UNIVERSITÀ DEGLI STUDI DI NAPOLI
FEDERICO II

SCUOLA POLITECNICA E DELLE SCIENZE DI BASE
DIPARTIMENTO DI INGEGNERIA CHIMICA, DEI MATERIALI E DELLA PRODUZIONE INDUSTRIALE

PHD THESIS IN INDUSTRIAL PRODUCTS AND PROCESS ENGINEERING
XXXV CYCLE

TIME AND SPACE MODULATION OF SUBSTRATE CURVATURE TO REGULATE CELL MECHANICAL IDENTITY

Supervisor:
Prof. Paolo Antonio Netti

Candidate:
Stefania Saporito

Advisor:
Ing. Valeria Panzetta

Coordinator:
Prof. Andrea D'Anna

2019-2022

Motivation and outline

Each cell can sense and transform external mechanical stimuli into internal chemical reactions thanks to two cell's abilities known as mechanosensing and mechanotransduction, respectively [1].

The mechanical cues can be either extracellular forces applied on the cell from the extracellular matrix (ECM) such as compression, tension and fluid shear stress, or intracellular forces like those arising from cellular responses to changes in extracellular matrix stiffness. These mechanical stresses could control cell shape, cell proliferation, cell polarity and cell differentiation; furthermore, in pathological conditions, such as cancers or neurodegenerative diseases, the mechanosensing and mechanotransduction pathways result different from normal cells [2, 3].

On the cell scale, the geometric form and the biological functions are inherently correlated and there is also increasing evidence of the effects of substrate curvature on cell behaviour, even if these effects are largely overlooked or underestimated during the design of new cell-material interfaces [4]. Moreover, there is a spatio-temporal dependence in the influence of cell response from its surrounding environment which has to be considered [4]. In fact, in the body, the cells especially those from blood, bone marrow, lungs, heart and musculoskeletal tissues are subjected to cyclically mechanical loading. To mimic such dynamic mechanical microenvironment, the controlled stress/strain could be applied to cell-seeded biomaterials designing specific microfluidic devices.

Different microfluidic platforms have been designed to analyse the cell responses to static [5-8] or dynamic mechanical loadings [9-13], but in all these studies, the effects of these solicitations are viewed at the end of stimulation and/or on confluent cells. Conversely, a real-time analysis on single live cells is necessary to disclose the role played by these mechanical cues on cell fate and behaviour. So, the aim of this project is to design a microfluidic platform where single adipose derived mesenchymal stem cells (ASCs) are statically or dynamically stretched modifying substrate curvature and then, their response is acquired in real time using the confocal microscopy technique. The real-time visualization with a confocal microscope is possible using the transfection technique, which here has been obtained by electroporation strategy.

Detailly, to study the response of single adipose stem cells to a static/dynamic curvature solicitation, the structural changes of the actin cytoskeleton and the focal adhesions (FAs) have been explored and quantified.

Moreover, the actin cytoskeleton can convert this mechanical stimulus into biochemical responses. Specifically, the actin cytoskeleton can directly regulate the activation of Yes-associated protein (YAP), a transcription factor implicated in cell proliferation, differentiation, and survival [14]. It is not well understood the role of curvature in the regulation of this specific transcription factor, particularly for concave surfaces. In fact, the convex substrates should be able to activate the YAP translocation from the cytoplasm to the nucleus and then, induces cellular proliferation [15,16]. Conversely, a correlation between concave morphologies and tight junctions for high-density cells should be responsible for YAP shuttling from the nucleus to the cytoplasm but this mechanism has not completely elucidated [17-19]. So, the designed microfluidic platform has been used to study the mechanotransduction response to a specific curvature variation in terms of YAP translocation (from the nucleus to the cytoplasm and *vice versa*) in ASCs cultured at high-density.

The designed microfluidic platform is able to induce macroscopic morphological topographies to adipose derived mesenchymal stem cells which are able to finely control actin stress fibers, focal adhesions, and YAP responses. Conversely, micro and nanoscopic mechanical features could be applied by designing specific patterns of hundreds of nanometres on the PDMS cell-seeded membrane of the chip. Being micropatterns characterized by morphological featured within the same order of magnitude of cell receptors, they are able to act at level of focal adhesions. So, a specific micropatterned substrate has been designed and fabricated using the two-photon polymerization technique which will be used as master for the PDMS membrane manufacture. In this way, the microfluidic platform can be considered as a tool to apply different mechanical insults on ASCs in a simultaneous manner.

This work is organized as followed: the theoretical background regarding the cell structures involved in mechanosensing and mechanotransduction pathways, the role of microenvironment curvature on the cell behaviour and state of the art about the design of microfluidic platforms as tools for cellular mechanical stimulation are given in **Chapter**

1, establishing relevant definitions for a sufficient background knowledge for the work presented in this thesis. The **Chapter 2** describes the design of a new microfluidic platform to stimulate in a static or dynamic way adipose derived mesenchymal stem cells and analyse their response in real time combining microfluidic device – confocal microscopy technique – electroporation strategy. In the **Chapter 3** the actin cytoskeleton organization and focal adhesions behaviour in static mechanical configurations have been analyzed; conversely the dynamic mechanical response of the same structures has been observed in **Chapter 4**. Then, the response of YAP to a specific curvature morphology and the design and fabrication of a specific micropatterned substrate were amply explained in the **Chapters 5** and **6**, respectively.

References

[1] J. HC Wang and B. Li, “Mechanics Rule of Cell Biology”, Sports Medicine, Arthroscopy, Rehabilitation, Therapy & Technology, 2010

[2] Dahl et al. “Nuclear Shape, Mechanics and Mechanotransduction”, Circulation research, 2008

[3] A. Garcia et al. “Modelling of the mechano-chemical behaviour of the nuclear pore complex: current research and perspectives”, Royal Society of Chemistry, 2016

[4] D. Baptista et al. “Overlooked? Underestimated? Effects of substrate curvature on cell behaviour”, Cell Press Reviews, August 2019, Vol.37, No. 8

[5] J. Y. Park et al. “Study of cellular behaviour on concave and convex microstructures fabricated from elastic PDMS membranes”. Lab Chip, 9, 2043-2049 (2009)

[6] D. A. Soscia et al.” Salivary gland cell differentiation and organization on micropatterned PLGA nanofiber craters”, Biomaterials, 34, 6773-6784, 2013

[7] E. M. Levina et al. “Cylindrical substratum induces different patterns of actin microfilament bundles in nontransformed and in ras-transformed epitheliocytes” Exp. Cell Res. 229, 159-165, 1996

[8] E. S. Fioretta et al. “Differential Responses of endothelial and endothelial colony forming cells on electrospun scaffolds with distinct microfiber diameters”, Biomacromolecules, 15, 821-829, 2014

[9] C. Moraes et al. “Microfabricated arrays for high-throughput screening of cellular response to cyclic substrate deformation”, Lab on a chip, 10, 227-234, 2010

[10] C. Moraes et al. “Microdevice array-based identification of distinct mechanobiological response profiles in layer-specific valve interstitial cells”, Integrative Biology, 2013

[11] F. Michielin et al. “Microfluidic-assisted cyclic mechanical stimulation affects cellular membrane integrity in a human muscular dystrophy in vitro model” RCS Advances, Royal Society of Chemistry, 5, 98429-98439, 2015

[12] C.H. Chiu et al. “Self-renewal and differentiation of adipose-derived stem cells (ADCSs) stimulated by multi-axial tensile strain in a pneumatic microdevice”, Micromachines, 9, 607, 2018

[13] N. Campillo et al. “A novel chip for cyclic stretch and intermittent hypoxia cell exposures mimicking obstructive sleep apnea”, Frontiers in physiology, Vol.7, 2016

[14] Aragona, Mariaceleste, et al. "A mechanical checkpoint controls multicellular growth through YAP/TAZ regulation by actin-processing factors." *Cell* 154.5 (2013): 1047-1059.

[15] Dupont, Sirio, et al. "Role of YAP/TAZ in mechanotransduction." *Nature* 474.7350 (2011): 179-183.

[16] Low, Boon Chuan, et al. "YAP/TAZ as mechanosensors and mechanotransducers in regulating organ size and tumor growth." *FEBS letters* 588.16 (2014): 2663-2670.

[17] Soscia, David A., et al. "Salivary gland cell differentiation and organization on micropatterned PLGA nanofiber craters." *Biomaterials* 34.28 (2013): 6773-6784.

[18] Oka, T., A. P. Schmitt, and M. Sudol. "Opposing roles of angiomotin-like-1 and zona occludens-2 on pro-apoptotic function of YAP." *Oncogene* 31.1 (2012): 128-134.

[19] Oka, Tsutomu, et al. "Functional complexes between YAP2 and ZO-2 are PDZ domain-dependent, and regulate YAP2 nuclear localization and signalling." *Biochemical Journal* 432.3 (2010): 461-478.

Table of contents

CHAPTER 3

Adipose stem cell behaviour to static mechanical cues: cytoskeleton and focal adhesions response

List of Figures

Chapter 1

Introduction

1.1 Cell Organization

The cell (Figure 1.1) is the basic structural, functional, and biological unit of all known organisms and it is defined as the smallest unit of life. Focusing the attention on a particular class of cells, known as eukaryotes, they are defined as cells containing organized organelles, which are enveloped by a membrane. Most important among these organelles is the nucleus in which the genetic material is stored [1]

These cells have a complex structure but for this project, only the parts involved in the mechanosensing and mechanotransduction pathways will be analysed.

The **cell membrane**, also known as the plasma membrane, is a biological semipermeable membrane that separates and protects the cell from its surrounding environment. It consists of a double layer of phospholipids combined with proteins and carbohydrates.

The cell membrane is classified as a semi-permeable membrane because it regulates what enters and exits from the cells, thus facilitating the transport of materials needed for cell survival [2]. In addition, cell membranes are involved in a variety of cellular processes such as cell adhesion, ion conductivity, and cell signalling. Moreover, it serves as attachment surface for several extracellular structures or for other cells to hold them together to form tissues [3] and it allows mechanosensing through focal adhesions [4].

The **cytoplasm** is all the material inside a cell, enclosed by the cell membrane, except for the nucleus. The main components are cytosol and organelles. The former makes up about 70% of the cell volume and it is a complex mixture of cytoskeleton filaments, dissolved molecules, and water [5,6]. The latter are membrane-bound structures inside the cell such as mitochondria, endoplasmic reticulum and Golgi apparatus that have a fundamental importance in fulfilling specific functions enabling cell viability [7]. So far have not been shown to play a significant role in mechanotransduction and therefore will not be analysed in this context [7].

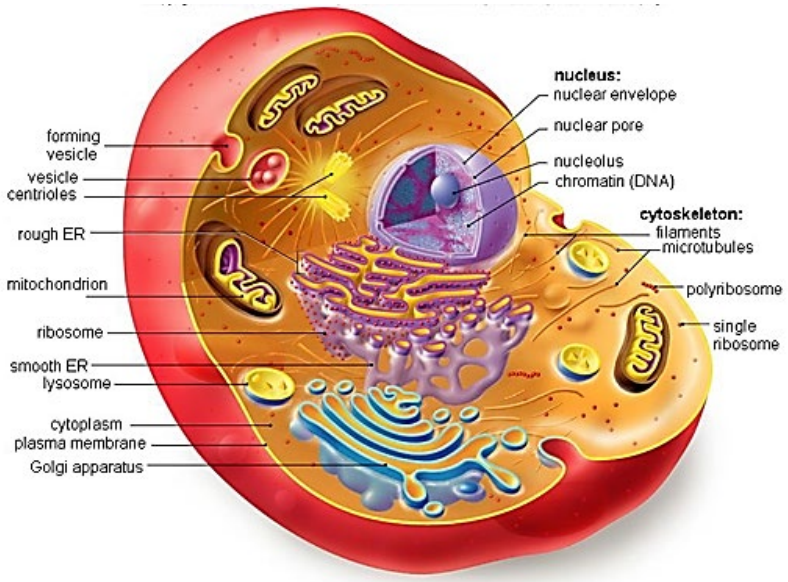

Figure 1.1: Eukaryotic cell organization [1]

The **cytoskeleton** is composed of actin filaments, microtubules, and intermediate filaments. **Actin filaments** are flexible structures composed of two stranded helical polymers of the globular actin protein. They are central to the formation of a variety of mechanosensing structures including linear bundles (e.g., lamellipodia and protrusions), two-dimensional and three-dimensional networks (Figure 1.2) [8,9]. Actin, in contrast to microtubules, is continuously assembled and disassembled in multiple areas of the cell and has the capability to associate with myosin II. The association between actin filaments and myosin (actomyosin) allows cell contractility, exhibiting a muscle-like contractile behaviour. Consequently, actomyosin present in the actin stress fibers is highly involved in mechanosensing and mechanotransduction [9-12] given its attachment to the focal adhesions or to the nuclear membrane.

Microtubules are composed of a protein called tubulin, which can form hollow cylinders and they have the most complex assembly and disassembly dynamics. They play an important role in providing strength under compressive load in cells and they are involved in intracellular transport, cell division, and chromosome separation [8,13]. Additionally, together with actin filaments, microtubules are involved in processes of force

transduction and hence cellular processes involving mechanosensing by tuning the degree of cellular deformation [14-16]

Finally, the **intermediate filaments** can provide strength to tensile forces much more effectively than compressive ones [8,17]. One class of intermediate filaments, known as nuclear lamins, contribute to the mechanical integrity of the cell nucleus [18].

Thanks to this specific organization, the cell cytoskeleton actively participates in the ability of cells to sense and convert mechanical stresses to biological responses [19,20].

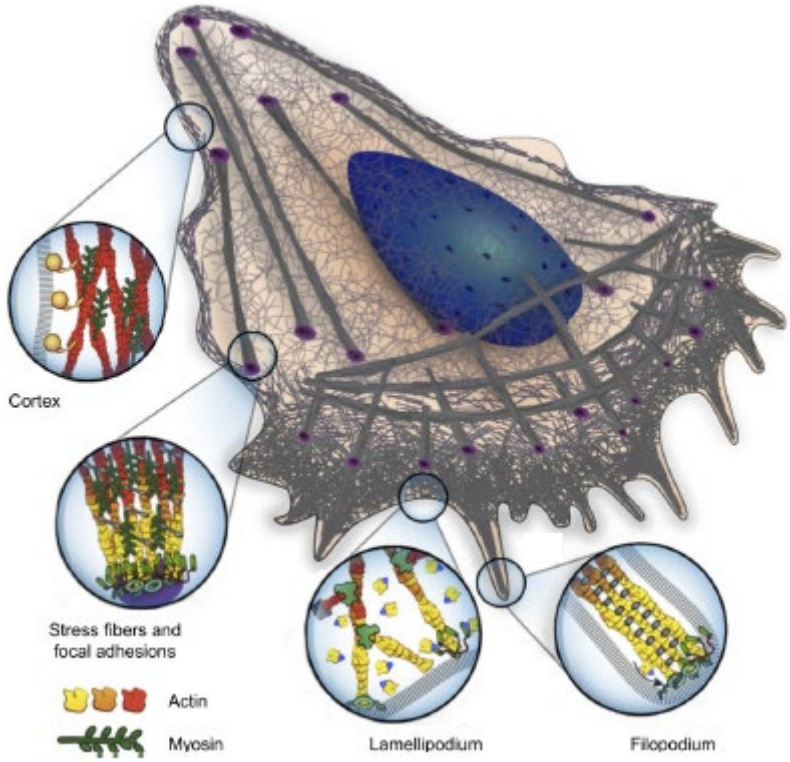

Figure 1.2: Actin cytoskeleton architecture and mechanics in the cell. The association of actin and myosin (actomyosin) confers contraction capacity in specific regions of the cell such as the cortex or actin stress fibers [21]

The cell **nucleus** can be structurally and functionally divided into two parts: the nuclear envelope (NE) and the nuclear interior. The NE is composed of two phospholipid bilayer membranes (inner and outer) and the nuclear lamina. In particular, the two membranes join at the nuclear pore complexes (NPCs), which allow nuclear-cytoplasmic transport, whereas the nuclear lamina can provide mechanical support to the nucleus and its anchors both to the inner nuclear membrane and peripheral DNA and chromatin [19].
The nuclear interior houses the genetic material that is organized in chromosomes and here occurred almost all DNA replications and RNA synthesis [19].

1.2 Mechanosensing and Mechanotransduction pathways

Mechanical forces act on human bodies at different levels, from the whole body to individual organs, tissues, and cells, can potentially influence the growth and shape of every tissue and organ. Focusing the attention on the cellular level, each cell can sense mechanical cues, through a process known as mechanosensing and respond to these signals by translating mechanical stimuli into biochemical ones, through mechanotransduction. These mechanical cues can be either forces applied on the cell from the extracellular matrix (ECM), or intracellular forces generated in response to variations in the ECM stiffness. Even if the physical pathway responsible to transmit these signals from the ECM to the nucleus is well known, how the mechanical cues are transduced into biochemical ones remains an open challenge. This topic results of great interest inasmuch the mechanical cues are involved in cell proliferation, differentiation, survival, apoptosis and, in pathology like cancers or neurodegenerative diseases, the mechanosensing and the mechanotransduction pathways are compromised [19,22].
The cells can communicate with the extracellular matrix [24], which is a complex microenvironment surrounding cells composed by proteins and macromolecules (collagen, proteoglycans, elastin, and fibronectin), using focal adhesions (FAs). To exert forces to their surroundings and probe the mechanical environment, cells required focal adhesions. Moreover, FAs have the capacity to adapt according to the forces exerted to the substrate, increasing their size as force increases or dissipating when the forces decrease [25]. The FAs are discrete complexes formed by membrane-spanning integrins and other proteins, such as focal adhesion kinase, talin, vinculin and paxillin. The focal

adhesions create a direct communication between the ECM and the cell's cytoskeleton; in particular, the ECM's stiffness can regulate cell adhesion, shape, differentiation, and motility [23].

A physical connection between the cytoskeleton and the nuclear envelope, known as the LINC complex, provides a mechanism to transmit extracellular and cytoskeletal forces to the nucleus. This coupling is established with specific outer nuclear membrane proteins (Nesprin 1 and 2), which can bind with both cytoskeleton's filaments and inner nuclear membrane proteins (SUN 1 and 2). SUN proteins can bind lamins of the nuclear lamina and other nuclear membrane proteins, which, in turn can bind DNA and chromatin (Figure 1.3) [23].

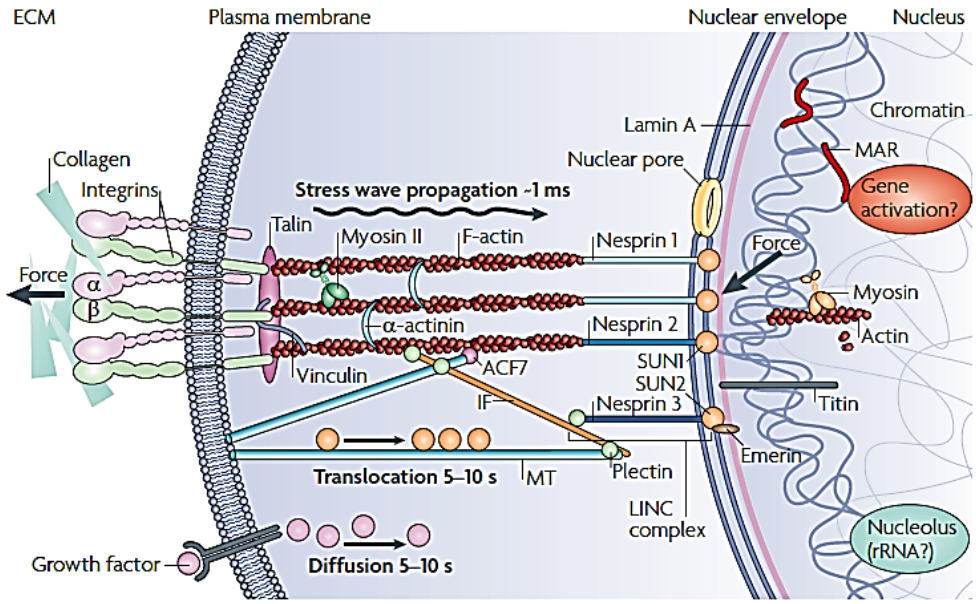

Figure 1.3: Molecular connectivity from the ECM to the nucleus [23]

Other than the physical connection previously described, there is a specific physical pathway for a direct transmission of stresses and strains from the ECM to the nucleus known as actin cap. It has been proved that the actin cap can regulate nuclear shape, mechanosensing, and mechanotransduction [26]. The actin cap is composed of thick, parallel, and highly contractile actomyosin filament bundles, which result functionally, molecularly, and topologically different from actin filaments. The former is typically

highly organized and oriented with the long axis of the cell, whereas the latter are confined to the basal layer and arranged in different directions [20].

Consequently, cells can sense the mechanical environment, inducing motility and signalling responses that regulate several cellular processes (Figure 1.4). By pulling on the substrate, the cells will modify the ECM creating additional signals. These signals can be translated into intracellular cues that will alter the expression of the cell, the cellular forces, and the secreted matrix [4]. Therefore, cell mechanosensing and the associated mechanotransduction of mechanical inputs in biochemical reactions greatly influence cellular behaviour and ECM organization.

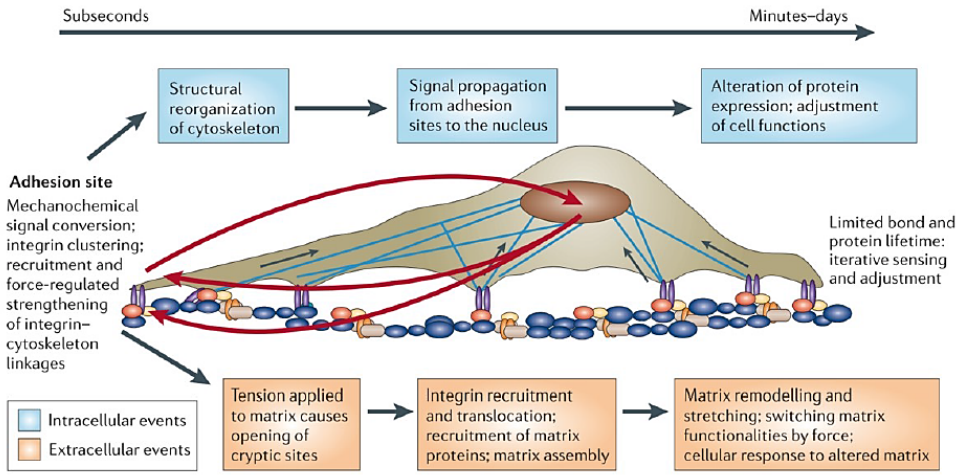

Figure 1.4: Cell cytoskeleton and mechanosensing. Diagram depicting the steps in mechanosensing involving substrate testing, substrate modification and changes in cellular protein content [4].

1.3 Role of curvature on cell behaviour

On the cell scale, the geometric form and the biological functions are inherently correlated; in fact, there is increasing evidence of the effects of substrate curvature on cell behaviour, even if these phenomena are largely overlooked or underestimated during the design of new cell-material interfaces [27]. The cells can discriminate between planar, convex, and concave surfaces. Fibroblasts, for example, can differentiate on spherical convex substrates up to a curvature diameter of 2 mm above which they have a response like cells on planar surfaces [28].

The mechanosensing and the mechanotransduction pathways of cells on convex and concave substrates are different. On the former (convex substrates), the response is

mediated by the Bin/amphiphysin/Rvs (BAR) domain proteins able to recognize and induce a corresponding bending of the cell membrane; in fact, upon contact, the BAR domain releases small enzymes (GTPases) and bind to the membrane inducing curvature [29]. As a result, there is a regulation of proliferation, cell shape, polarity, and locomotion because of the crucial effect of the convex substrate on the cell cycle and cytoskeleton. On the latter (concave substrates), a key role is played by inverse BAR (i-BAR) domain proteins on cell mechanotransduction, even if the function of these proteins to sense membrane curvature or to promote membrane bending is not fully understood [29].

Park and colleagues [30] have analyzed the response of fibroblasts on concave and convex microstructures realized in polydimethylsiloxane (PDMS) observing a preference of cells to climb on the convex structures with respect to enter on concave surfaces. On the contrary, cells of two immortalized salivary glands epithelial cell lines, seeded inside hemispherical craters realized in PDMS and coated with lactic-co-glycolic (PLGA) nanofibers, successfully stay and form curved confluent monolayers lining the concavities [31].

Cylindrically curved structures such as fibers, tubes and rounded ridges are often used to induce cell body elongation and alignment along the longitudinal axis of the structure. In some studies [32,33], the cells are oriented transversely to the cylindrical axis of the channels; whereas in others the cells have acquired a polarized cell morphology forming microfilament bundles and ECM fibrils oriented approximately longitudinally to the fiber axes.

So, for anisotropically curved substrates, like circular cylindrical surfaces, there is an anisotropic morphological response of cells due to elongation and alignment along a preferential direction. Conversely, for isotropically curved surfaces, such as spherical ones, if there are not direct stimuli, either isotropic or random anisotropic cell responses can be observed.

The curvature-induced cell orientation pointed to the remodelling of the cytoskeleton towards a reduction of the energetic penalty associated with the bending of the actin stress fibers [34-36].

1.4 Microfluidic platforms as a tool for cellular mechanical stimulation: State of the art

In all studies previously introduced, the role of curvature on cell behaviour and the interaction between the cell and the extracellular matrix are analyzed using static mechanically responsive platforms. Conversely, there is a spatio-temporal dependence in the influence of cell response from its surrounding environment, which has to be considered. In fact, in the human body, cells especially those from blood, bone marrow, lungs, heart, or musculoskeletal tissues, are subjected to cyclically mechanical loading. To mimic such mechanical microenvironment, the controlled stress/strain is applied to cell-seeded biomaterials designing specific microfluidic devices.

Currently, most existing studies for engineering the stress/strain microenvironment of cells have been focused on 2D substrates since it is easier to apply mechanical forces to cells cultured on 2D surfaces with respect to 3D configurations.

For example, *Moraes and colleagues* [37], have developed and characterized an array-based micro-fabricated platform able to simultaneously apply cyclic equibiaxial substrate strains ranging in magnitude from 2% to 15% to small populations of cardiac valve mesenchymal progenitor cells (Figure 1.5). In this way, a high-throughput screening of the effects of strain magnitude on cell behaviour has been made. The device consists of multiple layers of patterned poly(dimethylsiloxane) fabricated using multilayer soft lithography. Each unit of the microfabricated array is composed of a loading post suspended over an actuation cavity where, applying a positive pressure (30 kPa), the loading post can move upward and deform the flexible cell culture substrate. Simultaneous applications of a range of substrate strains across the array was achieved by changing the size of the actuation cavities, while keeping constant the size of the loading posts and the pressure applied. The cells are cyclically stimulated at 1 Hz for 3h and 6h and, as a result, the accumulation of β-catenin in the nuclei of primary mesenchymal progenitor cells, depending on temporal and strain magnitude solicitation, has been analyzed. Generally, this protein is accumulated inside the cytoplasm, but the cyclically mechanical stimulation can affect the translocation inside the nucleus. In fact, after 3h of stimulation, there is a general increase in nuclear β-catenin with increasing strain levels; in particular, largest β-catenin accumulation was obtained for cells

stimulated at 15% strain. On the contrary, after 6h of stimulation, elevated β-catenin levels in the nucleus are recorded for 3%, 5% and 8% strain, whereas for 15% strain the level returns to these comparable to static control. Since the levels of β-catenin inside the nuclei results elevated for valvular interstitial cells of diseased aortic valves, an understanding of how mechanical strains modulate their nuclear accumulation in valve-derived mesenchymal progenitors results very useful to study valvular diseases.

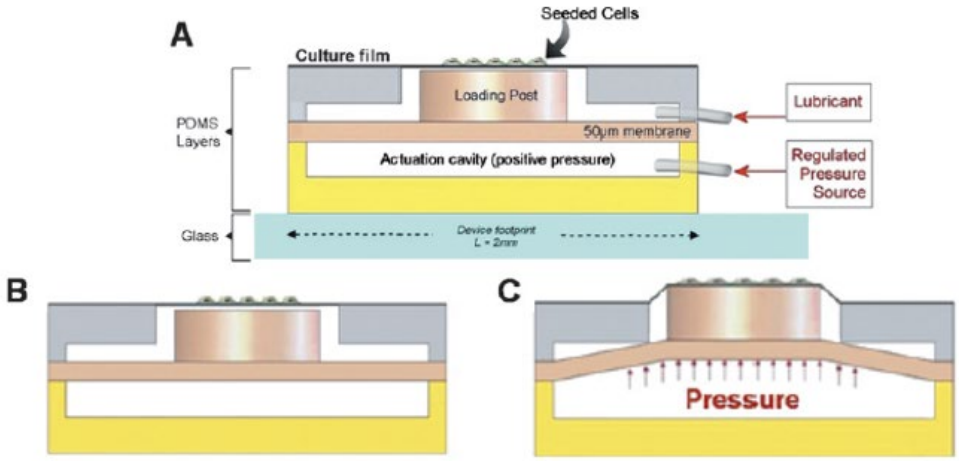

Figure 1.5: Microfluidic device structure. (A) Schematic cross-sectional view of a single mechanically active unit of the array. (B, C) Schematic of a unit in its (B) resting and (C) actuated positions [37].

The same group [38] has realized a development of this study, in which the cyclically mechanical stimulation is coupled with matrix proteins and soluble cues. The goal is to analyze the response of valvular interstitial cells (VICs) to these different signals in function of their origin. In fact, these cells are taken from two different tissues of aortic heart valve: ventricularis and fibrosa. These different cues should be involved in the dysfunctional differentiation of VICs into myofibroblasts. The level of a specific marker involved in this mechanism, called α-smooth muscle actin (α-SMA), has been analyzed. As a result, a consistent increase of α-SMA levels has been observed in cells from the ventricularis with respect to these from the fibrosa. This means that the VICs of ventricularis region tend to differentiate more easily into myofibroblasts when are subjected to a cyclic mechanical stimulation and there are more possibilities for these to develop aortic heart valve dysfunctions.

Michielin et al [39] have designed a microfluidic device able to investigate the effects of cyclic physiological stretching on early pathological events in dystrophic myotubes by using a human Duchenne Muscular Dystrophy (DMD) in vitro model. DMD is a disease characterized by a lack of the protein dystrophin, which plays a structural and regulatory role in preserving membrane integrity and homeostasis; in particular, mechanical cues seem to enhance the pathogenesis of muscle fibers. So, with ad hoc microfluidic-based cell-stretching device, external stimuli in terms of both frequency and intensity are applied to primary myoblasts and myotubes cell cultures. The results show that the human myotubes are more sensitive to mechanical stretching than the myoblasts. Moreover, the DMD myotubes have a higher stretch-induced membrane permeability compared to the healthy ones, when both are subjected to 90 min cyclic strain of 15%. Conversely, after only 45 min of the identical solicitation, the same effect has not been observed. This means that the absence of dystrophin makes the membrane more fragile and more susceptible to mechanical stress in specific conditions, leading to increased membrane permeability. So, with this microfluidic approach, an accurate and temporally defined mechanical stimulation at single or subcellular level can be done. Moreover, it could be used to study early pathological events or potential therapeutic approaches on a skeletal muscle disease in vitro model subjected to stress conditions normally experienced by muscle fibers in vivo.

Chiu and colleagues [40] to apply multi-axial mechanical tensile stretching on adipose derived stem cells (ASCs) have developed a PDMS-based microfluidic device (Figure 1.6). It is composed of nine culture chambers with a pneumatic mechanism; in particular, for each one, there is a deflective membrane actuated by compressed air. An in-house built instrument can control the pressure and actuation frequency and it is composed by an air pump, a pressure gauge, and an electronic valve actuated by a microcontroller. The results show an up-regulation of genes involved in the self-renewal after three days of cyclically stimulation, and, also, an increase of cell proliferation for cells harvested by some patients. On the contrary, an up-regulation of genes involved in the cell differentiation is recorded after the cyclical stimulation for cells taken from other patients; in particular, an osteogenic differentiation. This means that the response of ASCs to cyclic stimulation results patient-dependent.

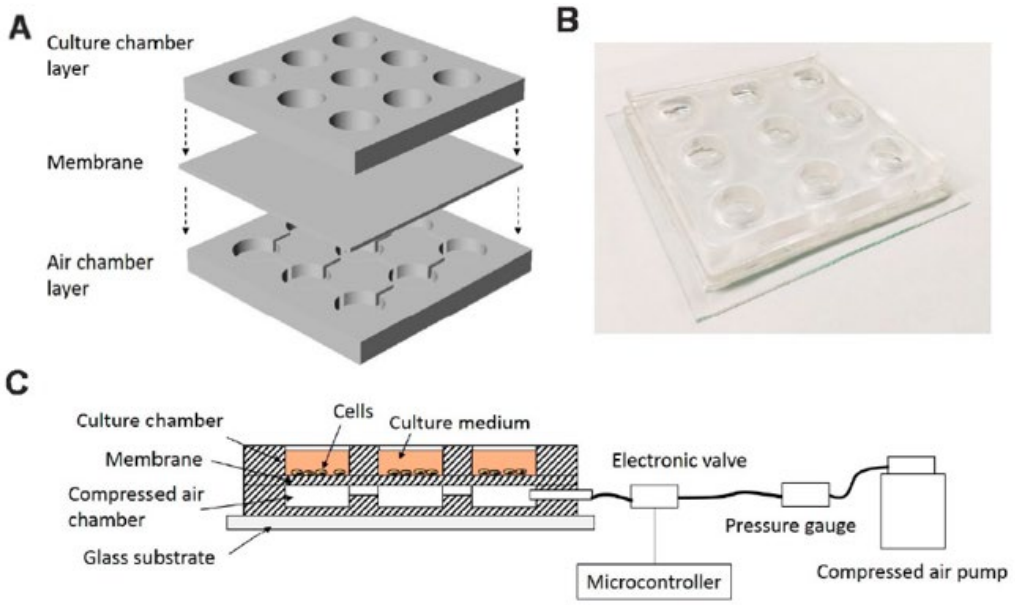

Figure 1.6: Microfluidic platform design. (A) Illustration of the design of the microdevice. (B) Photograph of the microdevice. (C) Illustration of the experimental setup of the cells stimulated by the multi-axial tensile strain[40].

Moreover, a chip able to mimic the obstructive sleep apnea (OSA) [41] has been fabricated. Due to this disease, the cells are subjected to cyclic stretch and different gas partial pressure, but the molecular mechanisms underlying these in vivo pathological responses remain poorly understood. The chip, made by PDMS, consists of a cylinder well-covered by a thin membrane on which cells are seeded and subjected to both fast changes in oxygen concentration and cyclic stretch at cardiac or respiratory frequencies. As a result, the oxygen concentration and cyclic stimulation are both responsible to increase the concentration of a specific factor involved in the pathology (hypoxia-inducible factor 1α). So, the chip provides a versatile tool for the study of cellular responses to cyclical hypoxia and stretch.

For all these microfluidic platforms, the cellular responses were analyzed at the end of mechanical stimulation fixing the samples into a specific configuration. Combining the immunostaining technique with the confocal microscopy the cellular behaviour in all the different configurations was observed. Conversely, an on-line visualization of cell response could be useful in order to visualize in real-time the cellular reaction to a specific mechanical cue. *Yamashita et al.* [42] have designed an air-pressure-driven separable

microdevice for live observations of human aortic smooth muscle cells (SMCs) to dynamic changes of anisotropic curvature (Figure 1.7). Briefly, the microfluidic device consists of three different components: a cell culture chamber with a thin elastic silicon bottom, a micro-slit with penetrating rectangular holes and a thin vacuum chamber. With an air-pressure control, a modulation of curvature was performed. A staining of cell nuclei was done to observe in real time with a low magnification objective the nuclear response. After 24h from the application of mechanical stimulation which induce a uniaxial stretching along the longitudinal microchannel direction, a nuclear alignment was obtained for high cell density configuration, whereas non-aligned nuclei for low cell density. Since the three different layers were not irreversibly bonded, a rotation of the 90° of the cell culture chamber was performed in order to apply the same uniaxial loading conditions orthogonally to the previous one. As a consequence, the nuclei that are aligned along the first preferential direction re-orient along the second one in 24h. All these results were observed for cells seeded on the culture chamber at high confluency, so the interaction between cells could have a relevant role in this nuclear response. On the contrary, on low cell density configuration, the nuclear response to a specific curvature variation was not well understood.

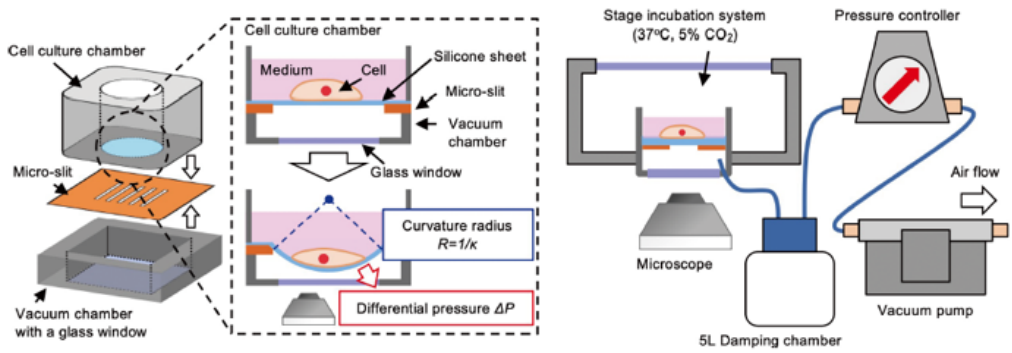

Figure 1.7: Design of the microdevice. The microdevice is composed of a cell culture chamber with a thin bottom made of silicon sheet, a micro-slit made of SU-8 and a vacuum chamber with a glass bottom. The microdevice installed in the stage incubator system was connected to a vacuum pump via a pressure controller that allows flexible modulation of the differential pressure applying to the cell culture surface[42].

From our knowledge, there were not designed microfluidic platforms able to induce and acquire single cell responses to uniaxial stretching conditions in real time. Moreover, the cytoskeleton architecture and focal adhesions organization in these specific mechanical conditions were not analyzed. So, to understand the single cell response, particularly in terms of actin stress fibers organization and FAs structure induced by uniaxial static and dynamic cues, a real-time accessible microfluidic platform has been designed and detailed described in the Chapter 2. Moreover, the same platform has been used to study the role of curvature on transcription factors trafficking between cytoplasm and nucleus focusing the attention on a specific molecule called Yes-associated protein.

References

[1]http://legacy.hopkinsville.kctcs.edu/instructors/JasonArnold/VLI/Module%202/m2cellstructure/m2cellstructure_print.html

[2] Holsbeeks, Inge, et al. "The eukaryotic plasma membrane as a nutrient-sensing device." *Trends in biochemical sciences* 29.10 (2004): 556-564.

[3] Ikeda, Mika, Akio Kihara, and Yasuyuki Igarashi. "Lipid asymmetry of the eukaryotic plasma membrane: functions and related enzymes." *Biological and Pharmaceutical Bulletin* 29.8 (2006): 1542-1546.

[4] V. Vogel, M. Sheetz, Local force and geometry sensing regulate cell functions., Nat. Rev. Mol. Cell Biol. 7 (2006) 265–275. doi:10.1038/nrm1890.

[5] D.A. Fletcher, R.D. Mullins, Cell mechanics and the cytoskeleton, Nature. 463 (2010) 485–492. doi:10.1038/nature08908

[6] C.T. Lim, E.H. Zhou, S.T. Quek, Mechanical models for living cells - A review, J. Biomech. 39 (2006) 195–216. doi:10.1016/j.jbiomech.2004.12.008.

[7] V.A. Shepherd, "The cytomatrix as a cooperative system of macromolecular and water networks", Current Topics in Developmental Biology, 2006

[8] D.A. Fletcher, R.D. Mullins, Cell mechanics and the cytoskeleton, Nature. 463 (2010) 485–492. doi:10.1038/nature08908.

[9] S. Tojkander, G. Gateva, P. Lappalainen, Actin stress fibers - assembly, dynamics and biological roles, J. Cell Sci. 125 (2012) 1855–1864. doi:10.1242/jcs.098087.

[10] G.W.G. Luxton, Linear Arrays of Nuclear Envelope Flow for Nuclear Movement, Science (80-.). 956 (2010) 956–960. doi:10.1126/science.1189072.

[11] J. Colombelli, A. Besser, H. Kress, E.G. Reynaud, P. Girard, E. Caussinus, U. Haselmann, J. V. Small, U.S. Schwarz, E.H.K. Stelzer, Mechanosensing in actin stress fibers revealed by a close correlation between force and protein localization, J. Cell Sci. 122 (2009) 1665–1679. doi:10.1242/jcs.054577.

[12] J. Swift, D.E. Discher, The nuclear lamina is mechano-responsive to ECM elasticity in mature tissue, J. Cell Sci. 127 (2014) 3005–3015. doi:10.1242/jcs.149203.

[13] C.P. Brangwynne, F.C. MacKintosh, S. Kumar, N.A. Geisse, J. Talbot, L. Mahadevan, K.K. Parker, D.E. Ingber, D.A. Weitz, Microtubules can bear enhanced

compressive loads in living cells because of lateral reinforcement, J. Cell Biol. 173 (2006) 733–741. doi:10.1083/jcb.200601060.

[14] L.G. Vincent, Y.S. Choi, B. Alonso-Latorre, J.C. Del Álamo, A.J. Engler, Mesenchymal stem cell durotaxis depends on substrate stiffness gradient strength, Biotechnol. J. 8 (2013) 472–484. doi:10.1002/biot.201200205.

[15] K.A. Kilian, B. Bugarija, B.T. Lahn, M. Mrksich, Geometric cues for directing the differentiation of mesenchymal stem cells., Proc. Natl. Acad. Sci. U. S. A. 107 (2010) 4872–7. doi:10.1073/pnas.0903269107.

[16] L. Pieuchot, J. Marteau, A. Guignandon, T. Dos Santos, I. Brigaud, P.F. Chauvy, T. Cloatre, A. Ponche, T. Petithory, P. Rougerie, M. Vassaux, J.L. Milan, N. Tusamda Wakhloo, A. Spangenberg, M. Bigerelle, K. Anselme, Curvotaxis directs cell migration through cell-scale curvature landscapes, Nat. Commun. 9 (2018). doi:10.1038/s41467-018-06494-6.

[17] D.E. Ingber, Tensegrity: the architectural basis of cellular mechanotransduction., Annu. Rev. Physiol. 59 (1997) 575–99. doi:10.1146/annurev.physiol.59.1.575.

[18] M.Y. Tsai, S. Wang, J.M. Heidinger, D.K. Shumaker, S.A. Adam, R.D. Goldman, Y. Zheng, A mitotic lamin B matrix induced by RanGTP required for spindle assembly, Science (80-.). 311 (2006) 1887–1893. doi:10.1126/science.1122771.

[19] Dahl et al. “Nuclear Shape, Mechanics and Mechanotransduction”, Circulation research, 2008

[20] M. M. Nava et al. “Bio-chemo-mechanical models for nuclear deformation in adherent eukaryotic cells”, Biomech Model Mechanobiol Review Paper, 2014

[21] L. Blanchoin, R. Boujemaa-Paterski, C. Sykes, J. Plastino, Actin Dynamics, Architecture, and Mechanics in Cell Motility, Physiol. Rev. 94 (2014) 235–263. doi:10.1152/physrev.00018.2013.

[22] A. Garcia et al. “Modelling of the mechano-chemical behaviour of the nuclear pore complex: current research and perspectives”, Royal Society of Chemistry, 2016

[23] N. Wang et al. “Mechanotransduction at a distance: mechanically coupling the extracellular matrix with the nucleus”, Nature reviews: Molecular Cell Biology, 2009

[24] J.K. Mouw, G. Ou, V.M. Weaver, Extracellular matrix assembly: a multiscale deconstruction, Nat. Rev. 15 (2014) 771–785. doi:10.1038/nrm3902.

[25] N.Q. Balaban, U.S. Schwarz, D. Riveline, P. Goichberg, G. Tzur, I. Sabanay, D. Mahalu, S. Safran, A. Bershadsky, L. Addadi, B. Geiger, Force and focal adhesion assembly: a close relationship studied using elastic micropatterned substrates., Nat. Cell Biol. 3 (2001) 466–72. doi:10.1038/35074532.

[26] Kim, Dong-Hwee, Allison B. Chambliss, and Denis Wirtz. "The multi-faceted role of the actin cap in cellular mechanosensation and mechanotransduction." *Soft matter* 9.23 (2013): 5516-5523.

[27] D. Baptista et al. “Overlooked? Underestimated? Effects of substrate curvature on cell behaviour”, Cell Press Reviews, August 2019, Vol.37, No. 8

[28] S. J. Lee and S- Yang “Micro glass ball embedded gels to study cell mechanobiological responses to substrate curvatures”, Rev. Sci. Instrum., 2012

[29] A. Frost et al., “The BAR domain superfamily: membrane molding macromolecules”, Cell, 137, 191-196, 2009

[30] J. Y. Park et al. “Study of cellular behaviour on concave and convex microstructures fabricated from elastic PDMS membranes”. Lab Chip, 9, 2043-2049 (2009)

[31] D. A. Soscia et al.” Salivary gland cell differentiation and organization on micropatterned PLGA nanofiber craters”, Biomaterials, 34, 6773-6784, 2013

[32] E. M. Levina et al. “Cylindrical substratum induces different patterns of actin microfilament bundles in nontransformed and in ras-transformed epitheliocytes” Exp. Cell Res. 229, 159-165, 1996

[33] E. S. Fioretta et al. “Differential Responses of endothelial and andothelial colony forming cells on electrospun scaffolds with distinct microfiber diameters”, Biomacromolecules, 15, 821-829, 2014

[34] N.D. Bade, T. Xu, R.D. Kamien, R.K. Assoian, K.J. Stebe, Gaussian Curvature Directs Stress Fiber Orientation and Cell Migration, Biophys. J. 114 (2018) 1467–1476. doi:10.1016/j.bpj.2018.01.039.

[35] N.D. Bade, R.D. Kamien, R.K. Assoian, K.J. Stebe, Curvature and Rho activation differentially control the alignment of cells and stress fibers, Sci. Adv. 3 (2017) e1700150. doi:10.1126/sciadv.1700150.

[36] G.A. Dunn, J.P. Heath, A new hypothesis of contact guidance in tissue cells, Exp. Cell Res. 101 (1976) 1–14. doi:10.1159/000457118.

[37] C. Moraes et al. “Microfabricated arrays for high-throughput screening of cellular response to cyclic substrate deformation”, Lab on a chip, 10, 227-234, 2010

[38] C. Moraes et al. “Microdevice array-based identification of distinct mechanobiological response profiles in layer-specific valve interstitial cells”, Integrative Biology, 2013

[39] F. Michielin et al. “Microfluidic-assisted cyclic mechanical stimulation affects cellular membrane integrity in a human muscular dystrophy in vitro model” RCS Advances, Royal Society of Chemistry, 5, 98429-98439, 2015

[40] C.H. Chiu et al. “Self-renewal and differentiation of adipose-derived stem cells (ADCSs) stimulated by multi-axial tensile strain in a pneumatic microdevice”, Micromachines, 9, 607, 2018

[41] N. Campillo et al. “A novel chip for cyclic stretch and intermittent hypoxia cell exposures mimicking obstructive sleep apnea”, Frontiers in physiology, Vol.7, 2016

[42] Yamashita, Tadahiro, et al. "Air-pressure-driven separable microdevice to control anisotropic curvature of cell culture surface." *Analytical Sciences* (2020): 20A001.

Chapter 2

Design of a microfluidic platform to study the role of static and dynamic mechanical loading on cell fate and behavior

2.1 Introduction

It is well known that mechanical cues influence cell proliferation, differentiation, migration, and apoptosis; so, different physiological activities could be mechanically regulated, for instance, cardiomyocyte orientation, osteogenesis, and angiogenesis [1,2]. Besides, many human tissues and organs, such as blood vessels, muscles, lungs, and heart, are affected by periodic stretching stimuli.

To study the cellular mechanobiology, microdevices for cell stretching can be a powerful tool. There are two different kinds of cell stretchers: motor-driven platform and microfluidic devices [3-5]. Starting from the motor driven devices, they are integrated machines, in which a motor (electric, electromagnetic, or stepper) is used to stretch the elastic membranes where cells are seeded. [6-8]. One of the most versatile motor driven devices is the commercialized system called "FlexCell" (FlexCell International Cooperation, Hillsborough, NC, USA) composed by six testing wells in parallel where tensile or compressive strains to cells can be applied. The drawbacks of this platform are related to the high number of cells and reagent useful in each experiment and the inability to test different mechanical environments in high-throughput manner [9].

In contrast, a microfluidic platform works using small quantities of cells and reagent, moreover, the materials involved in their fabrication are not only transparent and accessible for confocal microscopy technique, but also biocompatible for cells such as, polydimethylsiloxane [10, 11]. In literature there are a lot of microfluidic platforms, as explained in the section 1.4, able to mechanically stimulate cells in a static or dynamic way [12-19]. In function of platform design, it is possible to apply uniaxial or biaxial

stretches to cells but generally the effects of substrate curvature on cell response during the design of new cell-material interfaces are overlooked or underestimated [20].

It is well known that on convex substrates the cell response is mediated by the Bin/amphiphysin/Rvs (BAR) domain proteins able to recognize and induce a corresponding bending of the cell membrane. As a consequence, a regulation of cell proliferation, shape, polarity, and locomotion was observed [21]. Conversely, on the concave surfaces a key role is played by the inverse BAR (i-BAR) domain proteins on cell mechanotransduction, even if the cell response to these specific topographies is not fully understood. Moreover, for all these microfluidic platforms, the cell responses were analyzed at the end of mechanical stimulation on fixed samples using the immunostaining technique or in real-time on high confluency cells and not on low-density cells.

Considering all these aspects, the aim of this project consists in the design of a microfluidic device where low-density adipose-derived mesenchymal stem cells (ASCs) are statically - dynamically stretched and their response is acquired in real-time. This device, used as solicitation platform, is designed to modify the curvature of the membrane where cells are seeded at different frequencies. To do that, the system is connected to a pressure controller able to modify the pressure inside a microfluidic channel which, as a consequence, induce a variation of the membrane curvature. This means that anisotropic mechanical cues along a preferential direction (microchannel length) are applied on cells. Since the role of concave morphologies on cell response is not clear, the attention has been focused on the application of static or dynamic mechanical cues able to modify the membrane from a flat to a concave configuration.

All the layers of the previous fabricated microfluidic platforms [12-19] were made using the PDMS, that is a biocompatible and gas permeable material. As a consequence, to mechanically deform the layer of interest avoiding the modification of the others, the thicknesses between these layers should be different some order of magnitude or, another strategy, could be the modification of the pre-polymer/cross-linker ratio between the different layers. This further complicates their real-time accessibility. For this reason, the microfluidic device described in this work has been designed using the combination of two materials: polymethylmethacrylate (PMMA) and polydimethylsiloxane (PDMS). In this way, the PDMS membrane is attached to a more rigid polymer like PMMA, ensuring

to mechanically solicitate only the substrate where cells are seeded, and their response is viewed in real time using both low and high magnification objectives. In fact, using this design, the microfluidic platform is easily accessible to confocal microscopes.
Moreover, to quantify the stresses and strains developed on the PDMS surface during the mechanical load, a specific 3D finite element model (FEM) has been formulated using the software "Abaqus CAE" and validated comparing the simulated response of the platform with the experimental one. These FEM models are a useful tool to evaluate the stresses and strains field developed in the different regions of the membrane, particularly in the part of membrane in contact with cells which they will be the fields sensed by the cells themselves.

2.2 Materials and Method

2.2.1 Device Fabrication

The microfluidic platform consists of five different layers (Figure 2.1) realized with two different materials: polymethylmethacrylate (PMMA) and polydimethylsiloxane (PDMS). Particularly, the PMMA layers were designed by AutoCAD and carved with Micromilling machine (Minitech CNC Mini-Mill); whereas the nanoparticles functionalized PDMS layer was fabricated with the spin coater instrument (Model WS-650MZ-23NPPB, Laurell Technologies Corporation).
Each layer of the microfluidic platform has a specific function, and it is fabricated with specific parameters:

- Layer 1 "Housing for NanoPorts" (Figure 2.1) was made with 1.1mm PMMA sheet. This layer needs to house connectors in order to change the medium in the culture chamber and modify the air pressure inside the microchannel. These housings have a diameter of 9.5 mm and a thickness of 550 μm. At the center of these holes, 3 other small holes were dug with a diameter of 3mm and a thickness of 550 μm, necessary for the passage of culture medium and air, respectively. The different parts were made using a 1mm tip, spindle RPM of 7000, feed-rate of 70, plunge rate of 70, x-y step of 0.2 mm and z step size of 0.2 mm.

- The second PMMA layer (Figure 2.1) contains the microfluidic channel having a width of 400 µm, a thickness of 500 µm and a length of 4 cm. Due to the microchannel width, a tip having a diameter of 400 µm has been used on 1.1mm PMMA sheet with specific parameters: spindle RPM of 7000, feed-rate of 20, plunge rate of 20, x-y step of 0.1 mm and z step size of 0.05 mm. To create a communication between the upper and lower layers, 3 holes with 3mm diameter were fabricated using a tip of 1mm for the whole thickness of the sheet.
- Layer 3 of PDMS was embedded with fluorescent polystyrene nanoparticles and was manufactured with a thickness of approx. 70 µm that is deformed by air pressure variations. Aligned with other layers, 3 mm diameter holes were made using a specific punch having the same diameter.
- The PMMA layer 4 (Figure 2.1) is the chamber containing cell medium and a sheet of 1.1mm thickness was employed. The chamber medium has a dimension of 4 cm length, 1.4 cm width and 1.1 mm thickness. Furthermore, the channels from the holes to the chamber medium have a width of 3mm equal to the diameter of NanoPorts tubes, in this way the load losses associated with the transition between the different layers can be reduce. Due to the dimensions of the different parts composing this layer, 1mm tip was used.
- The PMMA layer 5 (Figure 2.1) needs to close the cell medium chamber. A 500 µm PMMA sheet was employed and a contour of the selection with dimensions of 5.9 cm length and 3.9 cm width was fabricated with the micro-milling instrument.

PMMA is a thermoplastic polymer that can be melted and used in different fabrication processes; on the contrary, PDMS is a thermoset polymer that cannot be remoulded, and its final shape cannot be changed [22]. Even though PMMA and PDMS are two polymers with characteristics completely different, they have been chosen to design the microfluidic device inasmuch the combination of these two materials permits to have the PDMS substrate attached to a more rigid polymer like PMMA, ensuring to mechanically solicitate only the membrane where cells are seeded without deformations of other device layers. Furthermore, the chip can be reused several times with an appropriate washing

protocol that will be explained later (Chapter 3 – Materials and Method) and it is easily accessible to the confocal microscopes.

The irreversible bonding between PMMA and PDMS was made using a protocol developed by *Norouzi and colleagues* [23] where a thin intermediate layer of SiO_2 is used to enhance PMMA surface's hydrophilicity and increase PMMA stickiness to PDMS via O_2 plasma activation. Instead, the protocol for the bonding between PMMA layers, developed by *Bamshad and colleagues* [24], consists in a rapid and simple thermally solvent method in which a thin film of 70% isopropyl alcohol is dispersed between PMMA sheets and placed at 68 °C for 15 min. Applying these two bonding protocols, each layer of the microfluidic platform is irreversible bonded to the others.

Fluorescent polystyrene nanoparticles (Fluoresbrite Carboxylate YG 0.50 Micron Microspheres - Polysciences) embedded in the PDMS layer have been used as fiducial markers to quantify the membrane deformation due to the different pressures applied, using the confocal microscopy technique. To avoid the formation of polystyrene nanoparticle aggregates inside the PDMS, the inclusion is made with a specific protocol using the 2-Methoxyethanol (2-Methoxyethanol anhydrous 99.8% - Sigma-Aldrich). So, an equal mass of PDMS pre-polymer and 2-Methoxyethanol with 5% of polystyrene nanoparticles (1:20 v/w) were mixed. After the complete solvent evaporation, the PDMS cross linker was added (19:1 pre-polymer crosslinker ratio) and PDMS substrates with a thickness approx. of 70 μm were produced setting the spin rates at 700 rpm for 1 min and curing at 70 °C for 4h. Since the PDMS substrates were custom made with the protocol previously introduced, in literature there are no information about the mechanical properties of these membranes. So, specific tension tests were made with the Instron Machine (BioPlus - Instron) (solicitation speed 1 mm/s, pre-load 0.1 N) to quantify the right mechanical characteristics of this customized material (Young Modulus, stress/strain curve).

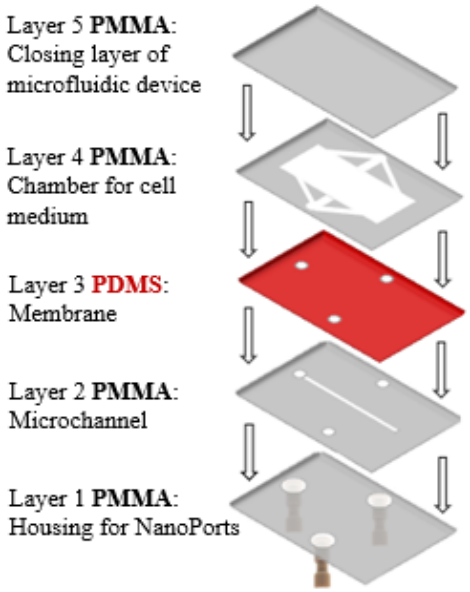

Figure 2.1: 3D view of the microfluidic platform

2.2.2 Computer interface and microfluidic control system for programmable cyclic loading

To obtain accurate and programmable device control, a pressure control system was used. The microfluidic platform was connected to the pressure controller OB1 MK4 (ElveFlow OB1 pressure controller – ElveFlow an ELVESYS brand) in order to apply specific pressure variations in the microfluidic channel which are able to modify the curvature of the PDMS membrane. Particularly, for positive pressures the substrate moves from flat to convex configuration, conversely for negative pressures from flat to concave one. Due to the full control software, the pressure variations can be applied in different ways: linear ramp, square profile, custom made scenarios and so on.

For experimental needs, different pressures ranging between -100 mbar and -600 mbar were applied as linear ramp (-100 mbar/min) and kept constants over time for static mechanical experiments on cells. On the contrary, dynamic mechanical stimulation of -500 mbar having a solicitation period of 1 s, 1 min or 10 min and a duty cycle of 50% were developed to study the cellular behaviour in cyclic mechanical cases.

2.2.3 Stretching experiments and curvature reconstruction protocol

To test the microfluidic platform response to different pressures (ΔP) ranging between -100 mbar and -600 mbar, specific stretching experiments have been developed using the pressure controller OB1 combined with the confocal microscope (Confocal Zeiss Axio Observer.Z1). For each test, the pressure has been applied as a linear ramp (-100 mbar/min) and this configuration was kept constant over time to scan the whole microchannel. Selecting at least ten specific regions along the microchannel, different z-stacks were acquired. Starting from these acquisitions, using the software FiJi, a reconstruction of the substrate curvatures towards the corresponding coordinates has been performed. Briefly, starting from the acquired z-stacks, the orthogonal view able to show the curvature variations induced by pressure was saved as .tiff. Then, after a contrast improvement (Enhance contrast 0.3%), the image was binarized and the coordinates of the part of PDMS membrane in contact with cells were quantified using in sequence different software functions: Erode, Skeletonize and Properties.

Knowing the membrane profile in the different configurations, the substrate curvature can be quantified using the equation (1) only if this profile can be associated to that of an arc of circumference:

$$R_C = \frac{w^2+H^2}{2H} \quad (1)$$

R_C = Radius of curvature of the deformed membrane under pressure.

w = Microchannel width.

H = Change of the height at the center of the membrane under pressure.

To verify if the equation (1) can be used to determine the radius of curvature (R_C) of experimental profiles, the experimental data have been compared with the Cartesian equation of a circle passing through three points of the experimental profile. The last one can be compared with that of the arc of circumference only if the coefficient of determination R^2 was close to 1. R^2 provides a measure of how well observed outcomes are replicated by the model, based on the proportion of the total variation of results explained by the model. Since R^2 results always greater than 0.96 for all pressures, the

experimental profiles can be modelled as an arc of circumference and, as a consequence, the radius of curvature quantified with equation (1).

2.2.4 Hypothesis and formulation of the 3D Finite Element Models

To quantify stresses and strains developed on the PDMS substrate during the mechanical load, a specific 3D finite element method (FEM) model has been formulated with a software based on the finite element approach called "Abaqus CAE". By using FEM, a complex domain is subdivided into a finite number of small elements with specific characteristics. The response of each element is expressed in terms of a finite number of degrees of freedom characterized as the value of unknown equation/equations, at a set of nodal points. In this way, the equations that model the single elements are assembled into a larger system of equations that model the entire structure.

Knowing the mechanical properties of the PDMS membrane obtained by the tension tests and the pressure variations applied during the experiments, the stress/strain field on the material surface has been quantified to estimate the mechanical stimuli to which cells will be subjected.

The first thing that has been performed in the Abaqus CAE software was the design of the different parts: PMMA and PDMS layers. To reduce the time of simulation, they have not been created all the layers of the microfluidic platform but only the parts involving in the membrane deformation, that is the PMMA layer 2 having the microchannel and the PDMS membrane (Figure S1A). Both were modelled as 3D deformable solid structures.

The PMMA layer was modelled as an incompressible isotropic elastic material that has Young's modulus of 4088 MPa, whereas, for the PDMS membrane, the stress/strain curve obtained from the tension tests was given as constitutive law. The load applied to the PDMS substrate is the experimental pressure and as a result, the von Mises stress distribution on the curved substrate was quantified.

The PDMS layer was modelled with the mesh element: solid continuum element of the first order with 8 nodes and a hybrid formulation (C3D8H) (Figure S1B). The solid continuum element has been chosen because it is used for linear and non-linear complex analysis of a solid involving contact and large deformations; whereas the hybrid

formulation is required by the software when the materials are characterized by hyper-elastic behaviour. Moreover, an element of the first order is characterized by a constant volumetric strain throughout the element. The PMMA layer was modelled with the mesh element: four-node linear tetrahedron (C3D4) chosen to reduce the simulation time as much as possible (Figure S1B). In fact, among the different types of elements, it is the one with the least number of nodes. This choice was possible because the part subjected to pressure is the PDMS layer and not the PMMA one, consequently a reduction in the number of nodes does not affect the final result. The PMMA layer is divided into a number of elements equal to 10902 having an approximate global size of 0.4, whereas PDMS substrate has a number of elements of 20000 and a global size of 0.2. Since Abaqus CAE is an a-dimensional software, all the different parameters have been defined in a coherent way: length unit millimetre (mm), force unit newton (N), masse unit tonne and Young's Modulus unit MPa.

Between the PMMA and the PDMS layers, an interaction has been defined. In the model this is one of the most important conditions because it avoids the interpenetration of the PDMS layer into the PMMA one. It is used a surface-surface interaction where the upper part of the PMMA layer is the master surface and the lower part of the PDMS substrate is the slave one. Generally, the master surface is one with the stiffer body and the coarser mesh (PMMA layer), conversely, the slave one should have more finely mesh and it cannot penetrate in the master surface (PDMS layer). The interaction has specific properties to normal and tangential loads; in particular, the tangential behaviour is set rough (no slip will occur once points are in contact) and isotropic, whereas the normal behaviour is characterized by a hard contact between the surfaces. These conditions are able to simulate the irreversible experimental bonding between the PDMS and the PMMA. Finally, to validate the FEM models, the experimental profiles and the simulative ones have been compared in order to quantify the R^2 parameters. For values $\geq$ 0.9 a good correspondence was observed.

2.3 Results

2.3.1 PDMS substrate fabrication and tension tests

The polydimethylsiloxane layer, as previously introduced, has been embedded with fluorescent polystyrene nanoparticles (Figure 2.2A), in this way it can be visualized using a confocal microscope. To obtain a thickness of approximately 70 μm, different rates of the spin coater instrument were tested, observing that the right combination is a speed of 700 rpm for 1 min with an acceleration of 85 rpm/s. These parameters have been optimized to the fabrication of these layers on PMMA sheets. The choice of these substrates was due to the anti-adhesiveness between PMMA and PDMS; so, the peeling off of the PDMS layer during the device assembly has been easy and rapid. Moreover, the pre-polymer/cross-linker ratio of 19:1 was used to have a membrane that is easily deformable as the pressure is changed in the underlying microchannel.

The thickness of the PDMS membrane was quantified using a confocal microscope and the experiments have been repeated three different times. As shown in Figure 2.2.B, there are not statistically significant differences between the different layer thicknesses.

Knowing the protocol for the PDMS substrates fabrication, it needs to know their mechanical properties. To do that, specific tension tests on specimens having the shape of dog bone were performed (Figure 2.2.C-D). Following the machine protocol, a pre-load of 0.1 N was set and then a solicitation time of 1mm/s was applied. The force-displacement curve (Figure 2.2.E) was the result of these tests. Knowing the specimen section, initial length, and thickness, from the force-displacement curve, the stress-strain plot can be quantified (Figure 2.2.F) which is characterized by a linear elastic behaviour up to 10% of strain following by a non-linear elastic one.

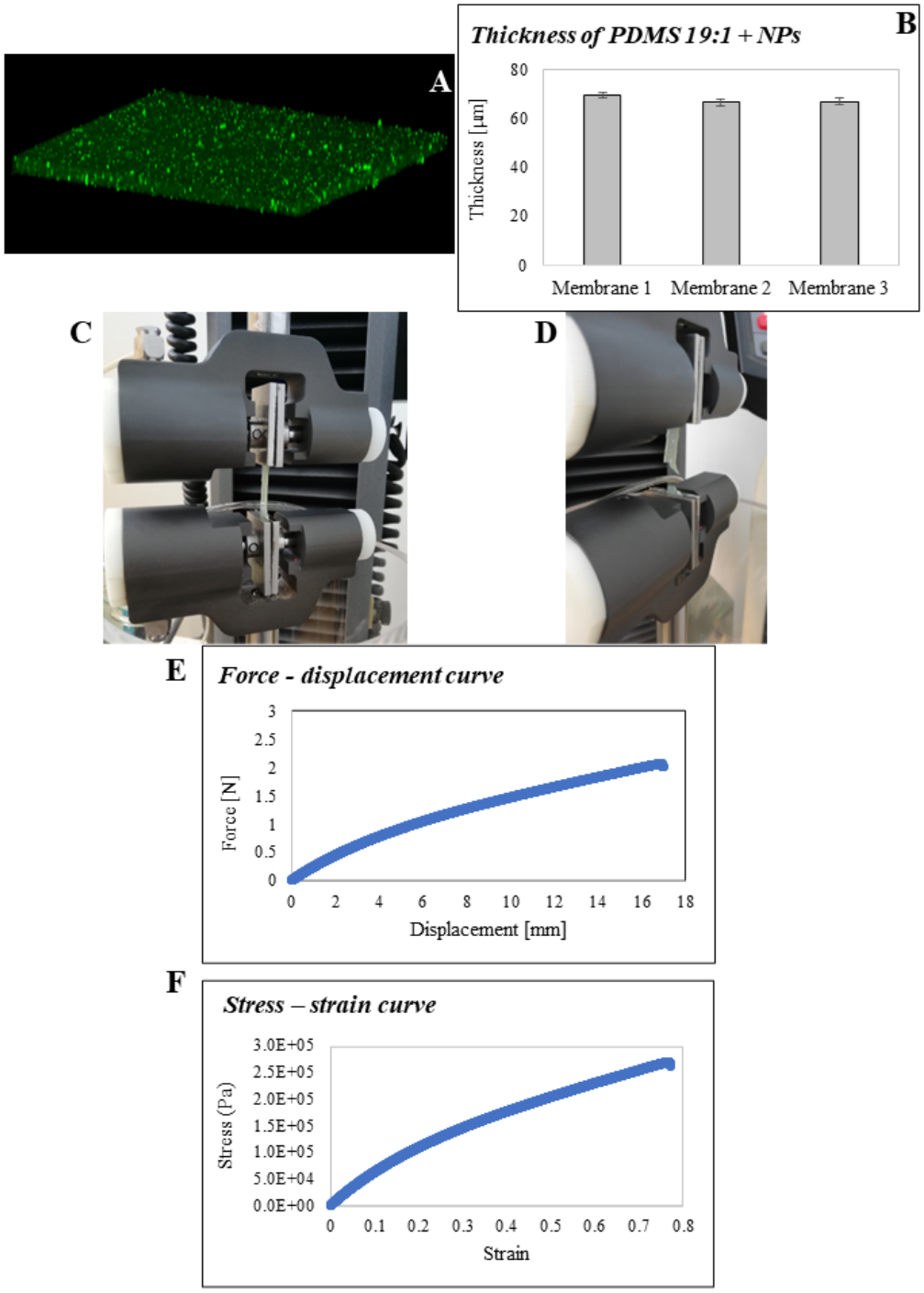

Figure 2.2: PDMS membrane characterization. A: 3D view of embedded polystyrene nanoparticles PDMS B: Thickness quantification on three independent PDMS substrates; C-D: Photos of the tension test made during the experiment (C) and at the end of it (D); E: Force-displacement plot obtained by tension tests on PDMS substrates with embedded fluorescent nanoparticles; F: Stress-strain curve derived by the force-displacement plot. All experiments have been repeated three times and data are expressed as mean ± s.e.m.

2.3.2 Microfluidic platform design, fabrication, and functioning

As previously introduced in the materials and methods section, the microfluidic platform was fabricated using two different materials: PMMA and PDMS. Each PMMA layer was designed using the AutoCAD software and performed with the micro-milling machine, whereas the PDMS substrate fabricated with the spin coating technique.
Particularly, each layer has a specific function:

- Layer 1 of PMMA needed to house three NanoPorts, with specific tasks – (i) cell medium influx, (ii) cell medium outflux and (iii) variation of air pressure inside the upper microchannel.
- Layer 2 of PMMA, having an empty microchannel at the center in which the air pressure was modified (length = 4cm, width = 400 μm and thickness = 500 μm).
- Layer 3 of PDMS embedded with fluorescent polystyrene nanoparticles and manufactured with a thickness of approx. 70 μm that is deformed by air pressure variations.
- Layer 4 of PMMA, having an empty chamber and microfluidic channels useful to contain the cell medium and to permit periodic cell culture medium replacement, respectively.
- Layer 5 of PMMA needed to close the microfluidic platform.

All PMMA thicknesses have been accurately chosen to create a microfluidic platform accessible to a confocal microscope with high magnification objectives. In fact, the working distance of these objectives is close to 2/2.5 mm that is a value close to the distance of the PDMS membrane from the objectives themselves. Since all the layers are completely transparent, the microfluidic platform is accessible using both upright and inverted confocal microscopes, that is, the objectives can be located in the lower or upper part of the instrument, respectively.
After the fabrication of each microfluidic platform part, all the layers were irreversible assembled as described in the materials and method section; so, the correct functioning has been tested.

The microfluidic platform was linked to the OB1 pressure controller and mounted on a confocal microscope. Different pressures were applied in the range [-100 mbar; -600 mbar]. The attention has been focalized on negative pressures inasmuch it is not clear the response of low-density cells in concave configurations with respect to the convex ones.

For each pressure applied, the pressure controller software was set in order to reduce the pressure inside the microchannel with a linear profile of -100 mbar/min assuming that 0 pressure corresponds to the configuration where the pressure inside and outside the microchannel is the same. After the application of a pressure variation, the PDMS membrane configuration was kept constant a time sufficient to acquire at least ten different z-stacks along the microchannel. From these acquisitions a quantification of the curvature variation can be made. Since different curvature changes have been tested, the results were organized in different sub-sections.

2.3.2.1 Test on microfluidic platform: ΔP = -100 mbar

Starting from the z-stacks acquired for the pressure variation of -100mbar, a reconstruction of the substrate curvatures towards the corresponding coordinates has been performed. As shown in Figure 2.3A, a change of the height at the center of the membrane of 39.95 μm has been obtained. To quantify the radius of curvature (R_C) and the corresponding curvature (κ) it needs to verify that this profile can be assumed to an arc of circumference profile. So, fixing three different points where this arc has to pass (central point and extreme points), the equation of a circumference passing through them has been calculated. Then, the two curves have been overlapped and the R^2 parameter quantified. As shown in Figure 2.3B a R^2 value of 0.9997 was obtained; so, the experimental profile can be assumed as an arc of circumference belonging to a circle having a radius of 538.73 μm ≈ 539 μm evaluated with equation (1). Knowing R_C, the curvature can be calculated using the equation (2):

$$\kappa = \frac{1}{R_C} \tag{2}$$

Particularly, For a pressure variation of -100 mbar, the curvature κ is equal to 0.00186 μm^{-1} and a 3D representative confocal image of the curvature change was shown in Figure 2.3C.

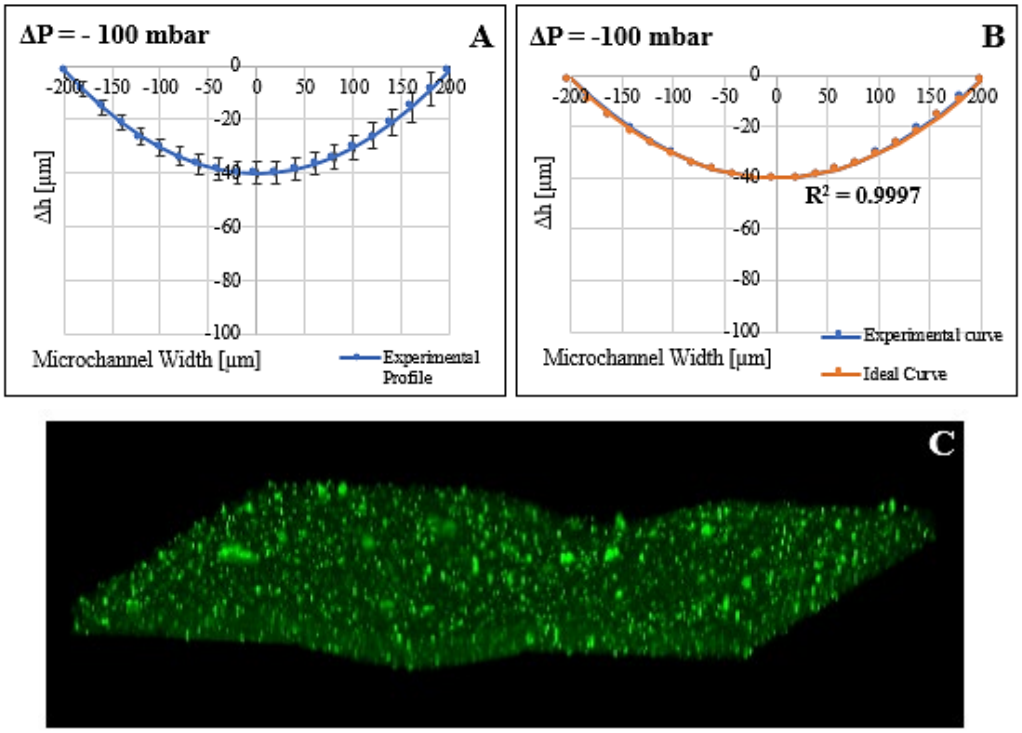

Figure 2.3: Microfluidic platform experiments for a pressure of -100mbar. A: Reconstruction of the experimental PDMS profile through the quantification of the corresponding coordinates. B: Overlapping of experimental and ideal profile. C: 3D representative confocal image. Each experiment has been repeated three different times and the data are expressed as mean ± standard deviation.

2.3.2.2 Test on microfluidic platform: ΔP = -200 mbar

A pressure of -200 mbar was applied on the microfluidic platform. Therefore, the substrate height variation (Δh) results equal to 71.22 μm (Figure 2.4A). Knowing the experimental profile, the ideal curve passing through the center and the vertexes of this profile has been determined (Figure 2.4B). Also in this case, there is a good agreement between the experimental and the ideal cases: $R^2 = 0.9970$. So, the radius of curvature results equal to 326.22 μm ≈ 326 μm, and, consequently, the curvature determined using the equation (2) corresponds to 0.00307 μm^{-1}. A representative 3D confocal image (Figure 2.4C) shows the 3D curvature change on the PDMS membrane.

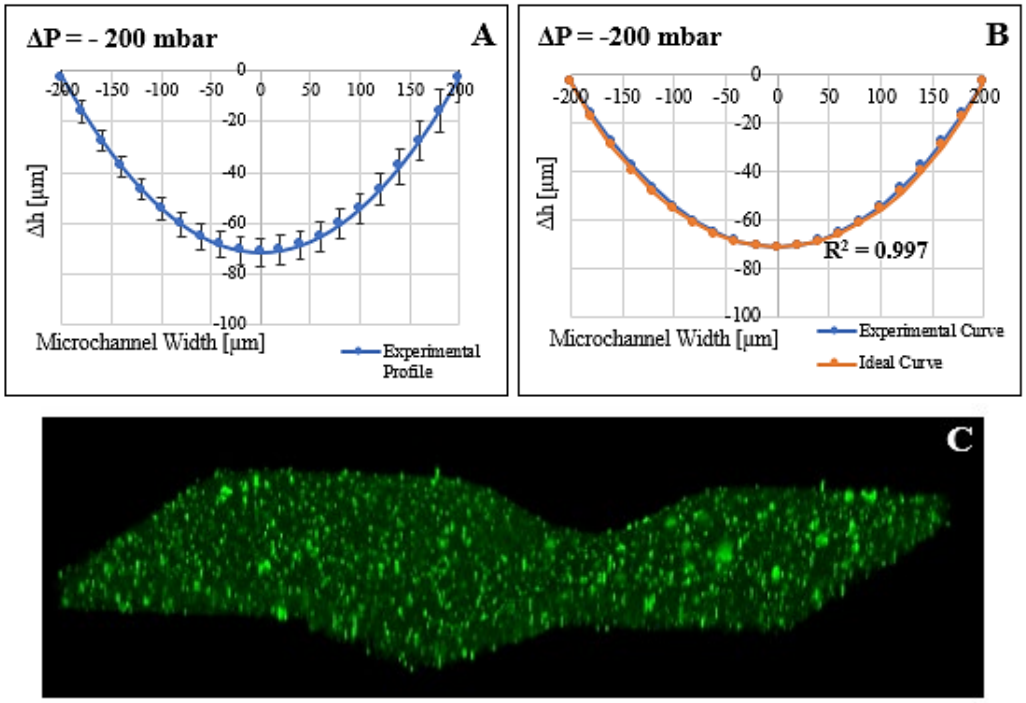

Figure 2.4: Microfluidic platform experiments for a pressure of -200mbar. A: Reconstruction of the experimental PDMS profile through the quantification of the corresponding coordinates. B: Overlapping of experimental and ideal profile. C: 3D representative confocal image. Each experiment has been repeated three different times and the data are expressed as mean ± standard deviation

2.3.2.3 Test on microfluidic platform: ΔP = -300 mbar

The third experiment developed to test the functioning of the microfluidic device consists in the application of a pressure equal to -300 mbar. From the corresponding coordinates obtained by the reconstruction of the PDMS profile (Figure 2.5A), a height variation of 105.92 µm was obtained. Then, an overlapping between the experimental curve and the ideal one (Figure 2.5B) shows a good approximation with R^2 equal to 0.994. Consequently, the radius of curvature is equal to 224.24 µm ≈ 224 µm, whereas the curvature κ results equal to 0.00446 μm^{-1}. The Figure 2.5C represents a 3D curvature profile of the solicitated PDMS membrane with embedded polystyrene nanoparticles.

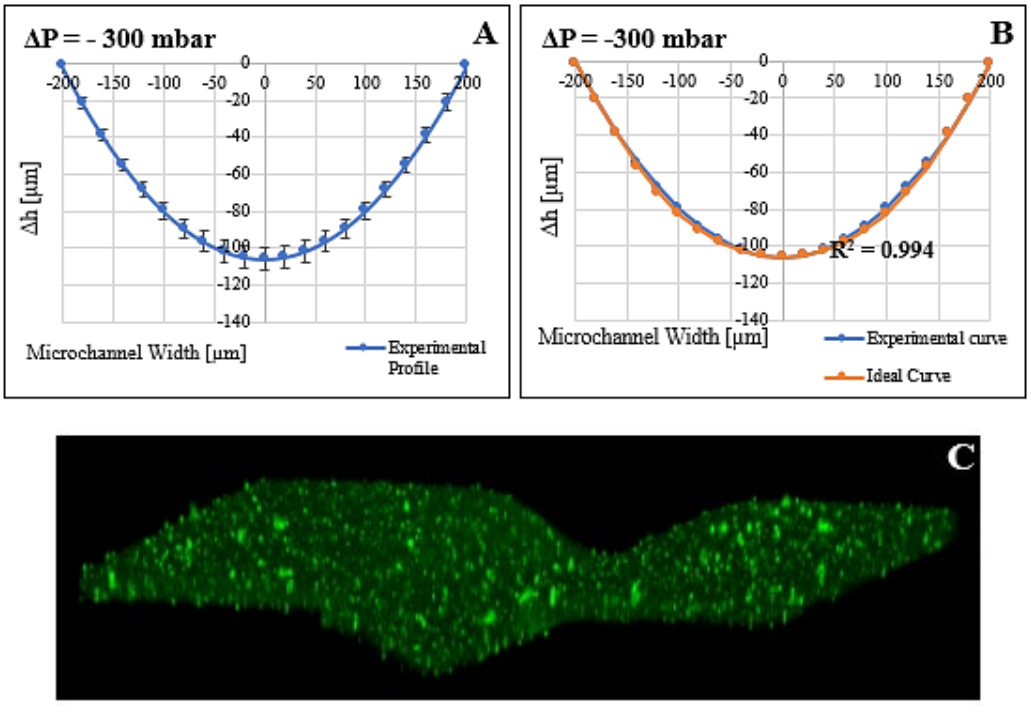

Figure 2.5: Microfluidic platform experiment for a pressure of -300mbar. A: Reconstruction of the experimental PDMS profile through the quantification of the corresponding coordinates. B: Overlapping of experimental and ideal profile. C: 3D representative confocal image. Each experiment has been repeated three different times and the data are expressed as mean ± standard deviation.

2.3.2.4 Test on microfluidic platform: ΔP = -400 mbar

Then, a pressure of -400 mbar was applied on the microfluidic platform observing a Δh = 136.49 μm (Figure 2.6A). Also in this case, a good correspondence between the ideal curve and the experimental one was obtained R^2 = 0.983 (Figure 2.6B). So, the experimental profile can be considered as an arc of circumference having a radius of curvature equal to 190.58 μm ≈ 191 μm and a curvature of 0.00525 μm^{-1}.

Increasing the pressure, a raise of PDMS membrane curvature was quantified and from a qualitative point of view this can be seen in the Figure 2.6C.

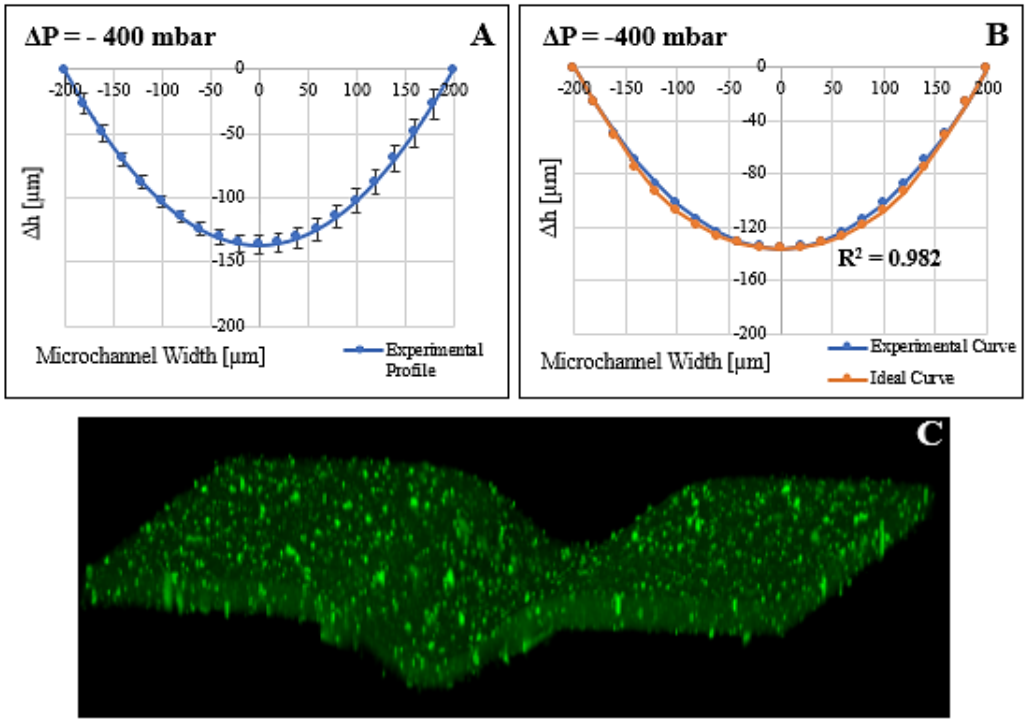

Figure 2.6: Microfluidic platform experiment for a pressure of -400mbar. A: Reconstruction of the experimental PDMS profile through the quantification of the corresponding coordinates. B: Overlapping of experimental and ideal profile. C: 3D representative confocal image. Each experiment has been repeated three different times and the data are expressed as mean ± standard deviation.

2.3.2.5 Test on microfluidic platform: ΔP = -500 mbar

Also, the response of the microfluidic platform to a pressure of -500 mbar was tested. In this case, a change of the height at the center of the membrane equal to 172.54 µm (Figure 2.7A) was obtained. As the previous cases, a comparison between the experimental curve and the ideal one was made (Figure 2.7B). As a result, a $R^2 = 0.965$ establishes a good agreement between them. So, the radius of curvature R_C is equal to 174.81 µm ≈ 175 µm and the curvature itself is 0.0057 μm^{-1}. The Figure 2.7C shows the 3D structure of the PDMS membrane with entrapped nanoparticles subjected to a pressure of -500 mbar.

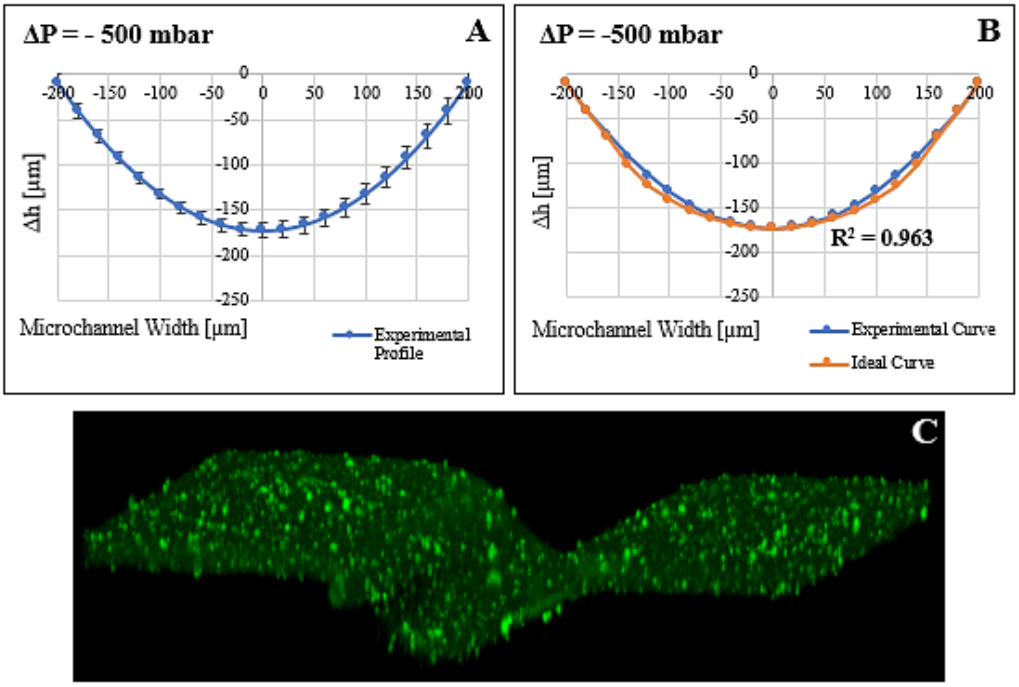

Figure 2.7: Microfluidic platform experiment for a pressure of -500mbar. A: Reconstruction of the experimental PDMS profile through the quantification of the corresponding coordinates. B: Overlapping of experimental and ideal profile. C: 3D representative confocal image. Each experiment has been repeated three different times and the data are expressed as mean ± standard deviation.

2.3.2.6 Test on microfluidic platform: ΔP = -600 mbar

Finally, the last experiment made consists into the application on the microfluidic platform of a pressure of -600 mbar. Here the height variation is equal to 194.21 µm (Figure 2.8A) and overlapping the ideal profile with the experimental curve, also for this configuration the arc of circumference is a good approximation (R^2 = 0.960). So, the radius of curvature is equal to 151.07 µm ≈ 151 µm and the corresponding curvature 0.0066 μm^{-1}. Then a 3D shape of the curved PDMS membrane was shown in Figure 2.8C.

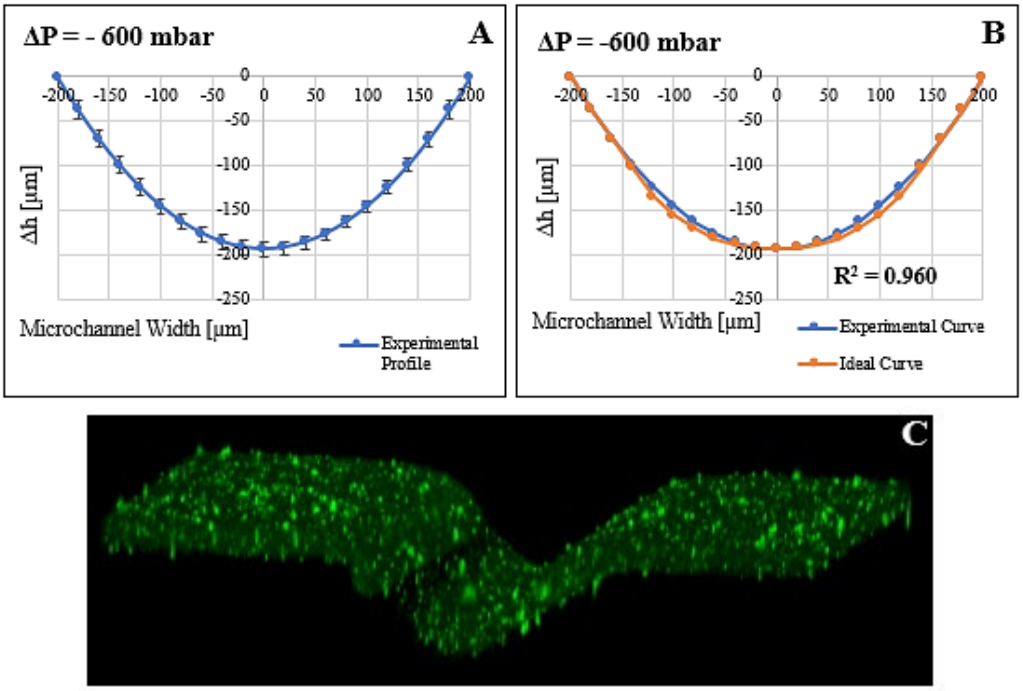

Figure 2.8: Microfluidic platform experiment for a pressure of -600mbar. A: Reconstruction of the experimental PDMS profile through the quantification of the corresponding coordinates. B: Overlapping of experimental and ideal profile. C: 3D representative confocal image. Each experiment has been repeated three different times and the data are expressed as mean ± standard deviation.

Knowing the microfluidic platform response to the different pressures, an overall evaluation of the height variation at the center of the membrane, the radius of curvature and the curvature itself with respect to ΔP was performed. Starting from Δh (Figure 2.9A), a linear correlation between this parameter and the pressure was observed. The same result was not obtained for the radius of curvature (Figure 2.9B) and, consequently, the curvature (Figure 2.9C). In fact, the correlation between R_C and ΔP can be expressed with a polynomial of the third order. Moreover, a fourth order polynomial equation needs to express the relationship between κ and ΔP.

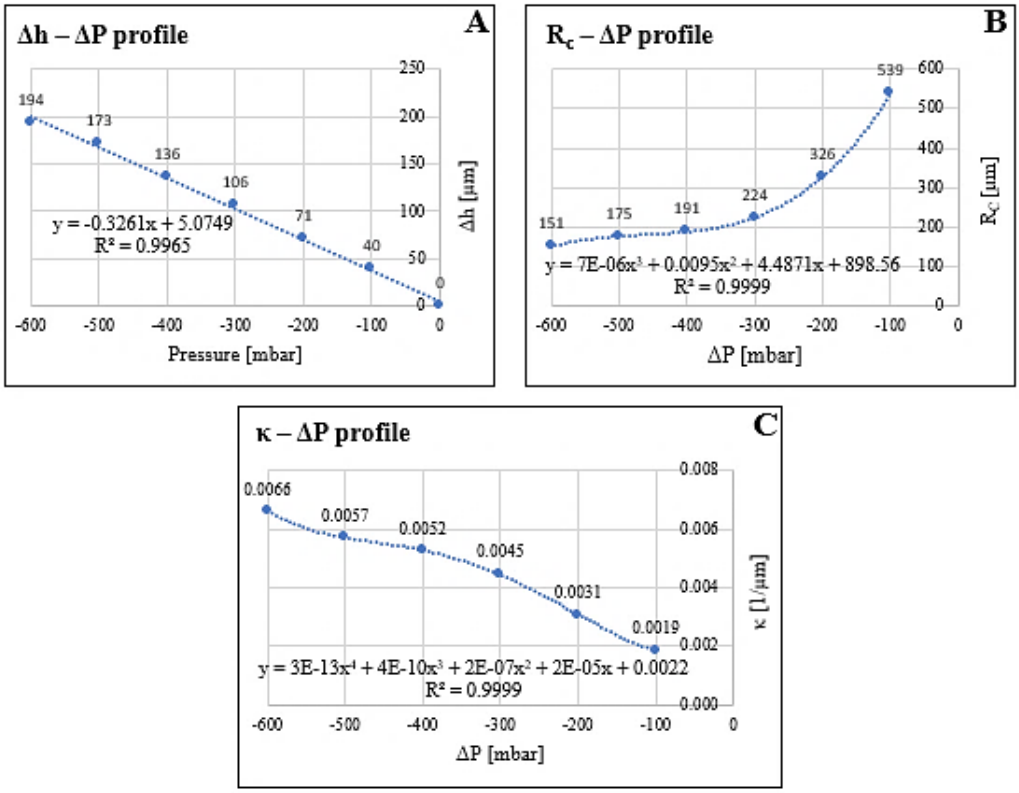

Figure 2.9: Evaluation of different experimental parameters with respect to pressure applied on the microfluidic platform. A:Height variation at the center of the membrane with respect to the pressure. B: Radius of curvature changes with respect to the pressure. C: Curvature profile with respect to the pressure.

2.3.3 FEM models development and validations

A specific 3D finite element model has been formulated to simulate the experimental PDMS substrate response on the microfluidic channel to the different pressure variations. As a result, the von Mises stress distribution on the upper part of the PDMS layer, that is the part in contact with cells, has been analyzed.

In the section 2.2.4 a detailed description of hypothesis and formulation of this model has been performed. So, starting from the pressure of -100 mbar, the von Mises stress distribution was studied (Figure 2.10A, S2A-B), observing a heterogeneous von Mises stress profile along the width of the microchannel. In fact, the stress value starts from 32 kPa up to 122 kPa. Particularly, the microchannel width of 400 μm has been divided into different parts: from 0 μm to 100 μm and from 300 μm to 400 μm are classified as side parts, whereas from 100 μm to 300 μm corresponds to the central one. This organization needs to discriminate the parts of PDMS membrane influenced by the side effects from the others where there are not these outcomes. The side effects are due to irreversible bonding between the PDMS and PMMA layers; in fact, only the part of PDMS substrate above the microchannel is free to deform during the pressure modifications. Due to this constraint, the von Mises stress distribution on the side parts has a minimum value of 32 kPa up to a maximum parameter of 122 kPa; conversely on the central part the von Mises outcomes belonging to the same order of magnitude [41.5 kPa – 58 kPa] (Figure 2.10A). To validate the 3D FEM model, a comparison between the experimental profile and the simulative one has been performed. It consists of overlapping the experimental profile of the PDMS membrane reconstructed by the z-stack acquisitions with the simulative one (Figure 2.10B). A quantification of how well observed outcomes are replicated by the model was provided by R^2 value. Particularly, for a pressure of -100 mbar, it is equal to 0.928, this means that the model is able to approximate in a good way the experimental results.

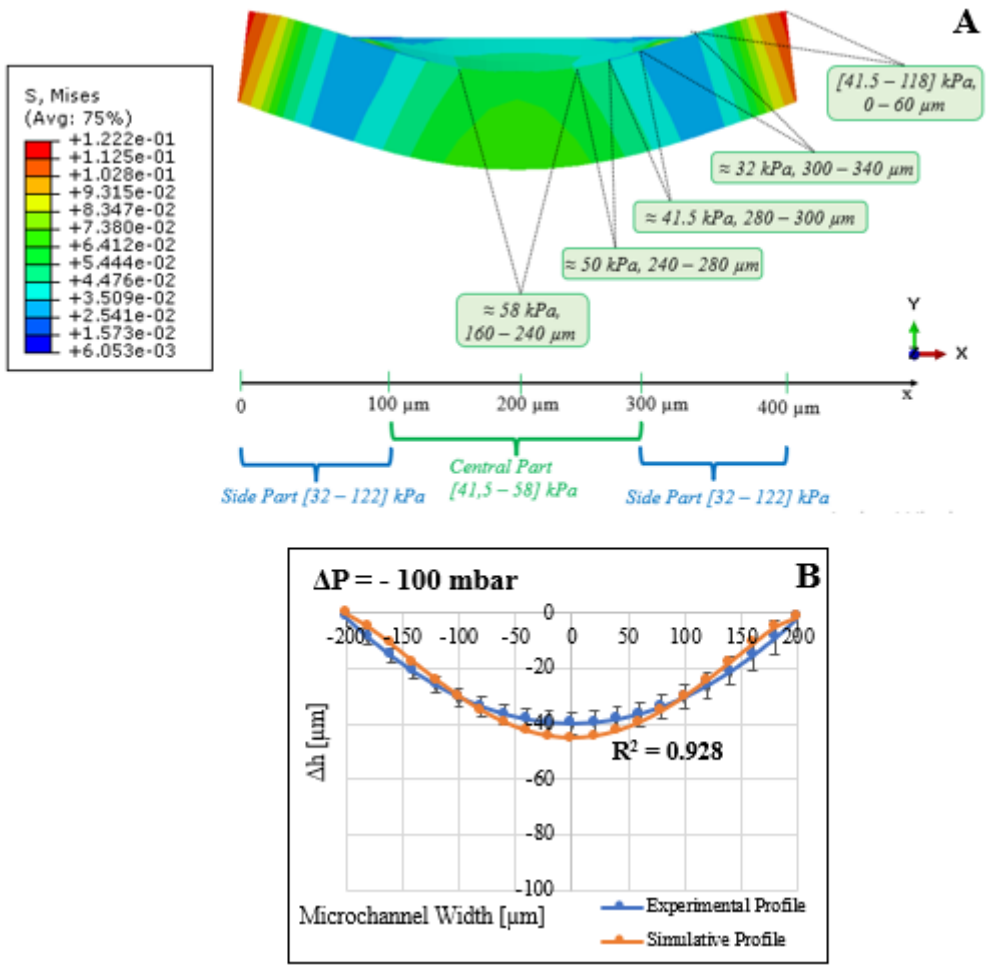

Figure 2.10: 3D finite element model formulation for pressure of -100mbar. A: von Mises stress distribution on the PDMS substrate along the microchannel width developed with a pressure of -100mbar (von Mises stress expressed in MPa on the colour map). B: 3D FEM model validation overlapping experimental profile with the simulative one.

With the same approach previously introduced, the 3D FEM model was developed for a pressure variation of -200 mbar. As shown in Figure 2.11A (Figure S2C-D), a heterogeneous von Mises stress distribution on the upper part of PDMS substrate along the microchannel width was obtained. Particularly, the side parts include [0 µm – 100 µm] and [300 µm – 400 µm] whereas the central part from 100 µm to 300 µm. On the formers, the von Mises stresses have a minimum of 40 kPa and a maximum of 229 kPa; on the latter the von Mises stress moves in the range [49.3 kPa – 68 kPa]. Overlapping the experimental reconstructed profile with the simulative one (Figure 2.11B), a good correspondence was observed. Indeed, the R^2 value is equal to 0.976.

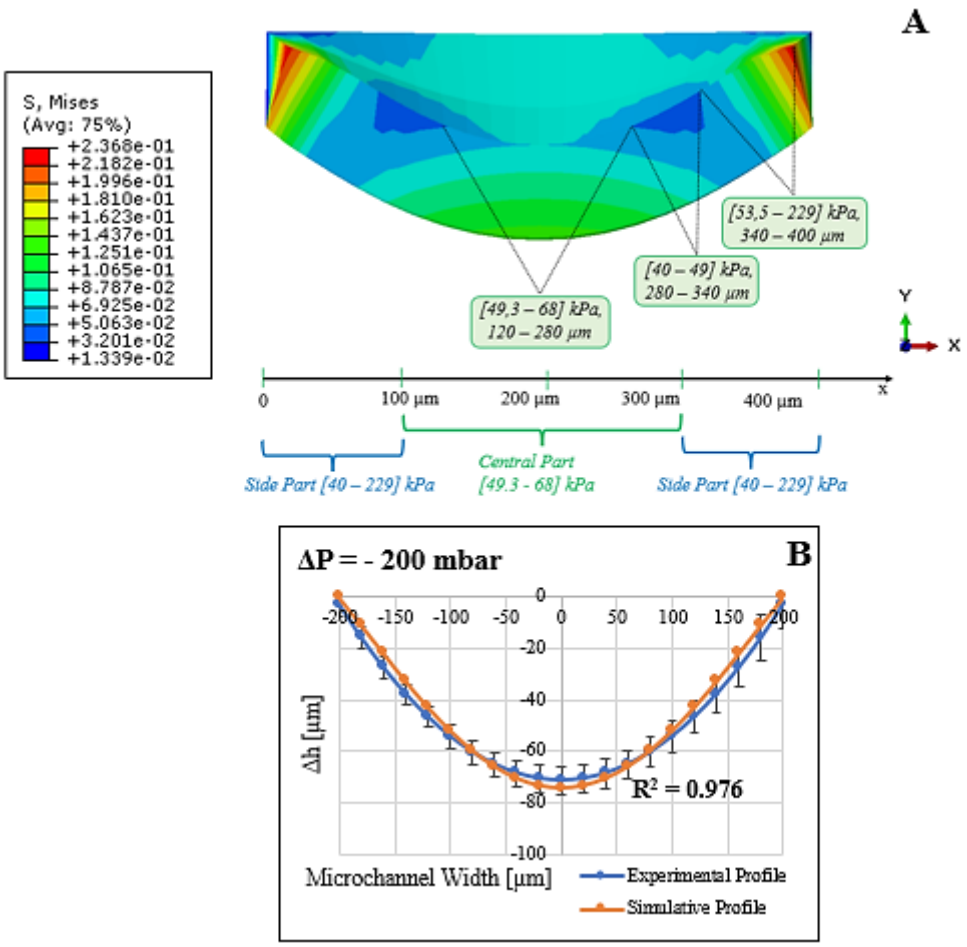

Figure 2.11: 3D finite element model formulation for pressure of -200mbar. A: von Mises stress distribution on the PDMS substrate along the microchannel width developed with a pressure of -200mbar (von Mises stress expressed in MPa on the colour map). B: 3D FEM model validation overlapping experimental profile with the simulative one.

Then, the third 3D FEM model developed was for the pressure of -300 mbar. Analysing the von Mises stress distribution (Figure 2.12A, S2E-F), it is possible to see a constant value approximately of 43 kPa in the central part of the microchannel [100 µm - 300 µm] and a heterogeneous stress distribution on the lateral ones [0 µm – 100 µm] [300 µm – 400 µm]. So, increasing the pressure applied on the membrane, a localization of the side effects on the edges and a constant von Mises stress distribution in the central part was recorded. Obviously, the stress distribution considered is related to the upper part of the PDMS membrane since, here, will be seeded the cells. In order to state that this simulated stress distribution is actually the experimentally obtained one, it is necessary to validate

the model. Comparing the experimental profile with the simulative curve (Figure 2.12B), the R^2 parameter results equal to 0.993, so a good correspondence between them.

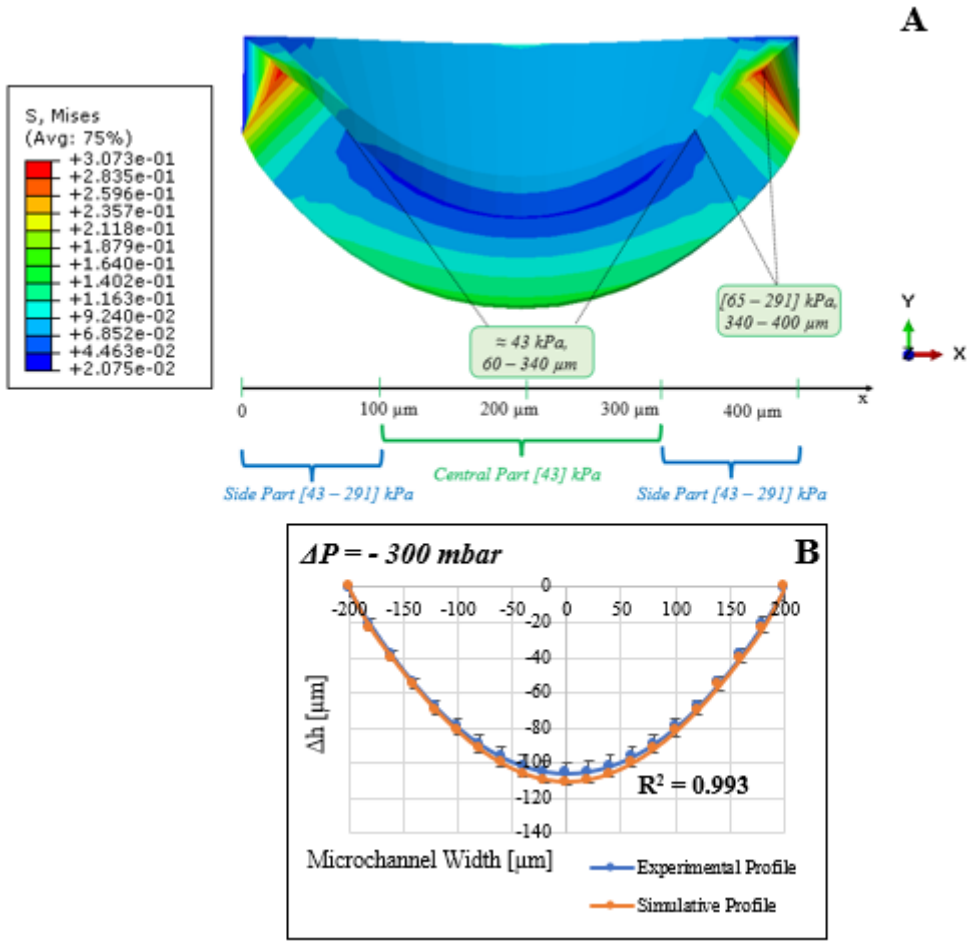

Figure 2.12: 3D finite element model formulation for pressure of -300mbar. A: von Mises stress distribution on the PDMS substrate along the microchannel width developed with a pressure of -300mbar (von Mises stress expressed in MPa on the colour map). B: 3D FEM model validation overlapping experimental profile with the simulative one.

Increasing the pressure imply an increment of von Mises stress developed on the PDMS membrane. In fact, analysing the stress distribution for ΔP = -400 mbar, a raise of stresses on the central and lateral parts with respect to the previous cases was observed (Figure 2.13A, S2G-H). A constant stress distribution of approx. 53 kPa characterizes the central part [100 µm – 300 µm], whereas the lateral regions have a heterogeneous von Mises profile [61 kPa – 362 kPa]. The comparison between experimental profile and simulative

one needs to validate the 3D FEM model (Figure 2.13B) and it shows a R^2 parameter close to 1 ($R^2 = 0.998$).

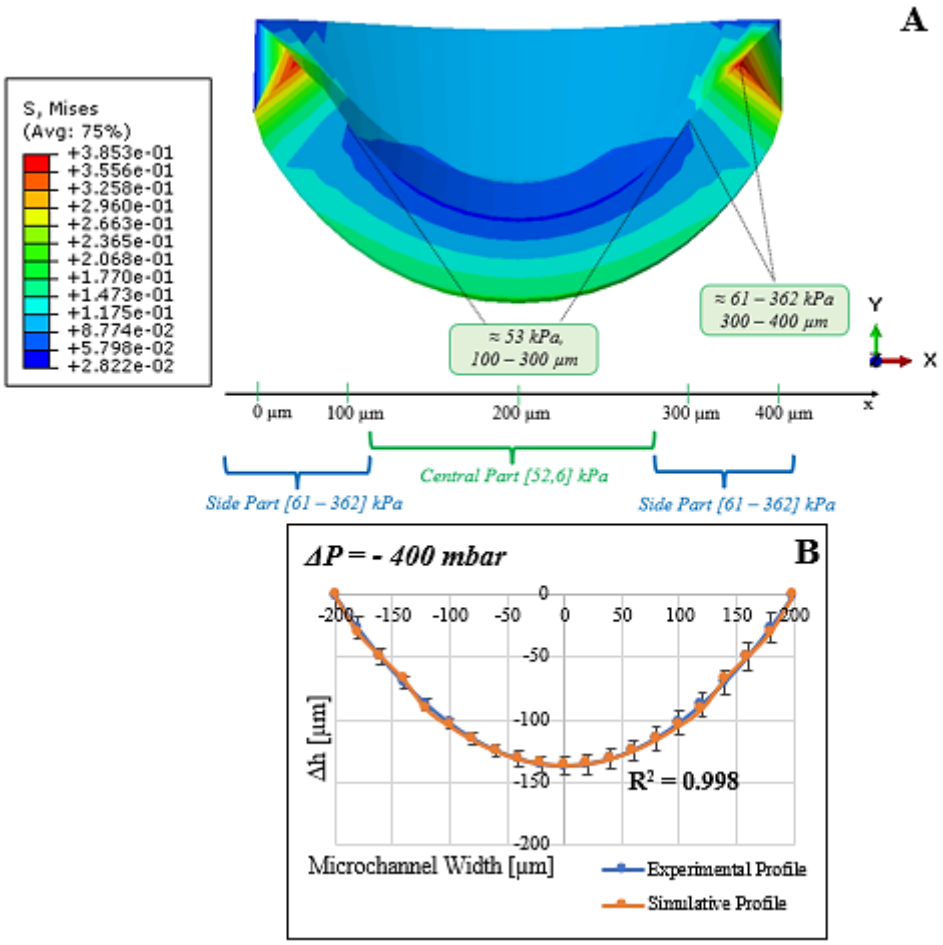

Figure 2.13: 3D finite element model formulation for pressure of -400mbar. A: von Mises stress distribution on the PDMS substrate along the microchannel width developed with a pressure of -400mbar (von Mises stress expressed in MPa on the colour map). B: 3D FEM model validation overlapping experimental profile with the simulative one.

Applying a pressure of -500 mbar on the 3D FEM model, a constant von Mises stress of ≈ 86 kPa on the central part of the PDMS layer and a heterogeneous stress [109 kPa – 415 kPa] on the side regions (Figure 2.14A, S2I-L) were obtained. Moreover, a good correspondence was observed comparing the experimental profile with the simulative one (Figure 2.14B).

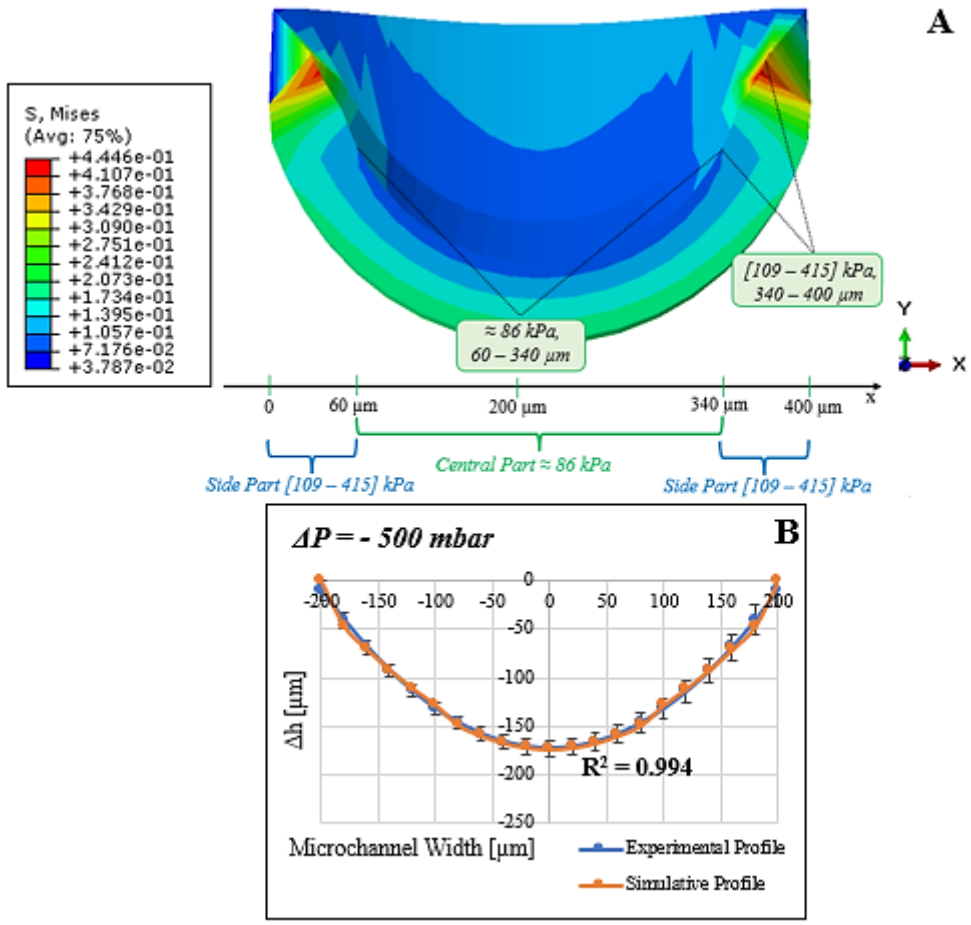

Figure 2.14: 3D finite element model formulation for pressure of -500mbar. A: von Mises stress distribution on the PDMS substrate along the microchannel width developed with a pressure of -500mbar (von Mises stress expressed in MPa on the colour map). B: 3D FEM model validation overlapping experimental profile with the simulative one.

Finally, the 3D FEM model for a pressure of -600 mbar was formulated. In agreement with the previous results, a constant von Mises stress distribution was observed in the central part (≈ 118 kPa) and a heterogeneous profile on the lateral regions [125 kPa – 485 kPa] (Figure 2.15A, S2M-N). Then, a perfect match between the simulative curve and the experimental one was performed with a $R^2 = 0.999$ (Figure 2.15B).

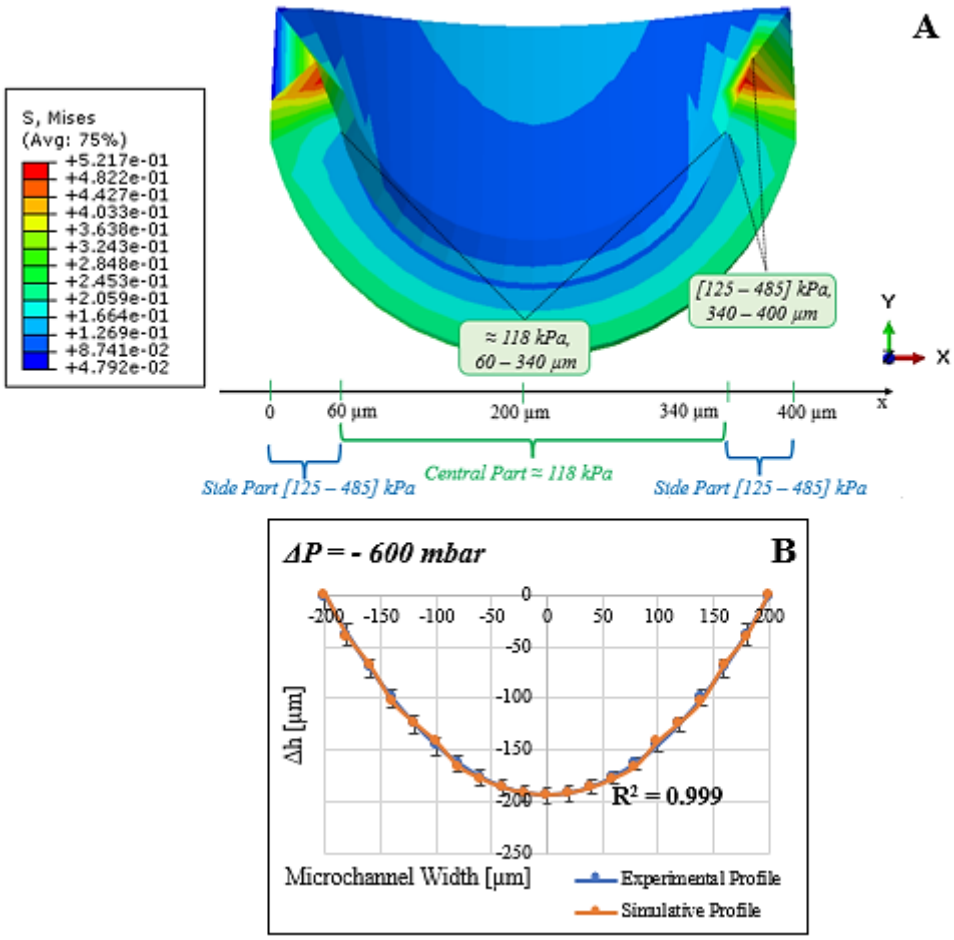

Figure 2.15: 3D finite element model formulation for pressure of -600mbar. A: von Mises stress distribution on the PDMS substrate along the microchannel width developed with a pressure of -600mbar (von Mises stress expressed in MPa on the colour map). B: 3D FEM model validation overlapping experimental profile with the simulative one.

Moreover, the 3D FEM models are able to reproduce the experimental thickness variations induced by the pressure applied. Both into experimental and simulative cases the PDMS membrane thickness was quantified in the central part of the structure itself, that is in the more solicited region. Starting from a PDMS membrane of approximatively 70 µm into undeformed configuration, after the application of a specific pressure, no statistically significant differences were highlighted between the experimental value and the simulative one (Figure 2.16). Obviously, the greater the pressure applied, the larger the reduction in thickness will be.

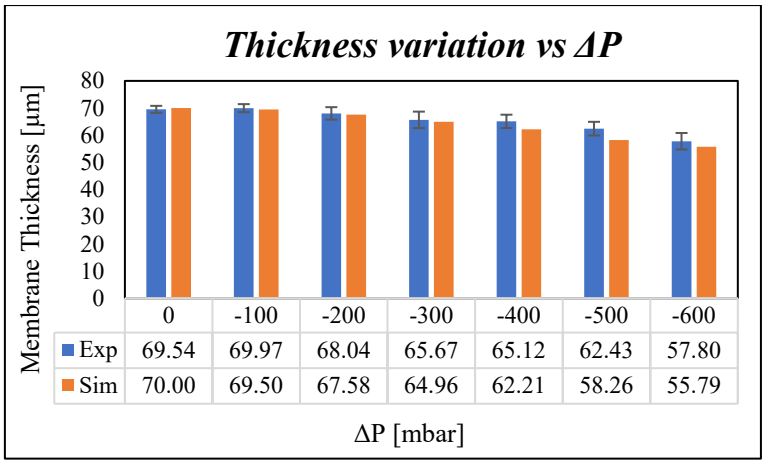

Figure 2.16: Thickness variation vs ΔP. Thickness variations of PDMS substrate in the microf00luidic platform induced by experimental pressures compared with the 3D FEM simulated ones.

2.4 Discussion and Conclusions

The microfluidic platform has been properly designed in order to ensure an accurate control of mechanical stimulation at the single-cell level. Moreover, an optical accessibility for on-line analysis and a high temporal resolution of static or cyclic mechanical stimulation have been guaranteed. Since the PDMS membrane has dimensions larger than the underneath microchannel (Figure 2.1), an internal non-stretched control in the microfluidic platform was obtained.

The microfluidic technology was chosen to perform an accurate control of pressure-driven mechanical deformation of the PDMS membrane where cells are seeded. This control of the mechanical load in terms of amplitude, temporal profile and frequency is possible connecting the microfluidic platform to a pressure controller (OB1). Modifying the pressure inside the microfluidic platform means an induction of mechanical deformation of the PDMS substrate and, consequently, a solicitation on the cultured cells. Due to the lack of information about the response of single adipose derived mesenchymal stem cells to the curvature variations in time and space, particularly for the modifications from flat to concave configurations, a reduction of the pressure inside the microfluidic channel was applied.

Before analysing the cellular response to these mechanical stresses, it was necessary not only to design the microfluidic device but also to test its correct operation. As detailed described in the sections 2.2 and 2.3 of this chapter, a multi-layer microfluidic platform

has been designed choosing PMMA and PDMS as materials. This choice is related to the need to design a microfluidic platform accessible to confocal microscopes not only using low magnification objectives but also high magnification ones. Thus, the total thickness of the platform becomes a design constraint. In order to be sure that the pressure deform only the PDMS substrate without other layer modifications considering the thickness constraint, materials with different mechanical properties have been used. In fact, the PMMA has a Young Modulus of 4088 MPa with respect to ≈ 600 kPa of 19:1 PDMS. The correct operation of the microfluidic device was tested by performing specific experiments at different pressures. The PDMS membrane response was acquired using confocal microscopy inasmuch the PDMS layer was correctly embedded with fluorescent nanoparticles.

A PDMS membrane curvature quantification was made comparing the experimental profile with the ideal one. Since the correspondence for all cases is high ($R^2 \geq 0.9$), each experimental profile can be expressed as an arc of circumference having a specific radius of curvature and consequently, a specific curvature itself. To quantify the stresses and strains field developed in the different experimental cases, a 3D FEM model of the PDMS membrane was developed and validated overlapping the experimental profile with the simulative one. Also, in this case a good agreement for all configurations ($R^2 \geq 0.9$) was recorded.

The microfluidic channel width was designed of 400µm since *Zhou et al.* [18] observe as threshold width a value of 200µm as minimum value to the alignment of confluent cells along the microchannel length moving from a flat to a convex configuration in a dynamic manner. Moreover, they observe a perfect alignment in the same solicitation conditions when the width of the microchannel was equal to 500µm [18]. Although in their project the modification of the curvature is different and, also, the type and density of cells changes, an intermediate parameter among those reported in literature has been chosen.

Even the sizing of the culture chamber was designed in such a way to create in future an array of microchannels and thus obtaining a high throughput microfluidic platform. In fact, as reported in literature [14, 18, 19] modifying the width of parallel microchannels, there is the possibility to generate different mechanical stresses and strains by applying a single pressure variation.

The strategy of designing a multilayer microfluidic device using two different materials is also innovative for another aspect. If instead of an anisotropic stress along a preferential direction of the microchannel, someone wanted to apply an isotropic mechanical load, for example, creating circular wells, it would be sufficient to re-design only PMMA layer 2 of the device rather than the whole platform.

In conclusion, a microfluidic multi-layer platform able to study the single-cell response to static or dynamic mechanical stimulations has been fabricated. With an ad hoc design, the chip is easily accessible to confocal microscopy and using the OB1 instrument a lot of different mechanical configurations can be studied. As we will see in the next chapters, this platform has proved to be an excellent tool for investigating cell signalling pathways induced by different mechanical cues.

References

[1] Ingber, Donald. “Mechanobiology and diseases of mechanotransduction.” *Annals of medicine* 35.8 (2003): 564-577.

[2] Stoppel, Whitney L., David L. Kaplan, and Lauren D. Black III. “Electrical and mechanical stimulation of cardiac cells and tissue constructs.” *Advanced drug delivery reviews* 96 (2016): 135-155.

[3] Riehl, Brandon D., et al. “Mechanical stretching for tissue engineering: two-dimensional and three-dimensional constructs.” *Tissue Engineering Part B: Reviews* 18.4 (2012): 288-300.

[4] Sears, Candice, and Roland Kaunas. “The many ways adherent cells respond to applied stretch.” *Journal of biomechanics* 49.8 (2016): 1347-1354.

[5] Kamble, Harshad, et al. “Cell stretching devices as research tools: engineering and biological considerations.” *Lab on a Chip* 16.17 (2016): 3193-3203.

[6] Ahmed, Wylie W., et al. “Myoblast morphology and organization on biochemically micro-patterned hydrogel coatings under cyclic mechanical strain.” *Biomaterials* 31.2 (2010): 250-258.

[7] Shao, Yue, et al. “Uniaxial cell stretching device for live-cell imaging of mechanosensitive cellular functions.” *Review of Scientific Instruments* 84.11 (2013): 114304.

[8] Ursekar, Chaitanya Prashant, et al. “Design and construction of an equibiaxial cell stretching system that is improved for biochemical analysis.” *PloS one* 9.3 (2014): e90665.

[9] Maul, Timothy M., et al. “Mechanical stimuli differentially control stem cell behavior: morphology, proliferation, and differentiation.” *Biomechanics and 61istema61g in mechanobiology* 10.6 (2011): 939-953.

[10] Whitesides, George M. “The origins and the future of microfluidics.” *Nature* 442.7101 (2006): 368-373.

[11] Sackmann, Eric K., Anna L. Fulton, and David J. Beebe. “The present and future role of microfluidics in biomedical research.” *Nature* 507.7491 (2014): 181-189.

[12] C. Moraes et al. “Microfabricated arrays for high-throughput screening of cellular response to cyclic substrate deformation”, Lab on a chip, 10, 227-234, 2010

[13] C. Moraes et al. “Microdevice array-based identification of distinct mechanobiological response profiles in layer-specific valve interstitial cells”, Integrative Biology, 2013

[14] F. Michielin et al. “Microfluidic-assisted cyclic mechanical stimulation affects cellular membrane integrity in a human muscular dystrophy in vitro model” RCS Advances, Royal Society of Chemistry, 5, 98429-98439, 2015

[15] C.H. Chiu et al. “Self-renewal and differentiation of adipose-derived stem cells (ADCSs) stimulated by multi-axial tensile strain in a pneumatic microdevice”, Micromachines, 9, 607, 2018

[16] N. Campillo et al. “A novel chip for cyclic stretch and intermittent hypoxia cell exposures mimicking obstructive sleep apnea”, Frontiers in physiology, Vol.7, 2016

[17] He, Yingning, et al. “A simplified yet enhanced and versatile microfluidic platform for cyclic cell stretching on an elastic polymer.” *Biofabrication* 12.4 (2020): 045032.

[18] Zhou, Jing, and Laura E. Niklason. “Microfluidic artificial “vessels” for dynamic mechanical stimulation of mesenchymal stem cells.” *Integrative Biology* 4.12 (2012): 1487-1497.

[19] Kamble, Harshad, et al. “Pneumatically actuated cell-stretching array platform for engineering cell patterns in vitro.” *Lab on a Chip* 18.5 (2018): 765-774.

[20] D. Baptista et al. “Overlooked? Underestimated? Effects of substrate curvature on cell behaviour”, Cell Press Reviews, August 2019, Vol.37, No. 8

[21] A. Frost et al., “The BAR domain superfamily: membrane molding macromolecules”, Cell, 137, 191-196, 2009

[22] Z. X. Chong et al. “Transfection types, methods and strategies: a technical review” PeerJ, 2021

[23] A. R. Norouzi et al. “PDMS-PMMA bonding improvement using SiO2 intermediate layer and its application in fabricating gas micro valves”, Microsystem Technologies, 24, 2018

[24] A. Bamshad et al. “ A new simple and fast thermally-solvent assisted method to bond PMMA-PMMA in micro-fluidics devices” J. Micromech. Microeng. 26, 2016

Chapter 3

Adipose stem cell behaviour to static mechanical cues: cytoskeleton and focal adhesions response

3.1 Introduction

Cells are capable of perceiving external stimuli, such as chemical, topographical, and mechanical signals present within the ECM, which act as important regulators of cell and tissue functions [1]. It has now been widely demonstrated that the propagation of these signals is mediated by the cell cytoskeleton, a structure which connects the cell membrane to the nucleus, capable of altering the epigenetic state of the cell and then, its gene expression profile. This is the foundation of mechanobiology which aims at combining the regulatory activity of biophysical signals on cellular functions (migration, differentiation, proliferation, etc.) with the state of tension of the cytoskeleton through the mutual interaction between the cytoskeletal forces and the deformations of the nucleus [2]. Consequently, using the knowledge of mechanobiology, it becomes in principle possible to finely control the functions and architectures of cells and tissues with physical and biochemical factors. To do this, it is essential to understand the mechanisms through which external signals influence biological and pathophysiological functions at different hierarchical levels, in order to be able to use them in an integrated way.

Mesenchymal stem cells (MSCs) present a great potential for therapy due to their ease of isolation, ability to proliferate in vitro, potential to differentiate in several cell types and to repair vital tissues [3]. MSCs reside in virtually all post-natal organs and tissues, and they can be isolated by three different sources: bone marrow, umbilical cord, and adipose tissue. The stem cells derived from human adipose tissue (ASCs) are similar to bone marrow derived MSCs in morphology and phenotype but show important differences in regard to harvest and cell yield. In fact, adipose tissue collection is less traumatic for patients than bone marrow harvest, and the frequency of stem cells is higher in that tissue,

indicating that ASCs represent an attractive and abundant cell type for regenerative medicine [4-6]. In fact, the adipose tissue can be easily obtained from the waste material generated by abdominoplasty or liposuction operations.

Therefore, the aim of this project is to understand the mechanisms through which the cell is able to perceive external signals (a process known as mechanosensing), and to translate them into biochemical activities which define the cellular functions (a process known as mechanotransduction). In particular, the attention is focused on the response of stem cells to the static or dynamic administration of biophysical signals. Understanding these complex processes can play a very important role in the design and engineering of a new generation of materials whose properties, could be finely controlled in space and time. In fact, they can constitute instructions capable of controlling the degree of structuring of the cytoskeleton and the extent of the forces exerted on the nucleus, allowing the direct transfer of information/instructions from the external material to the nucleus, regulating its shape and consequently controlling the state of compaction of the chromatin. Manipulating chromatin remodelling through the exposure of cells to material signals (biophysical and biochemical), means to control the mechanisms of epigenetic regulation and to guide in a highly specific way the processes of differentiation of stem cells, the biosynthetic events, and the processes of self-organization of cells in supracellular/tissue complexes.

To finely control these processes, a microfluidic platform has been designed (chapter 2) in order to apply in a static or in a dynamic way a specific mechanical cue. These signals are applied modifying in time and space the curvature of the cell-seeded membrane using a pressure control system. The combination of experimental approach with the simulative one (3D FEM models – Chapter 2) gives the possibility to exactly know the stress/strain fields developed on the cell-seeded material and so, applied on cell themselves. The role of these mechanical signals on ASCs behaviour has been studied analysing the cellular response in terms of cytoskeleton organization and focal adhesions (FAs) assembly. Particularly, the polarization with respect to the microfluidic channel of both actin stress fibers and FAs have been studied. Since there are not information about the cell response in both static and dynamic configurations into this microfluidic device, the investigation

started with an analysis of the effects of static mechanical curvature variations on stem cell behaviour. The role of dynamic stimuli was investigated in Chapter 4.

3.2 Materials and Methods

3.2.1 Isolation and culture of adipose-derived mesenchymal stem cells by human adipose tissue

Adipose tissue samples were obtained by six patients undergoing abdominoplasty or liposuction. The study has been approved by the Bioethical Committee of the University of Molise (protocol number: 19364) and all the patients were appropriately advised and signed the informed consent form. The mean age of the patients was 38 years (24-50 years). In order to reduce the variability in the biological properties of ASCs, related to numerous donor-dependent factors, and to increase the quality and reproducibility of the experimental data, the stem cells extracted from the tissues of at least 3 patients will be grouped (cell pooling) and used for experiments between passages 1 and 4.

The isolation procedure [4] consists basically in different steps: washing of the adipose tissue, enzymatic digestion, and centrifugation. Starting from the washing procedure, a solution of phosphate buffer saline (PBS) (D8537 – Merck) with 1% of pen-strep (P4333 – Merck) was used to extensively wash the tissue in order to remove as much blood as possible. Each wash lasts 10-15 minutes and their total number depends on the type of tissue and the amount of blood (generally 7-8 washes are needed).

The enzymatic digestion was carried out using collagenase A 0.1% w/v (Clostridium histolyticum, Roche, 11088793001) for 2 h at 37 °C, under gentle agitation. This process is useful to break down the native collagen that holds animal tissues together in order to isolate the different cellular populations forming the tissue itself. The last step of isolation procedure was consisted of a series of centrifugations in order to remove the collagenase type A and the stromal vascular fraction (SVF) from the cell population. The result of enzymatic digestion has been centrifuged at 3000 rpm for 10 min in order to divide the supernatant from the pellet. After the discharging of the supernatant, complete culture medium for ASCs was added to the pellet and a second centrifuge at 3000 rpm for 10 min was made.

Particularly, the adipose derive stem cells culture medium is composed by: Minimum Essential Medium Eagle (Alpha modification) (AL081 – Microtech S.R.L.), 10% of fetal bovine serum (F7524 – Merck), 1% of L-Glutamine (G7513 – Merck) and 1% of Pen-Strep (P4333 – Merck).

At the end of the second centrifuge, the supernatant was removed, and the complete culture medium of ASCs was added in order to suspend the pellet. Then, all the solution containing medium, and cells was put into a flask. Despite all the washings and centrifuges done, a small amount of red blood cells and stromal vascular fraction will be found in suspension in the flasks. Then, 24 hours after the ASCs extraction, three washes with PBS containing Pen Strep 1% and a culture medium change were carried out, in order to remove all the components in suspension. In this way only the ASCs remain adhered to the flask.

For all patients, the cells were kept in culture for 7 days, the time sufficient to reach a confluency of 80-85%, and subsequently, they were frozen and suitably stored or used.

3.2.2 Adipose derived mesenchymal stem cell differentiation

To verify the potential of differentiation of extracted ASCs, osteogenic and adipogenic differentiation was induced on confluent ASC cells at passage 1 in specific media, particularly, they were cultivated for 2 weeks with medium change every 3 days.

For osteogenic differentiation, the cell culture medium was composed by hMSC osteogenesis induction medium (Cat.-Nr.: 200 0903 – provitro) supplemented with 10% Fetal Bovine Serum (F7524 – Merck), 2% HEPES (221 1000 – FCS-kit, provitro), 1% L-Glutamine (222 1001 – FCS-kit, provitro), 1% Dexamethasone (238 0903 – FCS-kit, provitro), 1% Ascorbic-Acid-2-phosphate (238 0908 – FCS-kit, provitro), 1% β-Glycerol-phosphate (238 0909 – FCS-kit, provitro) and 1% Pen-Strep (P4333 – Merck).

To analyse the osteogenic differentiation of ASCs after two culturing weeks, the calcium depositions were observed using the Alizarin Red Stain Solution (Osteogenesis assay kit, Catalog. No. ECM815, Sigma-Aldrich). Briefly, the protocol consists of a careful aspiration of cell medium, washing with PBS, fixing with 4% paraformaldehyde at room temperature for 15 minutes, rinsing three times (5-10 minutes each) with distilled water and adding Alizarin Red Stain Solution at room temperature for at least 20 minutes. After

the incubation with stain solution, the excess dye was removed and four washes with deionized water (5 minutes each) have been done. It is important to wash gently as possible to avoid disturbing the calcium monolayer. At the end of this protocol, the calcium deposits appear bright red and different images have been captured using a microscope equipped with a colour camera (BX53 – OLYMPUS).

For adipogenic differentiation, the ASCs were cultured using a specific culture medium: hMSC adipogenesins induction medium (Cat.-Nr.: 200 0904 – provitro) supplemented with 10% Fetal Bovine Serum (F7524 – Merck), 2% HEPES (221 1000 – FCS-kit, provitro), 1% L-Glutamine (222 1001 – FCS-kit, provitro), 1% Dexamethasone (225 0904 – FCS-kit, provitro), 1% Indomethacine (229 0904 – FCS-kit, provitro), 1% 3-Isobutyl-1-methyl-xanthine (230 0904 – FCS-kit, provitro), 1% Insulin (246 0904 – FCS-kit, provitro) and 1% Pen-Strep (P4333 – Merck).

The adipocytes were visualized using the Lipid (Oil Red O) staining kit (Catalog. No. MAK194 – Sigma Aldrich) which consists of different steps. Starting from the medium removal and the gently wash of cells with PBS (repeated 2 times), then a fixing with 4% paraformaldehyde of 15 minutes at room temperature was performed. At the end of paraformaldehyde incubation, the samples were incubated for 5 minutes with 60% isopropanol solution. Finally, the Oil Red O staining solution was used to visualize the lipid droplets entrapped into adipocytes. The incubation lasts 5 minutes and then from 2 to 5 washes with water were carried out to remove the stain in excess. As for the calcium deposits of osteogenic cells, also the lipid droplets of adipocytes were visualized with the fluorescence microscope equipped with a colour camera (BX53 – OLYMPUS).

3.2.3. Electroporation of ASCs

The adipose-derived mesenchymal stem cell electroporation was performed using the Neon Transfection system (MPK5000 – ThermoFisher Scientific); particularly a co-transfection of the actin cytoskeleton and paxillin, a FA-associated protein, was made using the plasmids pCMV–LifeAct®–TagGFP2 (cat. 60101, ibidi) and pmKate2-paxillin vector (cat. FP323 – evrogen), respectively. The ASCs were trypsinized for 5 minutes and centrifuged at 1100 rpm for 5 minutes. After removal of the supernatant, PBS was added to ASCs for a second centrifuge (300 g for 5 min) necessary to remove all residues

of culture medium from cells. Since the total volume of the electroporator tip is 10 µL, a solution of this volume containing cells, buffer R, and plasmids was made. Particularly, this solution includes 300000 cells, 2 µg of pmKate2-paxillin vector, and 0.5 µg of p^{CMV}–LifeAct®–TagGFP2. The electroporator tip is immersed into an electroporator tube containing 3 mL of Buffer E and the instrument was set with a pulse voltage of 1200 V, a pulse width of 20 ms, and a pulse number equal to 2. After the electroporation step, the cells were put into a 6-well with 2 mL of complete ASCs culture medium without Pen-Strep. All buffers (E and R), tips and electroporation tubes belong to a specific kit provided by ThermoFisher Scientific (Catalog Number: MPK1096 – ThermoFisher Scientific).

3.2.4 Microfluidic platform sterilization and functionalization

In order to use the microfluidic platform as a tool to apply mechanical cues on cells, it needs to be sterilized and functionalized it in a specific way. Since the chip is completely closed, the sterilization and functionalization processes were made passing fluids through NanoPorts. Starting from the sterilization step, it consists of a wash with a 70% ethanol solution (5 minutes) followed by three washes with water (the operation is repeated three different times). Then a wash with a solution composed by PBS + Pen-Strep (2:1 v/v) followed by three washes with PBS was performed (the operation is repeated three times and the PBS + Pen-Strep solution stays into the microfluidic platform 6 minutes). At the end of the washing process, 1h of UV sterilization needed.

To make the PDMS membrane adhesive for ASCs, an incubation of 1 h with 50 µg/mL fibronectin solution (F0895-2MG – Sigma-Aldrich) at 37 °C was performed.

To reuse the microfluidic platform, it needs to remove not only the adhered ASCs but also the fibronectin functionalization from the PDMS membrane. To do that a solution containing 1% of sodium hypochlorite in deionized water for 5 minutes at room temperature was put into the cell culture chamber of the device. In this way a cleaning of the chamber without damaging the membrane itself can be carried out.

3.2.5 Cell culture and cell seeding on microfluidic platform

One week before the electroporation process, the ASCs at passage 1 were thawed and cultured into Minimum Essential Medium Eagle (Alpha modification) (AL081 – Microtech S.R.L.) supplemented with 10% of fetal bovine serum (F7524 – Merck), 1% of L-Glutamine (G7513 – Merck) and 1% of Pen-Strep (P4333 – Merck) at 37 °C in a humidified atmosphere of 95% air and 5% CO_2. One week in culture is enough time for cells to recover and reach approximately 80%-85% of confluency. 48h after the electroporation step (3.2.3 Section), the ASCs were detached with trypsin (Catalog. N° 25200056 Gibco, Thermo Fisher Scientific) and seeded at passages 3-4 on the fibronectin functionalized microfluidic platform at a density of 5000 cells/cm^2. The low seeding density was chosen to be able to study the response of single cells to mechanical stresses avoiding that it could be influenced by cell-cell interaction. The mechanical load of the cells was induced 24 h after seeding in order to be sure that all the cells were correctly adhered to the PDMS membrane. To visualize not only the actin stress fibers and focal adhesions, but also the cell nuclei, a staining with Hoechst dye (1:10000 for 15 min at 37 °C; Hoechst 33342, Catalog. N° H3570, Invitrogen) was performed 24 h after the cell seeding on the microfluidic platform.

3.2.6 Static mechanical stimulation of ASCs

The mechanical stimulation of adipose-derived mesenchymal stem cells was induced modifying in a static manner the curvature of cells-adhered membrane into microfluidic platform. The curvature variation was applied changing the pressure inside the underneath microfluidic channel using the pressure controller OB1. Different mechanical insults were studied starting from a pressure variation of -100 mbar up to -600 mbar; particularly the intermediate cases were -200 mbar, -300 mbar, -400 mbar and -500 mbar. Each pressure was applied with a linear ramp profile of -100 mbar/min and the cell response was analyzed into undeformed configuration and 24 h after the application and maintenance of the mechanical load. In this way, the cells have enough time to sense and respond to the curvature variations reaching their equilibrium configuration.

3.2.7 Confocal z-stacks acquisitions

As previously introduced (Chapter 2), the microfluidic platform is easily accessible to the confocal microscopes with both low and high magnification objectives thanks to its transparency and thickness. So, real-time acquisitions of single ASCs on the microfluidic device can be performed. To do that, it is fundamental to reproduce on the confocal microscope used (Confocal Zeiss Axio Observer.Z1) the same conditions of temperature, CO_2, and humidity of a cell culture incubator. This environment has been created equipping the microscope with a top stage incubator linked to temperature, CO_2 and humidity controllers produced by Okolab S.r.l. Moreover, the microfluidic platform has an unconventional shape and dimension with respect to the commercial microscope incubators, so a customized top stage incubator and sample holder were designed by Okolob S.r.l. As shown in figure 3.1, the customized top stage incubator has a custom riser needs to obtain a sufficient height able to prevent the tube restriction. Furthermore, the custom sample holder is designed in order to support not only the microfluidic device but also a 60 mm petri dish; particularly the latter can contain the cell culture medium opportunely oxygenated that is inflexed into the microfluidic platform using a peristaltic/syringe pump during long experiments. For 24h experiments, the medium change was not needed.

Figure 3.1: Photos of the customized top stage incubator mounted on the confocal microscope (figure on left side) with a zoom on the sample holder with the microfluidic platform (figure on the right side).

The response of single transfected ASCs was acquired for each static mechanical configuration before the stimulation (known as undeformed configuration) and 24 h after the application and maintenance of the stimulation itself (known as deformed

configuration). Due to the curvature variations, z-axis changes were obtained, so z-stack acquisitions need to be done. To quickly capture single ASCs to study the cytoskeleton response in both undeformed and deformed configurations, actin stress fibers were acquired using a 10x dry objective. Conversely, to study the focal adhesions response to the mechanical cues a 40x long distance water immersion objective was used. Particularly, samples were excited at 380 nm (nuclei), 488nm (actin stress fibers) and 555 (paxillin) and the emissions were collected in the 400-420 nm, 500-530 nm, and 560-600 nm ranges, respectively.

3.2.8 Confocal image analysis

The software Fiji was used to quantitatively analyse the actin cytoskeleton architecture and focal adhesions organization before and after the mechanical load. Starting from the actin cytoskeleton, to study the influence of static mechanical signals on the cytoskeleton structure, the orientation of the actin stress fibers with respect to the microchannel direction was quantified using the Fiji plug-in "Directionality". Since the plug-in setting is 0° in the East direction and the orientation is counterclockwise, the microchannel direction corresponds to the 90° angle. To have 0° as the angle indicating the microchannel direction, all the stress fibers orientation angles quantified by Directionality plug-in have been rotated of 90°. Knowing the actin stress fibers orientation in both undeformed and deformed configurations, specific histograms have been plotted into Excel in order to study the polarization changes of single ASCs induced by mechanical cues.

To have information about cell morphology, particularly cell area, into different cases, the Fiji plug-in "Measure" was employed. This analysis needs to evaluate the effects of mechanical curvature variations about cell spreading. Finally, from the 3D FEM models (Chapter 2 – 2.3.3 Section), it is known that the cells are subjected to a heterogeneous stress/strain field. So, to understand the role of not only substrate curvature but also mechanical field on cells, the microfluidic channel was divided into two different parts: side parts [0 μm – 100 μm] [300 μm – 400 μm] and central part [100 μm – 300 μm]. As a consequence, the exact position of single ASCs on the microfluidic channel has to be defined in order to divide them in the different groups. To do that the z-stacks of actin

stress fibers and nuclei were merged with the transmission z-stack of the microfluidic channel, then a z-projection was performed and manually the coordinates in x-y plane were quantified with the drawing tools of the Fiji software.

The focal adhesions morphology and polarization with respect to the microchannel direction were analyzed using the Fiji plug-in "Analyze Particles". In the 40x z-stacks were captured FAs paxillin, actin cytoskeleton, nucleus and microchannel in transmission. As a consequence, in the image post-processing the cell boundaries have been selected and used on the duplicated FAs stack to consider only the region of interest. Then, after a projection of the z-stack, the threshold tool was used to remove all the images background and Analyze Particle to select the focal adhesions of interest. Particularly, a range between 0.99 μm^2 and 9.99 μm^2 for FAs area was considered in order to only take into account single focal adhesions. As a result, single focal adhesion area and orientation were quantified and represented on box and whisker plots and histograms, respectively.

3.2.9 Statistical analysis

Each experiment has been performed on three different microfluidic platforms acquiring for the study of cytoskeleton polarization at least 80 cells/device, whereas for the FAs analysis at least 6 cells/device. All data are reported as mean ± standard deviation. Statistical comparisons were performed with ANOVA followed by Tukey's test for multiple comparison and P values of < 0.01 or < 0.05 denote statistically significant differences.

3.3 Results

3.3.1 Adipogenic and osteogenic differentiation

To verify the effectiveness of ASCs extraction process, specific experiments to evaluate the differentiation potential of these cells were carried out. As detailed explained into 3.2.2 section, the osteogenic and adipogenic differentiation have been induced.

Starting from the osteogenic differentiation, the calcium deposition was observed in differentiated cells after 2 weeks of culture with a specific differentiated culture medium. Particularly, in Figure 3.2A, these deposits appear bright red on confluent cells.

An adipogenic differentiation was obtained culturing the ASCs two weeks into a specific adipogenic differentiation medium. As a result (Figure 3.2B) the lipid droplets of adipocytes appear bright red on confluent ASCs.

So, these experiments were carried out for each ASCs extraction process, in order to verify that the procedure was actually successful.

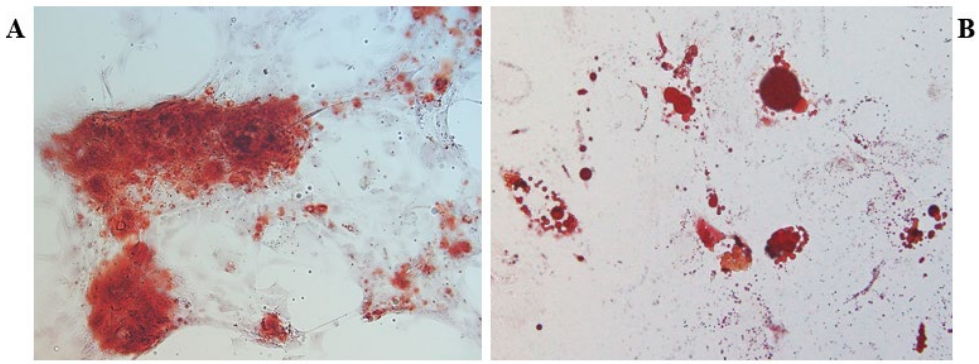

Figure 3.2: ASCs differentiation. A: Osteogenic differentiation of ASCs after 2 weeks in culture with osteogenic differentiation medium, calcium deposits in red. B: Adipogenic differentiation of ASCs after 2 weeks in culture with adipogenic differentiation medium, lipid droplets in red.

3.3.2 Actin cytoskeleton reorganization induced by static changes of cell-seeded membrane curvature

The actin stress fibers due to their attachment to the focal adhesions and nuclear membrane are highly involved in the mechanosensing and mechanotransduction pathways. In fact, the mechanical signals propagate from the extracellular matrix to the nucleus through the actin stress fibers, microtubules, and intermediate filaments. The attention has been focused on the actin stress fibers since the mechanical cues are able to

continuously assemble and disassemble them in different area of the cells with respect to other cytoskeleton filaments.

So, studying the polarization of the actin stress fibers induced by a specific mechanical insult could give information about the cellular mechanosensing and mechanotransduction pathways induced by the signal itself. The mechanical load has been applied modifying in a static way the curvature of the cell-seeded PDMS membrane into the microfluidic platform. Since different curvature changes have been considered, the results are detailed explained for each case in the sections below.

3.3.2.1 Actin stress fibers response to R_c = 539 µm

The first mechanical insult applied on single ASCs-seeded membrane of the microfluidic platform was able to generate on the PDMS substrate a radius of curvature equal to 539 µm which corresponds to a curvature of 0.0019 μm^{-1}. This specific mechanical cue was applied modifying the pressure inside the underneath microfluidic channel generating a pressure of -100 mbar. The actin stress fibers response was analyzed on three different microfluidic platforms acquiring at least 80 cells/device into undeformed configuration (flat PDMS membrane) and 24 h after the application and maintenance of the curvature change. Working with transfected ASCs, an on-line cell response can be observed. The actin stress fibers orientation of single adipose stem cells with respect to the microfluidic channel direction was evaluated in the two configurations in order to quantify the role played by this specific mechanical cue on the cytoskeleton re-organization.

Starting from undeformed configuration (Figure 3.3A), the cells are randomly polarized with respect to the microchannel direction. Particularly, the microchannel direction corresponds to the angle 0° and only the cells in the range [-20°; 20°] are considered aligned with the microfluidic channel itself. After 24 h from the application and maintenance of the curvature variation, on the whole microfluidic channel the cells continue to be randomly organized (Figure 3.3B). This means that the curvature variation is not enough to induce a sensitive variation of the cell polarization. The modification of the PDMS curvature along a microfluidic channel creates an anisotropic mechanical field due to not only to the specific shape of the channel but also to the side effects generated by the irreversible bonding between PDMS and PMMA layers. Analysing the 3D FEM

model results, a heterogeneous stress (Figure 3.3C, S2A-B) and strain (Figure 3.3D, S3A-B) field was observed along the radius of curvature. Starting from the stress field, in the central part of the microfluidic channel [100 – 300] μm the von Mises stress has a minimum of ≈ 41.5 kPa and a maximum of ≈ 58 kPa, resulting approximatively homogeneous. Conversely, on the side part [0 – 100] μm – [300 – 400] μm the von Mises stress distribution moves from ≈ 32 kPa to ≈ 122 kPa, showing an increase of almost one order of magnitude. The same occurs for the strain distribution, showing a value in the ranges [2.6 – 3.4] % and [2.6 – 12] % in the central and side parts, respectively. As a consequence, to deeply analyse the actin cytoskeleton organization variations induced by the curvature change without the influence of side effects, the stem cells have been divided into two different groups taking into account their position on the microfluidic channel: cells on central part and cells on side parts.

Starting from the cells on the lateral region, a random actin stress fibers organization was observed in both undeformed (Figure 3.3E) and deformed (Figure 3.3F) configurations generating a heterogeneous cellular polarization. The same occurs on the central part for undeformed (Figure 3.3G) and deformed (Figure 3.3H) cases.

Finally, the application of a radius of curvature of 539 μm on low-density ASCs resulted to be not sufficient to induce variations of actin cytoskeleton organization and cellular polarization in 24 h. Since 24 h is a sufficient time to observe a possible cellular response to mechanical signals, the absence of this leads us to believe that the specific signal does not induce any consequences on cellular mechanical identity.

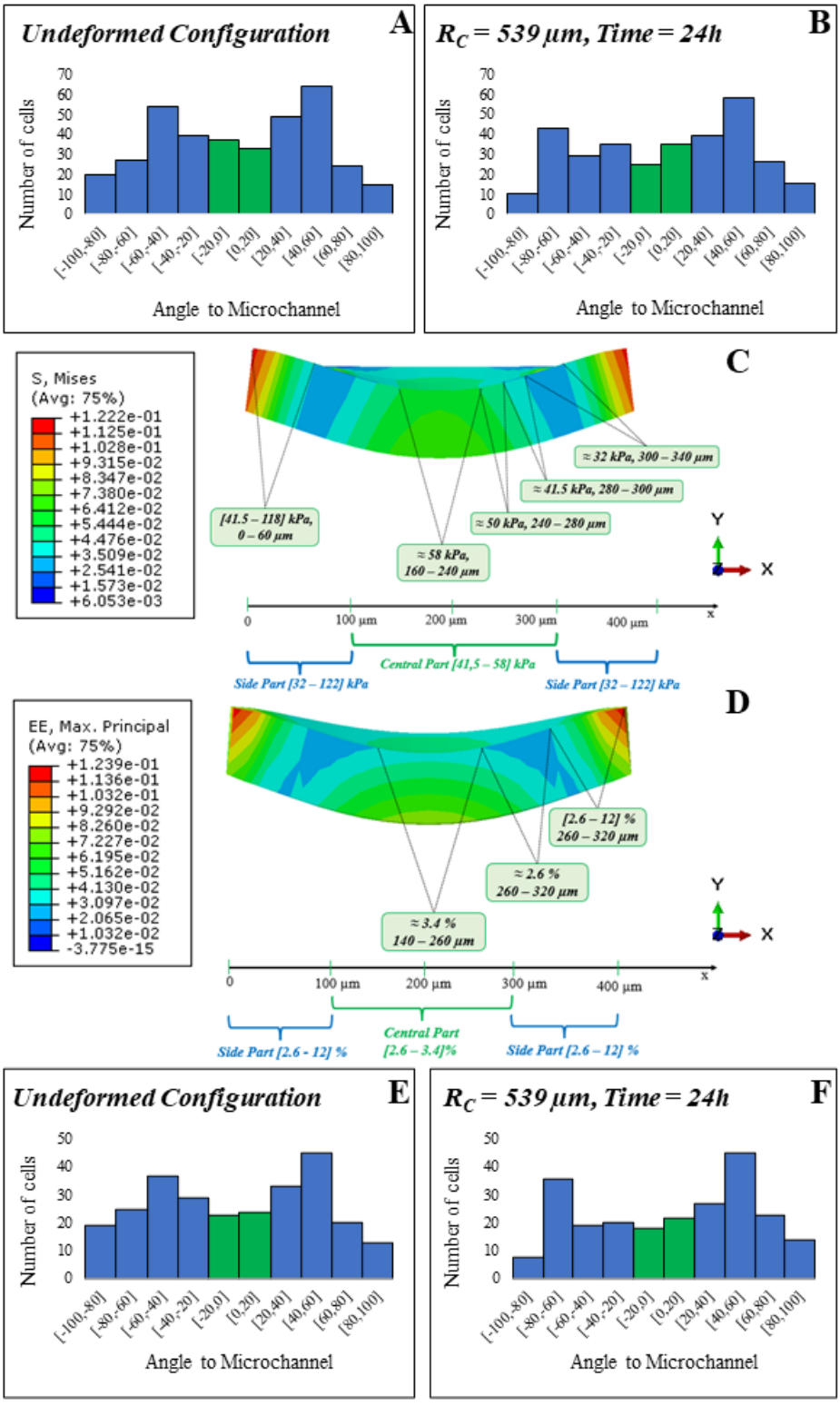
A
Undeformed Configuration
Number of cells
70
60
50
40
30
20
10
0
[-100,-80]
[-80,-60]
[-60,-40]
[-40,-20]
[-20,0]
[0,20]
[20,40]
[40,60]
[60,80]
[80,100]
Angle to Microchannel
B
R_C = 539 µm, Time = 24h
Number of cells
Angle to Microchannel
C
S, Mises
(Avg: 75%)
+1.222e-01
+1.125e-01
+1.028e-01
+9.315e-02
+8.347e-02
+7.380e-02
+6.412e-02
+5.444e-02
+4.476e-02
+3.509e-02
+2.541e-02
+1.573e-02
+6.053e-03
≈ 32 kPa, 300 – 340 µm
≈ 41.5 kPa, 280 – 300 µm
[41.5 – 118] kPa,
0 – 60 µm
≈ 50 kPa, 240 – 280 µm
≈ 58 kPa,
160 – 240 µm
Y
X
0
100 µm
200 µm
300 µm
400 µm
x
Central Part [41,5 – 58] kPa
Side Part [32 – 122] kPa
Side Part [32 – 122] kPa
D
EE, Max. Principal
(Avg: 75%)
+1.239e-01
+1.136e-01
+1.032e-01
+9.292e-02
+8.260e-02
+7.227e-02
+6.195e-02
+5.162e-02
+4.130e-02
+3.097e-02
+2.065e-02
+1.032e-02
-3.775e-15
[2.6 – 12] %
260 – 320 µm
≈ 2.6 %
260 – 320 µm
≈ 3.4 %
140 – 260 µm
Y
X
0
100 µm
200 µm
300 µm
400 µm
x
Central Part
[2.6 – 3.4]%
Side Part [2.6 - 12] %
Side Part [2.6 – 12] %
E
Undeformed Configuration
Number of cells
Angle to Microchannel
F
R_C = 539 µm, Time = 24h
Number of cells
Angle to Microchannel

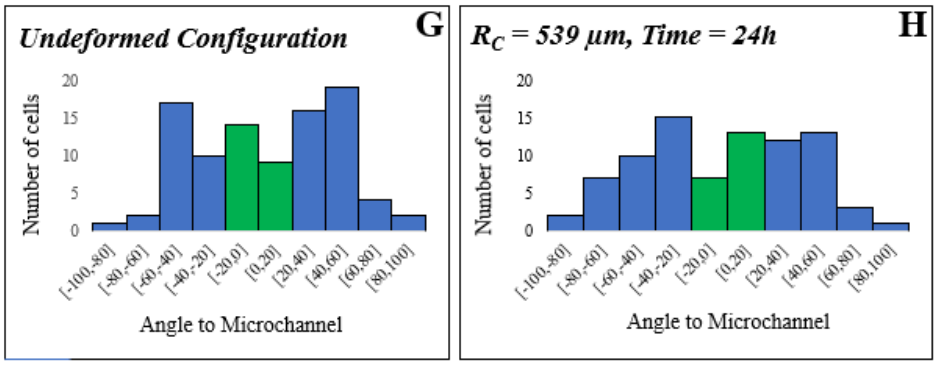

Figure 3.3: Adipose stem cells behaviour induced by a curvature variation of 0.0019 µm^{-1} on the microfluidic platform. A-B: Histograms showing ASCs polarization with respect to the microchannel direction (0°) into flat (A) and deformed (B) configurations. C: von Mises stress distribution on the curved cell-seeded PDMS membrane (colour map express the von Mises stress in MPa) D: elastic strain distribution on the curved cell-seeded PDMS membrane (colour map express the strain in a-dimensional way). E-F: Histograms showing ASCs polarization with respect to the microchannel direction (0°) into flat E and deformed (F) configurations on the lateral regions. G-H: Histograms showing ASCs polarization with respect to the microchannel direction (0°) into flat (G) and deformed (H) configurations on the central region.

3.3.2.2 Actin stress fibers response to R_c = 326 µm

Applying on the microfluidic platform a pressure of -200 mbar, a curvature variation on the cell-seeded membrane of 0.0031 µm^{-1}, corresponding to a R_C of 326 µm, was obtained. A randomly cellular polarization was observed in the undeformed configuration (Figure 3.4A) and the same occurs also into deformed one (Figure 3.4B). As previously introduced, the cellular polarization was quantified through the actin stress fibers direction with respect to the microfluidic channel orientation. This means that also this curvature variation along the microfluidic channel is not able to induce a cellular response. In this case, as in the previous one, the side effects are responsible for a heterogeneous stress (Figure 3.4C, S2C-D) and strain (Figure 3.4D, S3C-D) fields. In the central part, the von Mises stress has values from ≈ 49.3 kPa to ≈ 68 kPa while the strain varies from ≈ 3.4% to ≈ 4.6%. On the lateral part, the von Mises stress range corresponds to [40 – 229] kPa whereas the strain interval [3.4 – 22.4]%. Increasing the pressure on the microfluidic channel, a raise of curvature variation has occurred and, as a consequence, an increment of stress and strain fields.

Organizing the cells in the two different groups, starting from the ASCs on the microchannel side parts, a random organization was observed in both undeformed (Figure 3.4E) and 24 h deformed (Figure 3.4F) configurations. This means that the

curvature combined with the heterogeneous stress/strain distribution induced by side effects are not able to polarize cells along a specific direction. An analogous result was observed in the central part: adipose stem cells in undeformed (Figure 3.4G) and deformed (Figure 3.4H) configurations are randomly polarized. Since in the central part there is not the influence of the side effects and the stress/strain fields are approximatively uniform, the heterogeneous cellular organization, which means a random actin stress fibers direction, is due to a curvature variation too low to activate a consistent cellular response.

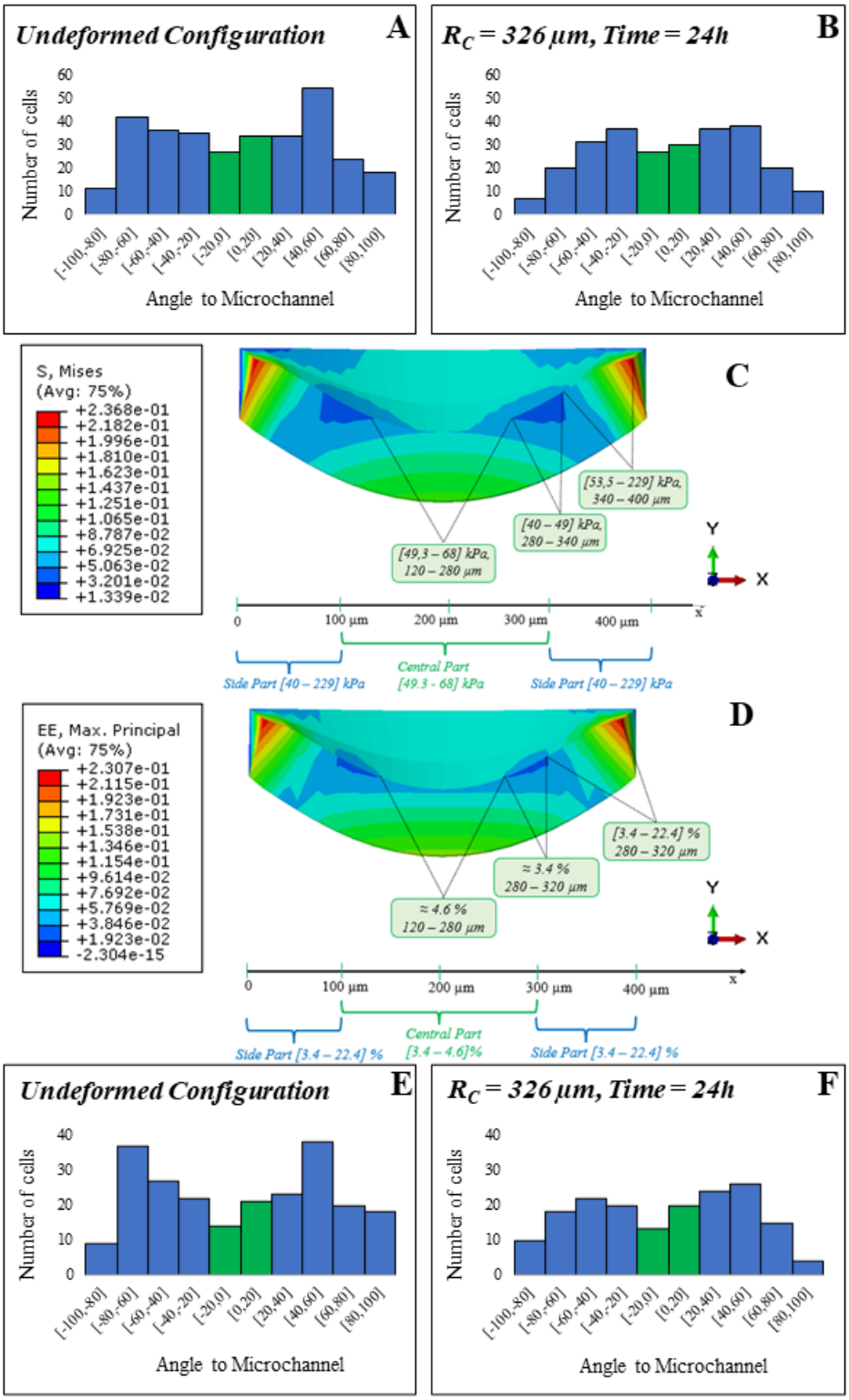
Undeformed Configuration
A
Number of cells
Angle to Microchannel
R_C = 326 µm, Time = 24h
B
S, Mises
(Avg: 75%)
+2.368e-01
+2.182e-01
+1.996e-01
+1.810e-01
+1.623e-01
+1.437e-01
+1.251e-01
+1.065e-01
+8.787e-02
+6.925e-02
+5.063e-02
+3.201e-02
+1.339e-02
C
[53,5 – 229] kPa,
340 – 400 µm
[40 – 49] kPa,
280 – 340 µm
[49,3 – 68] kPa,
120 – 280 µm
Y
X
0
100 µm
200 µm
300 µm
400 µm
x
Side Part [40 – 229] kPa
Central Part
[49.3 - 68] kPa
Side Part [40 – 229] kPa
EE, Max. Principal
(Avg: 75%)
+2.307e-01
+2.115e-01
+1.923e-01
+1.731e-01
+1.538e-01
+1.346e-01
+1.154e-01
+9.614e-02
+7.692e-02
+5.769e-02
+3.846e-02
+1.923e-02
-2.304e-15
D
[3.4 – 22.4] %
280 – 320 µm
≈ 3.4 %
280 – 320 µm
≈ 4.6 %
120 – 280 µm
Side Part [3.4 – 22.4] %
Central Part
[3.4 – 4.6]%
Side Part [3.4 – 22.4] %
Undeformed Configuration
E
R_C = 326 µm, Time = 24h
F

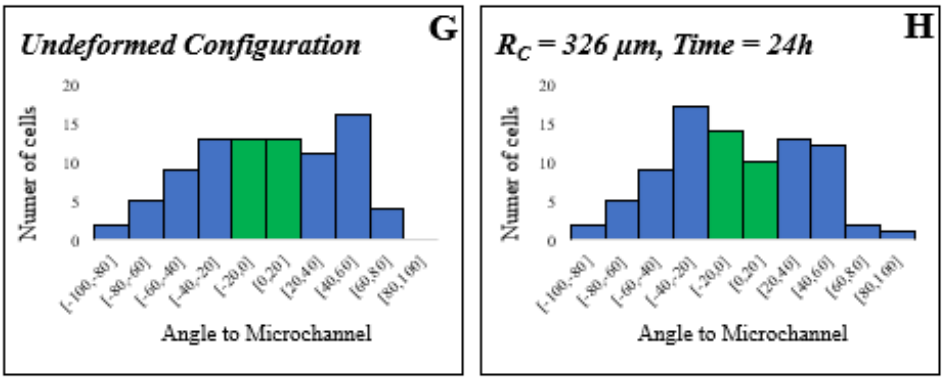

Figure 3.4: Adipose stem cells behaviour induced by a curvature variation of 0.0031 µm^{-1} on the microfluidic platform. A-B: Histograms showing ASCs polarization with respect to the microchannel direction (0°) into flat (A) and deformed (B) configurations. C: von Mises stress distribution on the curved cell-seeded PDMS membrane (colour map express the von Mises stress in MPa) D: elastic strain distribution on the curved cell-seeded PDMS membrane (colour map express the strain in a-dimensional way. E-F: Histograms showing ASCs polarization with respect to the microchannel direction (0°) into flat E and deformed (F) configurations on the lateral regions. G-H: Histograms showing ASCs polarization with respect to the microchannel direction (0°) into flat (G) and deformed (H) configurations on the central region.

3.3.2.3 Actin stress fibers response to R_c = 224 µm

A pressure of -300 mbar on the microfluidic platform was able to induce a radius of curvature of 224 µm corresponding to a curvature of 0.0045 µm^{-1}. Comparing the cellular polarization between undeformed (Figure 3.5A) and deformed (Figure 3.5B) configurations, a cellular response to the applied mechanical insult was observed. In fact, into undeformed configuration there is a random actin stress fibers orientation with respect to the microchannel direction; conversely, after 24 h from the membrane curvature change, a cytoskeleton re-organization has been obtained. The actin stress fibers response induces a cellular polarization along the preferential direction of the microfluidic channel (longitudinal axis). This means that the curvature modifications applied are enough to control the structure of ASC actin cytoskeleton.

In order to better understand this result, an analysis of 3D FEM stresses and strains created by the mechanical cue was done. Starting from the von Mises stress field (Figure 3.5C, S2E-F), a uniform stress distribution of ≈ 43 kPa in the central microchannel part was quantified. Then, in the lateral part, the side effects are more localized on the microchannel with a von Mises stress range of [65 – 291] kPa. The strain field (Figure 3.5D, S3E-F) developed on the different microchannel regions has the same profile of

the von Mises stress; that is uniform in the central part ≈ 5.5% and heterogeneous on the side ones [5.5 – 39]%.

Even if the side effects are more localized, we have always considered as central and lateral regions the same parts of the microchannel as previously defined.

From a detailed analysis of the ASCs polarization in the different microchannel parts a random cytoskeleton organization on the side regions in both undeformed (Figure 3.5E) and deformed (Figure 3.5F) configurations was observed. Conversely, in the central part, a heterogeneous cell polarization into flat case (Figure 3.5G) is followed by a defined cellular orientation into curved situation (Figure 3.5H). Particularly, the cells prefer to align along the longitudinal microchannel direction. This result means that the cell behaviour, particularly the actin stress fibers assembly, is controlled by the mechanical insult applied. So, the curvature value of 0.0045 μm^{-1} should be considered as a threshold parameter to observe an actin cytoskeleton re-organization of ASCs induced by PDMS membrane curvature variation.

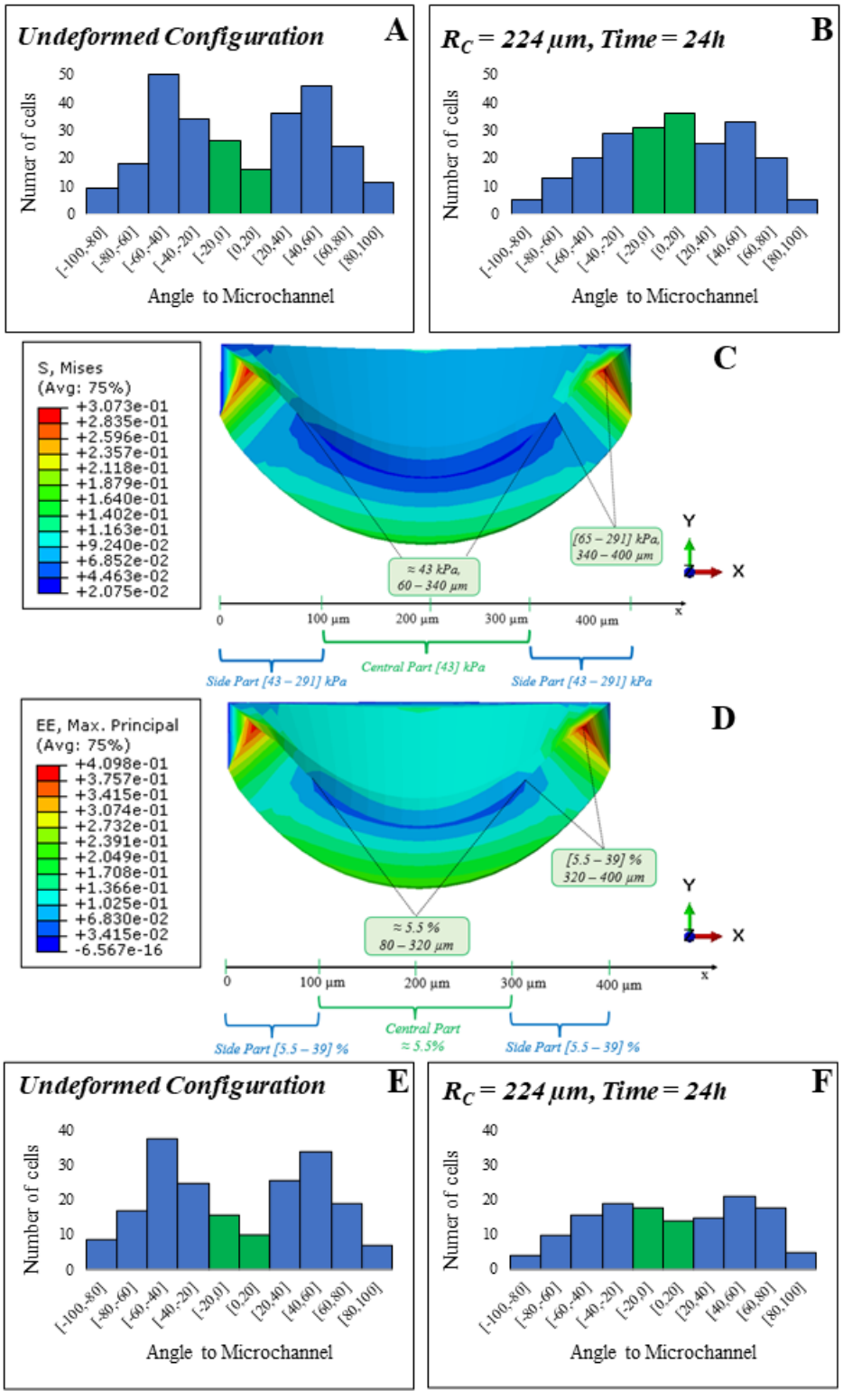
Undeformed Configuration
A
Numer of cells
Angle to Microchannel
R_C = 224 µm, Time = 24h
B
Number of cells
Angle to Microchannel
S, Mises
(Avg: 75%)
+3.073e-01
+2.835e-01
+2.596e-01
+2.357e-01
+2.118e-01
+1.879e-01
+1.640e-01
+1.402e-01
+1.163e-01
+9.240e-02
+6.852e-02
+4.463e-02
+2.075e-02
C
[65 – 291] kPa,
340 – 400 µm
≈ 43 kPa,
60 – 340 µm
Side Part [43 – 291] kPa
Central Part [43] kPa
Side Part [43 – 291] kPa
EE, Max. Principal
(Avg: 75%)
+4.098e-01
+3.757e-01
+3.415e-01
+3.074e-01
+2.732e-01
+2.391e-01
+2.049e-01
+1.708e-01
+1.366e-01
+1.025e-01
+6.830e-02
+3.415e-02
-6.567e-16
D
[5.5 – 39] %
320 – 400 µm
≈ 5.5 %
80 – 320 µm
Side Part [5.5 – 39] %
Central Part
≈ 5.5%
Side Part [5.5 – 39] %
Undeformed Configuration
E
Number of cells
Angle to Microchannel
R_C = 224 µm, Time = 24h
F
Numer of cells
Angle to Microchannel

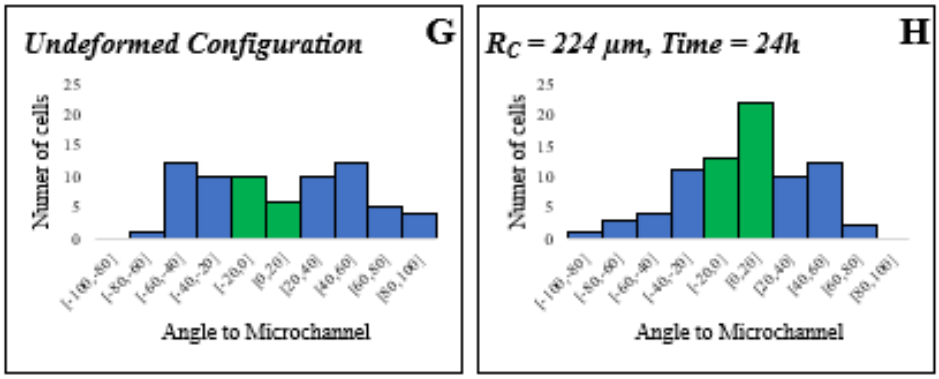

Figure 3.5: Adipose stem cells behaviour induced by a curvature variation of 0.0045 µm^{-1} on the microfluidic platform. A-B: Histograms showing ASCs polarization with respect to the microchannel direction (0°) into flat (A) and deformed (B) configurations. C: von Mises stress distribution on the curved cell-seeded PDMS membrane (colour map express the von Mises stress in MPa) D: elastic strain distribution on the curved cell-seeded PDMS membrane (colour map express the strain in a-dimensional way. E-F: Histograms showing ASCs polarization with respect to the microchannel direction (0°) into flat E and deformed (F) configurations on the lateral regions. G-H: Histograms showing ASCs polarization with respect to the microchannel direction (0°) into flat (G) and deformed (H) configurations on the central region.

3.3.2.4 Actin stress fibers response to R_c = 191 µm

A radius of curvature of 191 µm, corresponding to a curvature of 0.0052 µm^{-1}, was obtained applying a pressure of -400 mbar. This macroscopic topographic variation of PDMS substrate profile induces a response of the actin stress fibers. In fact, comparing the undeformed (Figure 3.6A) and 24h deformed (Figure 3.6B) results, an actin stress fibers re-organization shows a substantial cellular polarization along the longitudinal direction of the microchannel. Also, in this situation a uniform von Mises stress distribution (Figure 3.6C, S2G-H) was observed in the central region of the membrane ≈ 53 kPa, with respect to a heterogeneous one on the side parts [61 – 362] kPa. Similarly, constant strain field was quantified in the central part of the membrane 6.1% and a heterogeneous one on the side regions [6.1 – 46.7] % (Figure 3.6D, S3G-H).

In agreement with the previous results, the cells on the side part of the channel have actin cytoskeleton filaments randomly organized in both undeformed (Figure 3.6E) and deformed (Figure 3.6F) configurations. So, this cytoskeleton organization is not able to define a preferential polarization of cells along a specific direction.

Conversely, in the central part of the PDMS membrane, a cellular polarization along the microchannel length was obtained after 24 h of mechanical stimulation. In fact, the

randomly oriented cells in the undeformed configuration (Figure 3.6G) result polarized along the longitudinal microchannel direction after 24h (Figure 3.6H).

Moreover, one of the advantages to work with transfected cells is the possibility to analyse for each microfluidic device the same stem cells before and after the mechanical stimulation, this means that the actin stress fibers response is only due to the mechanical signals applied.

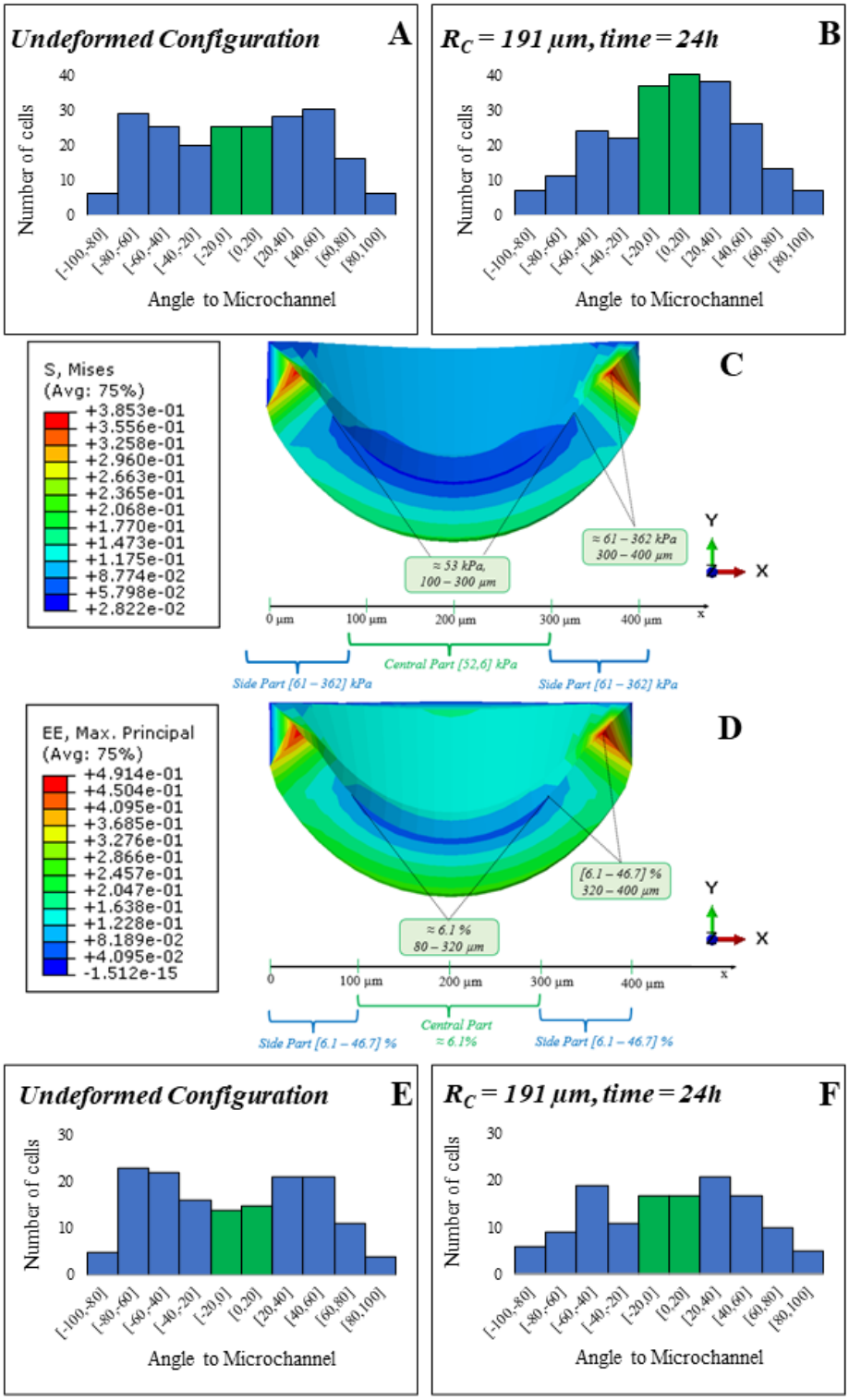
Undeformed Configuration
A
Number of cells
Angle to Microchannel
R_C = 191 µm, time = 24h
B
Number of cells
Angle to Microchannel
S, Mises
(Avg: 75%)
+3.853e-01
+3.556e-01
+3.258e-01
+2.960e-01
+2.663e-01
+2.365e-01
+2.068e-01
+1.770e-01
+1.473e-01
+1.175e-01
+8.774e-02
+5.798e-02
+2.822e-02
C
≈ 53 kPa, 100 – 300 µm
≈ 61 – 362 kPa 300 – 400 µm
Central Part [52,6] kPa
Side Part [61 – 362] kPa
Side Part [61 – 362] kPa
EE, Max. Principal
(Avg: 75%)
+4.914e-01
+4.504e-01
+4.095e-01
+3.685e-01
+3.276e-01
+2.866e-01
+2.457e-01
+2.047e-01
+1.638e-01
+1.228e-01
+8.189e-02
+4.095e-02
-1.512e-15
D
≈ 6.1 % 80 – 320 µm
[6.1 – 46.7] % 320 – 400 µm
Central Part ≈ 6.1%
Side Part [6.1 – 46.7] %
Side Part [6.1 – 46.7] %
Undeformed Configuration
E
Number of cells
Angle to Microchannel
R_C = 191 µm, time = 24h
F
Number of cells
Angle to Microchannel

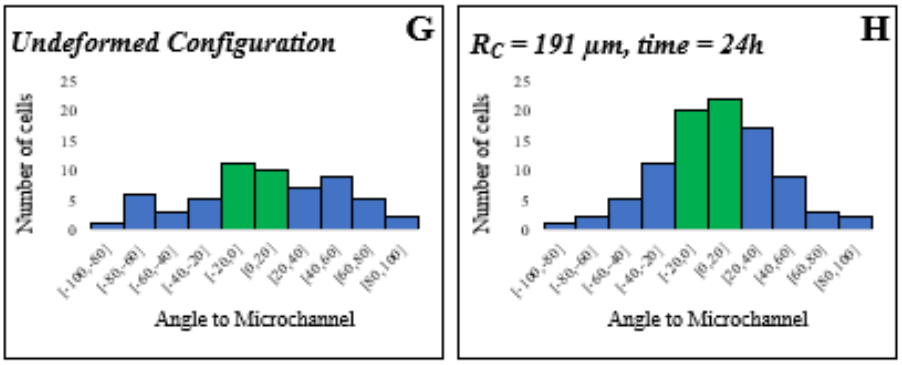

Figure 3.6: Adipose stem cells behaviour induced by a curvature variation of 0.0052 µm^{-1} on the microfluidic platform. A-B: Histograms showing ASCs polarization with respect to the microchannel direction (0°) into flat (A) and deformed (B) configurations. C: von Mises stress distribution on the curved cell-seeded PDMS membrane (colour map express the von Mises stress in MPa) D: maximum elastic strain distribution on the curved cell-seeded PDMS membrane (colour map express the strain in a-dimensional way. E-F: Histograms showing ASCs polarization with respect to the microchannel direction (0°) into flat E and deformed (F) configurations on the lateral regions. G-H: Histograms showing ASCs polarization with respect to the microchannel direction (0°) into flat (G) and deformed (H) configurations on the central region.

3.3.2.5 Actin stress fibers response to R_c = 175 µm

The curvature radii of 224 µm and 191 µm, as previously explained, are able to re-organize the stem cell cytoskeleton in the central part of the PDMS membrane inducing an alignment of actin stress fibers along the longitudinal microchannel direction. Conversely, on the lateral parts, due to side effects responsible of heterogeneous stresses and strains, a consistent cytoskeleton organization along a specific direction was not observed.

In order to have more information about the role of curvature variations on the cytoskeleton architecture, an analysis of stem cell response to a higher curvature has been performed. Particularly, a curvature of 0.0057 µm^{-1}, which corresponds to a R_c = 175 µm was applied on stem cells cultured at low density through a pressure of -500 mbar.

As a result, a re-organization of the actin cytoskeleton stress fibers was observed after 24 h from the application and maintenance of the mechanical cue. In fact, a random polarization of stem cells was observed in flat configuration (Figure 3.7A) with respect to the curved membrane configuration (Figure 3.7B). Increasing the pressure, there is not only a raise of the membrane curvature but, also, an increment of von Mises stresses and strains. In detail, a uniform von Mises stress field was observed in the central part of the PDMS membrane (Figure 3.7C, S2I-L) with a value of ≈ 86 kPa, and a heterogeneous

one on the side regions [109 – 415] kPa. The same occurred for the strain profile (Figure 3.7D, S3I-L) having a constant strain in the central part ≈ 14.4 % and a non-uniform one on the side parts: [14.4 – 60.1] %.

With the previous introduced approach, the cells were divided into two groups: stem cells on side parts and ASCs on the central one into both configurations (undeformed – deformed). Starting from the side regions, a heterogeneous actin stress fibers polarization was observed in both cases (Figure 3.7E, F) even if an increment in terms of total stem cell number aligned along the microfluidic channel was obtained into deformed case with respect to the undeformed one. Despite this increase, the histogram profile obtained does not show a preference of the stem cells to align along the longitudinal direction.

Then, in the central part, the role played by the curvature variation on the cell response was analyzed. Indeed, from a random cellular orientation in undeformed configuration (Figure 3.7G), polarized cells along the microfluidic channel have been captured (Figure 3.7H). In fact, the histogram profile is close to that of a gaussian curve.

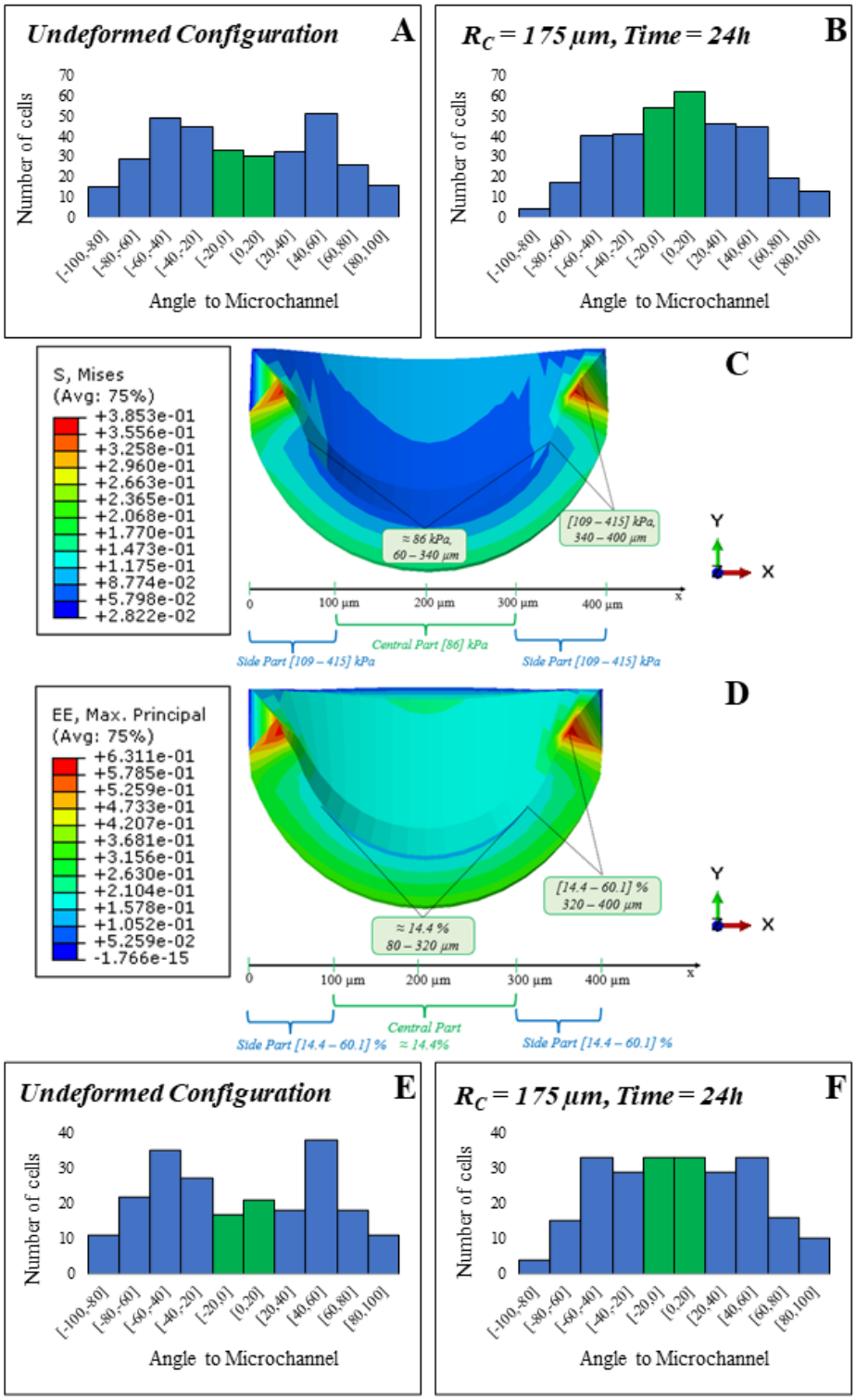
Undeformed Configuration
A
Number of cells
Angle to Microchannel
R_C = 175 µm, Time = 24h
B
Number of cells
Angle to Microchannel
S, Mises
(Avg: 75%)
+3.853e-01
+3.556e-01
+3.258e-01
+2.960e-01
+2.663e-01
+2.365e-01
+2.068e-01
+1.770e-01
+1.473e-01
+1.175e-01
+8.774e-02
+5.798e-02
+2.822e-02
C
≈ 86 kPa, 60 – 340 µm
[109 – 415] kPa, 340 – 400 µm
Central Part [86] kPa
Side Part [109 – 415] kPa
Side Part [109 – 415] kPa
EE, Max. Principal
(Avg: 75%)
+6.311e-01
+5.785e-01
+5.259e-01
+4.733e-01
+4.207e-01
+3.681e-01
+3.156e-01
+2.630e-01
+2.104e-01
+1.578e-01
+1.052e-01
+5.259e-02
-1.766e-15
D
[14.4 – 60.1] % 320 – 400 µm
≈ 14.4 % 80 – 320 µm
Central Part
Side Part [14.4 – 60.1] %
≈ 14.4%
Side Part [14.4 – 60.1] %
Undeformed Configuration
E
Number of cells
Angle to Microchannel
R_C = 175 µm, Time = 24h
F
Number of cells
Angle to Microchannel

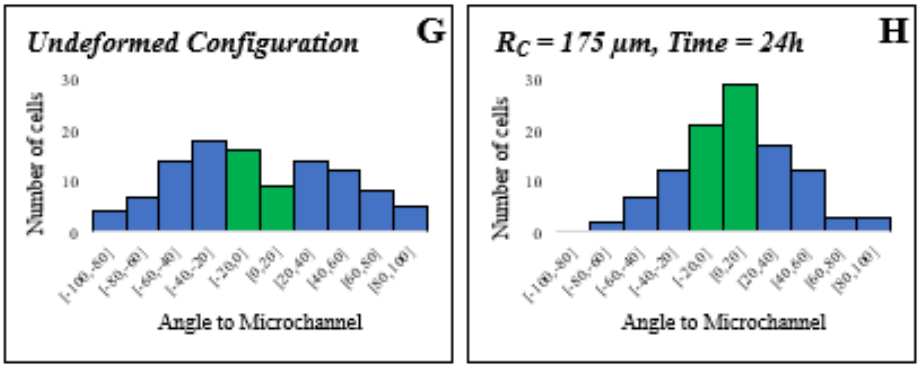

Figure 3.7: Adipose stem cells behaviour induced by a curvature variation of 0.0057 μm^{-1} on the microfluidic platform. A-B: Histograms showing ASCs polarization with respect to the microchannel direction (0°) into flat (A) and deformed (B) configurations. C: von Mises stress distribution on the curved cell-seeded PDMS membrane (colour map express the von Mises stress in MPa) D: maximum elastic strain distribution on the curved cell-seeded PDMS membrane (colour map express the strain in a-dimensional way. E-F: Histograms showing ASCs polarization with respect to the microchannel direction (0°) into flat E and deformed (F) configurations on the lateral regions. G-H: Histograms showing ASCs polarization with respect to the microchannel direction (0°) into flat (G) and deformed (H) configurations on the central region.

3.3.2.6 Actin stress fibers response to R_c = 151 µm

The last but not least static mechanical curvature variation applied on the ASCs-seeded on the microfluidic platform was equal to 0.0066 μm^{-1} which corresponds to a radius of curvature of 151 µm. This mechanical load was applied with a pressure of -600 mbar inside the microfluidic channel.

As a result, an actin cytoskeleton polarization along the microchannel direction was observed 24 h after the mechanical stimulation (Figure 3.8B) with respect to the random cellular organization in flat configuration (Figure 3.8A).

The von Mises stress distribution (Figure 3.8C, S2M-N) is constant in the central part ≈ 118 kPa with respect to the side ones [125 – 485] kPa. This profile is in agreement with the previous von Mises stress fields analyzed. The same occurred for the strain distribution having a constant value approximatively of ≈ 20% in the central part than the non-uniform one on the side regions [20 – 67.3] % (Figure 3.8D, S3M-N).

Dividing the stem cells in function of their positions on the microfluidic channel, a study on the central and side sections was made. As a result, a random cytoskeleton organization and, as a consequence, the absence of ASCs polarization with respect to the longitudinal direction, was observed on the side parts. In fact, in both undeformed (Figure 3.8E) and deformed (Figure 3.8F) profiles the ASCs are oriented in all directions.

Conversely, a cellular polarization was induced by the curvature variation applied in the central part after 24 h (Figure 3.8G-H). Moreover, a raise of total number of cells into central-part deformed configuration was observed with respect to the equivalent region into undeformed case. On the contrary, an opposite result was seen on the lateral zone. In fact, comparing the undeformed and deformed cases of side regions, a decreasing in the total cell number was obtained.

This could indicate that the increase in membrane curvature and, therefore, in the mechanical stresses/strains on the stem cells, not only induces a cytoskeleton re-organization along the longitudinal direction, but also a preference of the cells to move towards the central part of the microchannel with respect to the lateral one. The cellular displacement in the central part should be due to a more stable and uniform stress/strain field developed here with respect to the lateral heterogeneity.

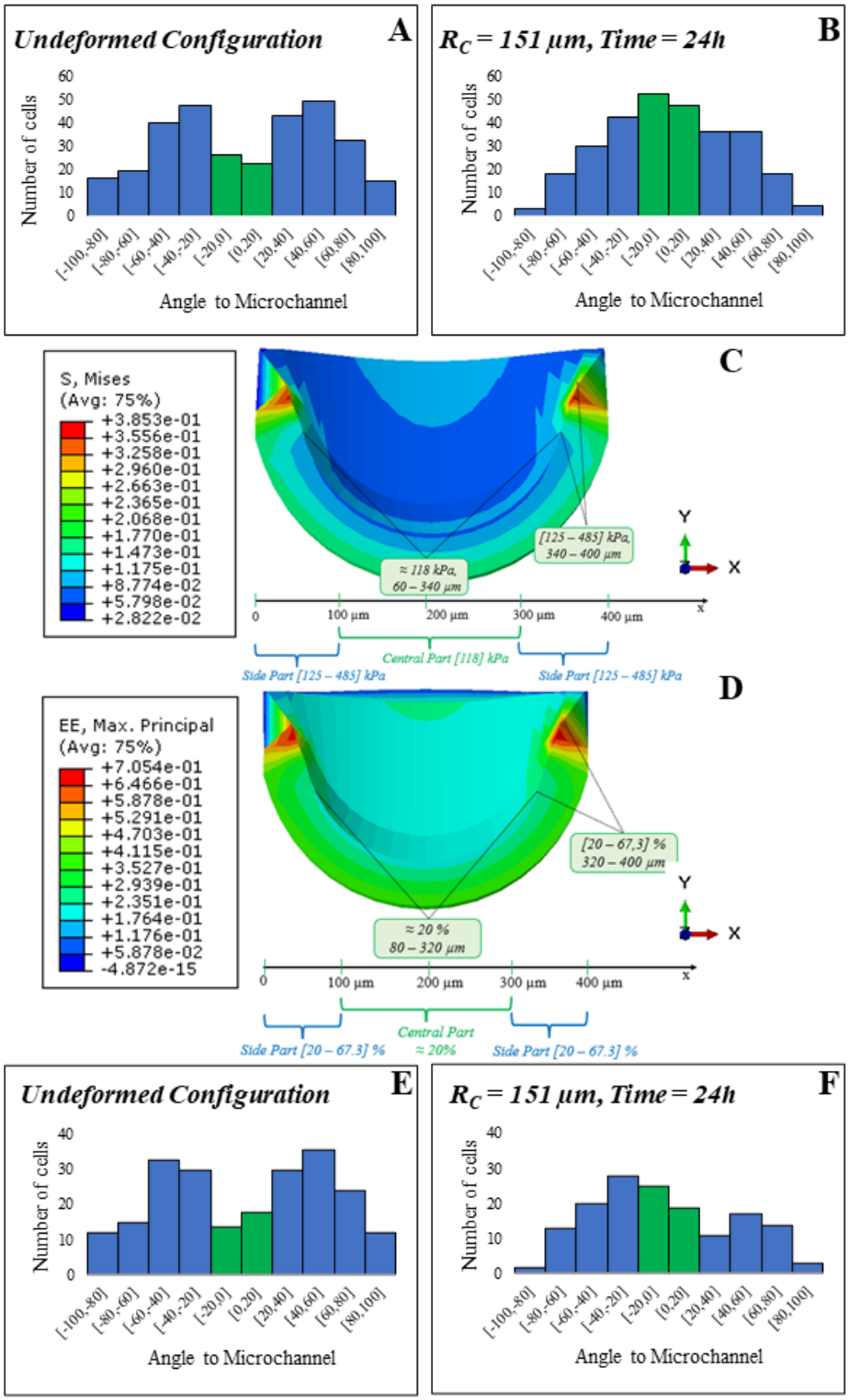
A
Undeformed Configuration
Number of cells
Angle to Microchannel
B
R_C = 151 µm, Time = 24h
Number of cells
Angle to Microchannel
C
S, Mises
(Avg: 75%)
+3.853e-01
+3.556e-01
+3.258e-01
+2.960e-01
+2.663e-01
+2.365e-01
+2.068e-01
+1.770e-01
+1.473e-01
+1.175e-01
+8.774e-02
+5.798e-02
+2.822e-02
[125 – 485] kPa,
340 – 400 µm
≈ 118 kPa,
60 – 340 µm
Central Part [118] kPa
Side Part [125 – 485] kPa
Side Part [125 – 485] kPa
D
EE, Max. Principal
(Avg: 75%)
+7.054e-01
+6.466e-01
+5.878e-01
+5.291e-01
+4.703e-01
+4.115e-01
+3.527e-01
+2.939e-01
+2.351e-01
+1.764e-01
+1.176e-01
+5.878e-02
-4.872e-15
[20 – 67,3] %
320 – 400 µm
≈ 20 %
80 – 320 µm
Central Part
≈ 20%
Side Part [20 – 67.3] %
Side Part [20 – 67.3] %
E
Undeformed Configuration
Number of cells
Angle to Microchannel
F
R_C = 151 µm, Time = 24h
Number of cells
Angle to Microchannel

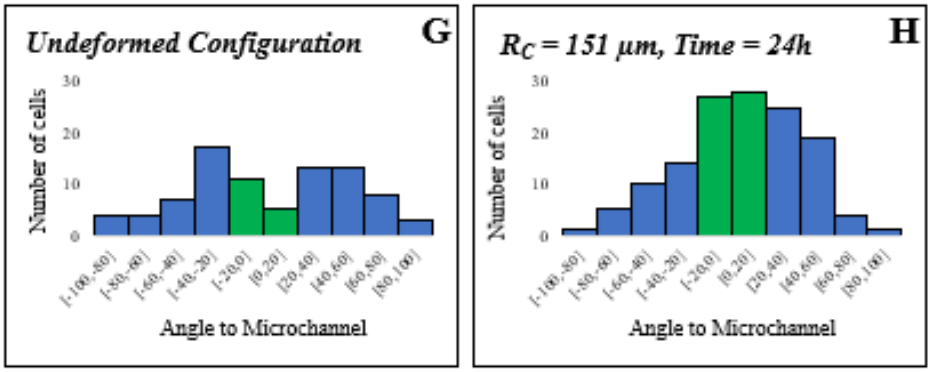

Figure 3.8: Adipose stem cells behaviour induced by a curvature variation of 0.0066 µm^{-1} on the microfluidic platform. A-B: Histograms showing ASCs polarization with respect to the microchannel direction (0°) into flat (A) and deformed (B) configurations. C: von Mises stress distribution on the curved cell-seeded PDMS membrane (colour map express the von Mises stress in MPa) D: maximum elastic strain distribution on the curved cell-seeded PDMS membrane (colour map express the strain in a-dimensional way. E-F: Histograms showing ASCs polarization with respect to the microchannel direction (0°) into flat E and deformed (F) configurations on the lateral regions. G-H: Histograms showing ASCs polarization with respect to the microchannel direction (0°) into flat (G) and deformed (H) configurations on the central region.

3.3.3 Cell morphology induced by static changes of cell-seeded membrane curvature

Cell morphology can influence aspects of cellular mechanosensation and curvotaxis by limiting the amount of area that cells are able to cover while adhered to a certain substrate. To unravel differences in cell morphology between both undeformed and deformed configurations in each curvature case, a comparison of ASCs area was performed.

This area was quantified from the z-stacks of the actin stress fibers using the command "Measure" of the software Fiji. The ASCs area for each curvature configuration has been divided into two groups: area of cells on side parts and that on central one comparing both undeformed and deformed cases. As shown in Figure 3.9, expect to side part with R_C = 151 µm, there are not statistically significant differences between undeformed and deformed arrangements. These results highlight the ASCs capacity to re-organize actin stress fibers polarization in function of amplitude of curvature variations without changing their adhesion area on the PDMS substrate.

The only statistical difference was observed on side parts of the highest curvature case (Figure 3.9F) where also, as previously introduced, a translocation into deformed configuration of ASCs from side to central regions was obtained. This curvature on the side part should be able to activate not only the cytoskeleton re-organization but also cell movement with a consequent cell area reduction with respect to the undeformed case.

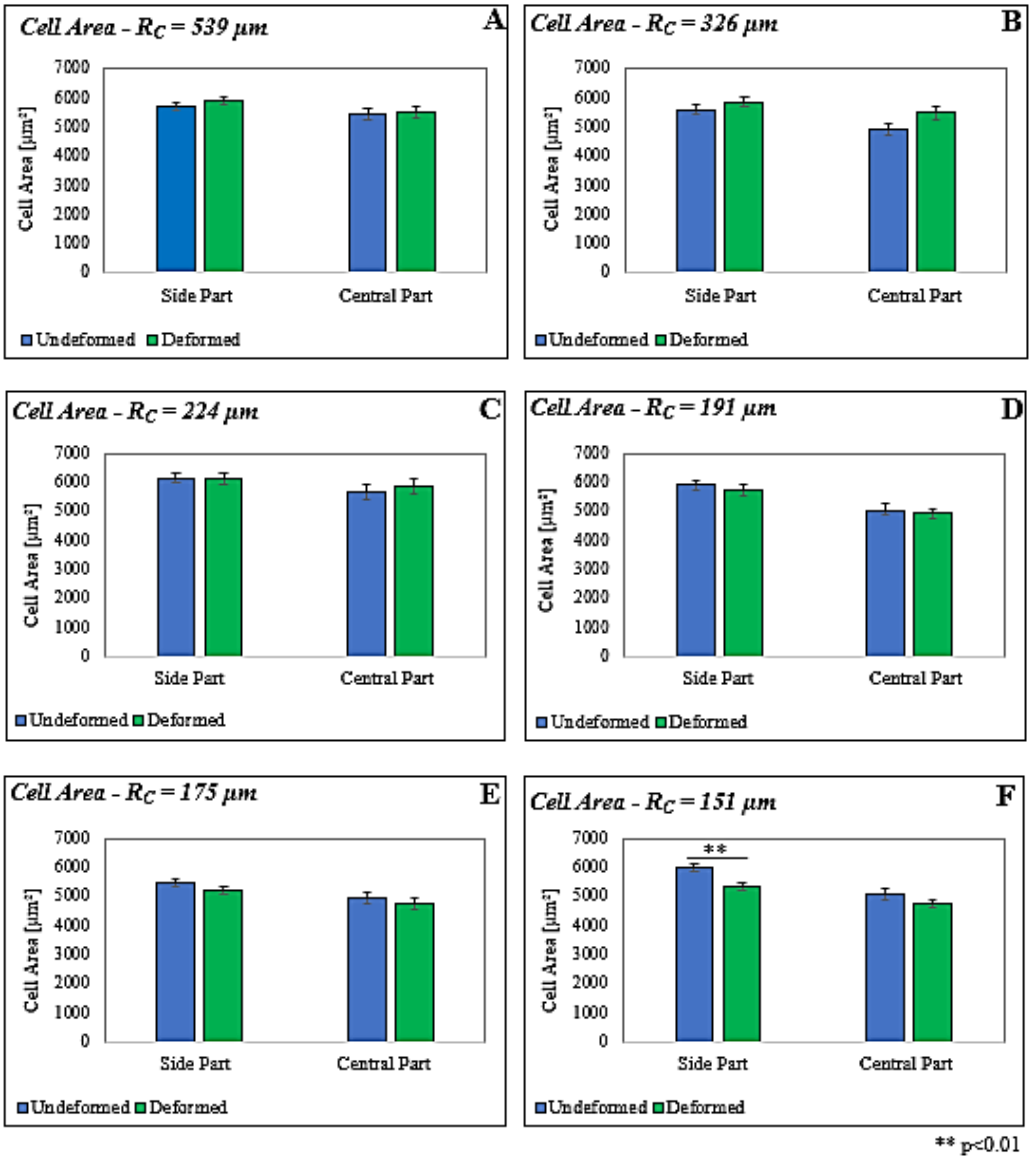

*Figure 3.9: Cell area distribution for undeformed and deformed configurations on both side and central regions of the microfluidic channel. A: Cell area distribution for R_C = 539 µm. B: Cell area distribution for R_C = 326 µm. C: Cell area distribution for R_C = 224 µm. D Cell area distribution for R_C = 191 µm. E: Cell area distribution for R_C = 175 µm. F: Cell area distribution for R_C = 151 µm. Each experiment was repeated three times on three different microfluidic platform and the histograms show the mean cell area ± s.e.m. ** p<0.01*

3.3.4 Focal Adhesions assembly induced by static changes of cell-seeded membrane curvature

Based on the differences observed in curvature-controlled cellular polarization /orientation, further analysis was performed at the level of the interaction of the cells with their substrate.

Cells adhere to the substrate by means of FAs, adhesion-complexes formed by transmembrane integrins and intracellular proteins, among which talin, α-actinin, vinculin, paxillin and tensin [7, 8]. Such adhesions are highly relevant for events such as cell migration, motility, mechanosensing and curvotaxis [9-11]. Therefore, the size and distribution of FAs in ASCs were compared between undeformed and 24 h deformed configuration for the different curvatures.

FAs characterization was done by analysis of paxillin, a protein localized at the FA intracellular layer. It has been chosen because it is involved to integrate mechanical cues arising from the ECM working as a multi-domain adaptor at the interface between the plasma membrane and the actin cytoskeleton [12, 13]. In the sections below, the FAs response to the different mechanical signals, that is to the different curvatures, has been studied.

3.3.4.1 Focal adhesions response to R_c = 539 µm

As observed in the section 3.3.1.1, the curvature variation applied on the low-density ASCs was not enough to activate a re-organization of actin stress fibers.

It is well known that the FA complexes create a direct communication between the ECM and the cells, being involved in the mechanical cues' propagation from the ECM to the cell and *viceversa*. To analyse the FAs behaviour to this specific mechanical insult, the FAs orientation with respect to the microchannel direction was quantified. For a specific microfluidic platform, at least 6 different ASCs in both undeformed and deformed configurations have been acquired with a high magnification long distance objective (40x) and each experiment was repeated three different times on independent microfluidic platforms. Moreover, considering the results about actin cytoskeleton re-organization already discussed, only the ASCs on the central part of the microchannel are taken into account in order to neglect the side effects.

Starting from undeformed configuration, assuming that only the FAs polarized in the range [-20°; 20°] are aligned along the microchannel direction, a random polarization was observed (Figure 3.10A). Also, in the 24h deformed configuration the same result was obtained (Figure 3.10B). In fact, as shown in representative confocal images (Figure 3.10C-D), the actin stress fibers and FAs polarization are randomly distributed with respect to the longitudinal direction in both arrangements.

Moreover, a FA size distribution was made to compare if the curvature was able to modify the FAs area between the two configurations. Particularly, the FAs have been organized in four different groups in function of their area: (i) FAs with an area ≤ 2.5 μm^2; (ii) FAs area in the range [2.5 – 5] μm^2; (iii) FAs area in the interval [5 – 7.5] μm^2; (iv) FAs area ≥ 7.5 μm^2; whereas the total number of FAs in each group was express in percentage in order to have for each ASC cell an amount of FAs that is independent from the total number of FAs of the cell itself. This means that if different cells have a specific total number of focal adhesions, normalizing their amount, all these values can be compared. In the box and whisker plot (Figure 3.10E) no statistical differences between the undeformed and 24 h curved configurations were observed, in agreement with the actin cytoskeleton results, even if the polarization of FAs with respect to the microchannel direction was not considered. In fact, the curvature of PDMS substrate should be responsible to change FAs size for those polarized along the longitudinal direction or orthogonally to this one. So, for each experimental configuration, a FAs size distribution was analyzed considering their polarization with respect to the microchannel direction. Then the FAs were organized in three different groups: (i) FAs aligned along the microchannel direction [-20°; 20°]; (ii) FAs having an angle intermediate between longitudinal and orthogonal direction of the channel [-60°; -20°], [20°; 60°]; (iii) FAs polarized orthogonally to the microchannel direction [-100°; -60°], [60°; 100°]. Starting from the undeformed configuration (Figure 3.10F), a statistical difference was observed only for FAs size ≤ 2.5 μm^2 aligned along the longitudinal direction and orthogonally to that one. In fact, a lower percentage of FAs having this area was obtained along the microchannel direction with respect to the other. The same analysis was done for 24h curved case (Figure 3.10G), where no statistical differences between the various cases were found.

So, in conclusion, the curvature 0.0019 μm^{-1} was not able to induce a consistent cytoskeleton and FA response after 24 h from the mechanical insult application.

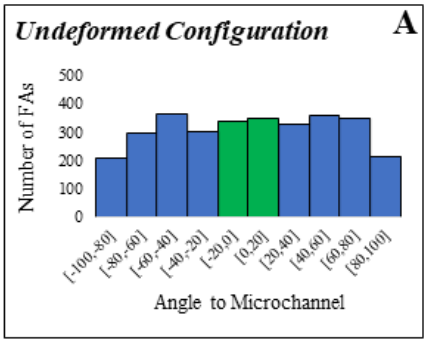

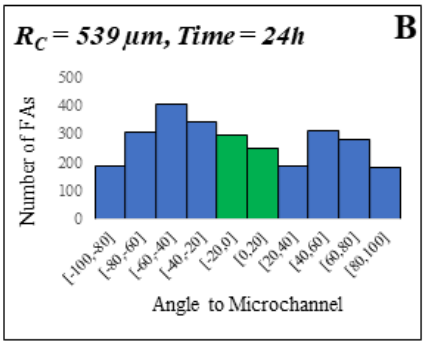

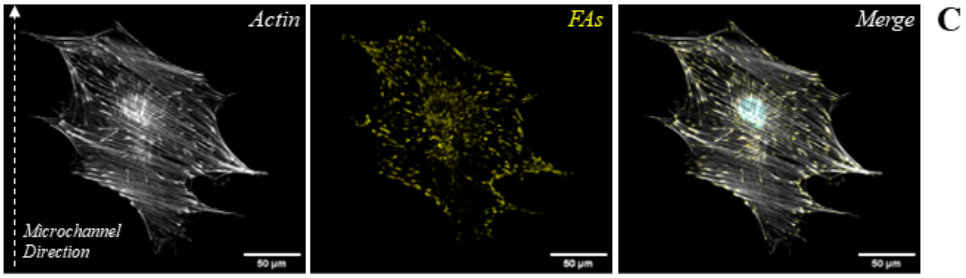

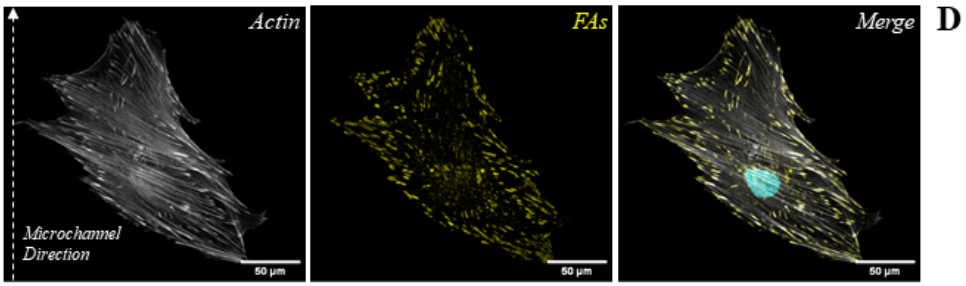

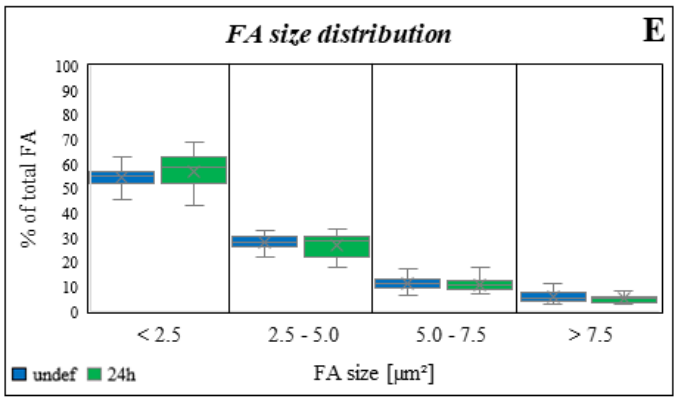

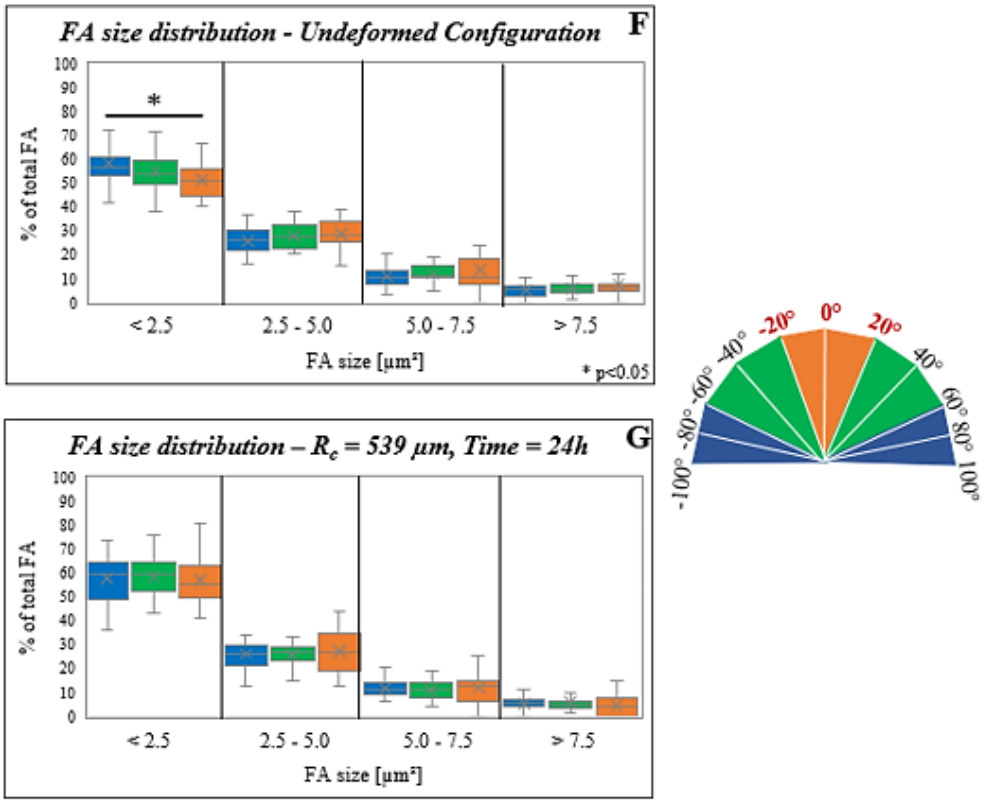

*Figure 3.10: Focal adhesions (FAs) behaviour induced by a curvature variation of 0.0019 µm^{-1} on the microfluidic platform. A-B: Histograms showing FAs polarization with respect to the microchannel direction (0°) into flat (A) and deformed (B) configurations. C: Confocal acquisition of a single adipose derived mesenchymal stem cell into undeformed configuration. Gray: Actin Cytoskeleton, Yellow: Focal Adhesions, Cyan: Nucleus. Scale bar: 50 µm. D: Confocal acquisition of a single adipose derived mesenchymal stem cell into deformed configuration. Gray: Actin Cytoskeleton, Yellow: Focal Adhesions, Cyan: Nucleus. Scale bar: 50 µm. E-G: Focal adhesions size distribution. E: Comparison of FA size distribution between deformed and deformed configuration. F: FA size distribution in function of polarization angle into undeformed configuration. G: FA size distribution in function of polarization angle into deformed configuration. Data are expressed as mean value ± standard deviation and each experiment was repeated three times on independent microfluidic platform. * p<0.05*

3.3.4.2 Focal adhesions response to R_c = 326 µm

Similarly to the previous case, the FA re-organization in terms of both size and direction was studied for curvature radius of 326 µm. Starting from the FA polarization with respect to the microchannel direction (Figure 3.11A-B); a random orientation of FAs was observed in flat and curved configurations. Also in the z-projections representative images of ASCs can be visualized a non-preferential alignment of FAs along the microchannel direction (Figure 3.11C-D).

Analysing the FAs size distribution between the undeformed and deformed PDMS membrane (Figure 3.11E), specific statistical differences can be viewed. In detail, a percentage increase of FAs having an area smaller than 2.5 µm² occurred after 24 h from the application of the mechanical insult with respect to the flat configuration. Conversely, a reduction of large FAs was obtained into 24 h curved profile than the undeformed one. To deeply investigate the FAs size distribution variation in function of their polarization; an organization of FAs depending not only on area but also on orientation with respect to the microchannel direction was performed.

Starting from undeformed configuration (Figure 3.11F), no statistically significant differences were observed between the different groups. The same occurred for 24 h deformed membrane profile (Figure 3.11G).

In conclusion, the different size distributions show relevant differences for FAs size between undeformed and deformed cases, but no relevant size distribution changes for each specific configuration. Moreover, the random FAs polarization showed in Figure 3.11A-B agrees with the heterogeneous actin cytoskeleton re-organization.

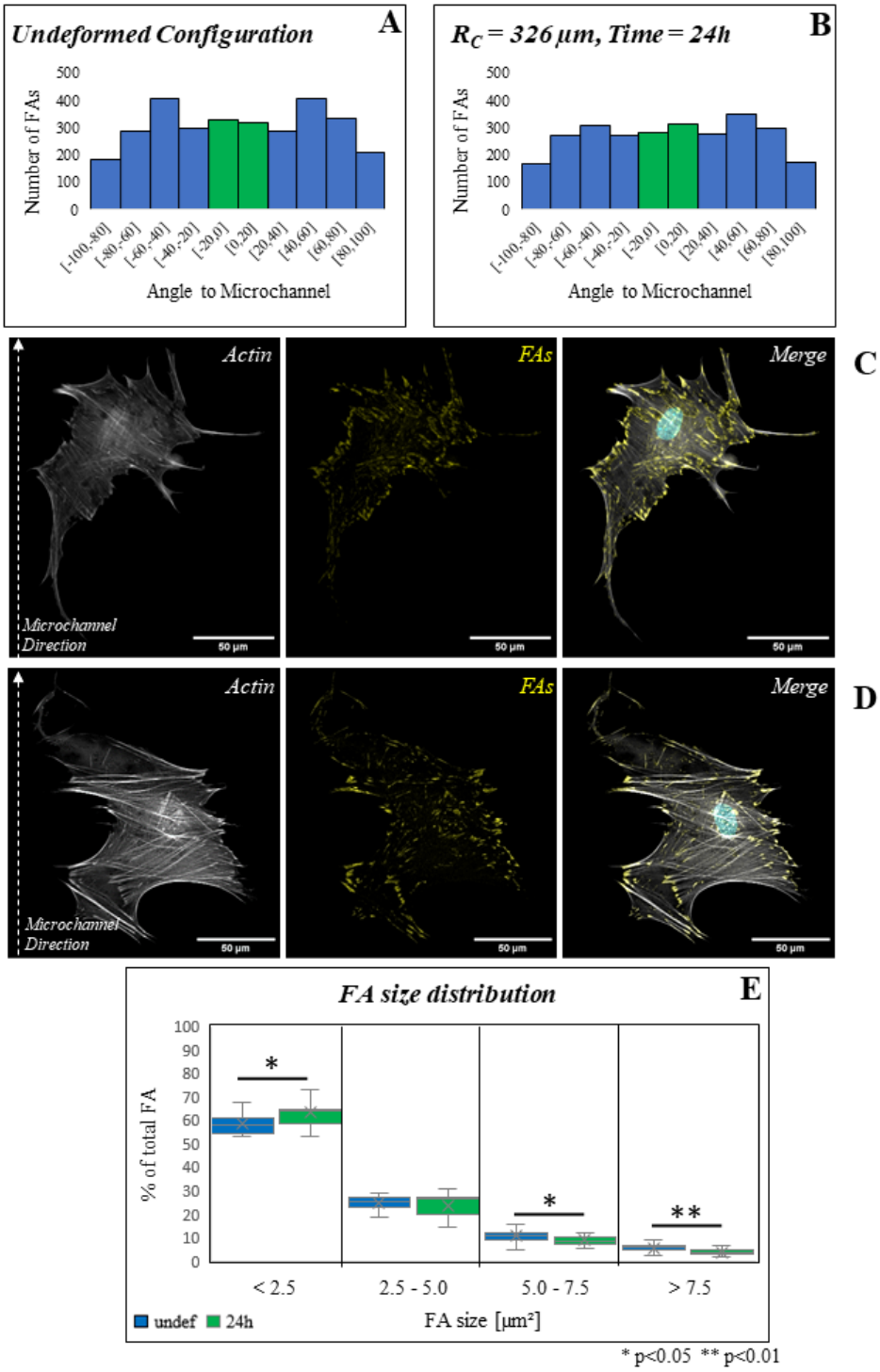
A
Undeformed Configuration
Number of FAs
Angle to Microchannel
B
R_C = 326 µm, Time = 24h
Number of FAs
Angle to Microchannel
C
Actin
FAs
Merge
Microchannel Direction
50 µm
D
Actin
FAs
Merge
Microchannel Direction
50 µm
E
FA size distribution
% of total FA
< 2.5
2.5 - 5.0
5.0 - 7.5
> 7.5
FA size [µm²]
undef
24h
* p<0.05 ** p<0.01

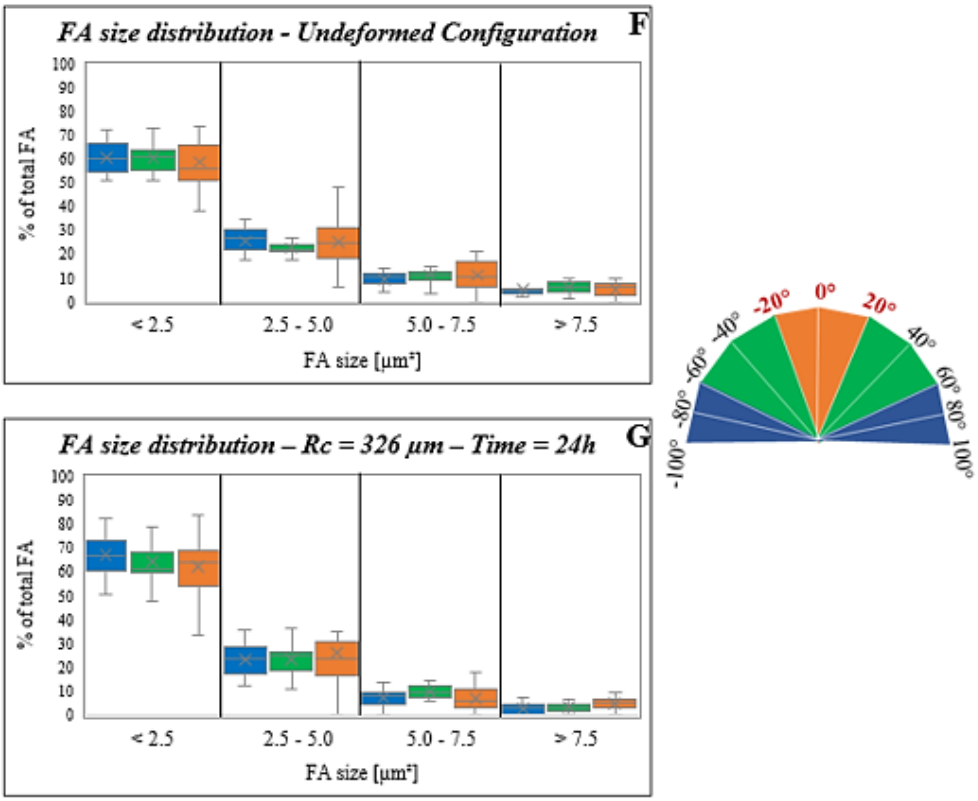

*Figure 3.11: Focal adhesions (FAs) behaviour induced by a curvature variation of 0.0031 μm^{-1} on the microfluidic platform. A-B: Histograms showing FAs polarization with respect to the microchannel direction (0°) into flat (A) and deformed (B) configurations. C: Confocal acquisition of a single adipose derived mesenchymal stem cell into undeformed configuration. Gray: Actin Cytoskeleton, Yellow: Focal Adhesions, Cyan: Nucleus. Scale bar: 50 µm. D: Confocal acquisition of a single adipose derived mesenchymal stem cell into deformed configuration. Gray: Actin Cytoskeleton, Yellow: Focal Adhesions, Cyan: Nucleus. Scale bar: 50 µm. E-G: Focal adhesions size distribution. E: Comparison of FA size distribution between deformed and deformed configuration. F: FA size distribution in function of polarization angle into undeformed configuration. G: FA size distribution in function of polarization angle into deformed configuration. Data are expressed as mean value ± standard deviation and each experiment was repeated three times on independent microfluidic platform. * $p<0.05$, ** $p<0.01$.*

3.3.4.3 Focal adhesions response to R_c = 224 μm

Applying a mechanical cue able to curve the PDMS membrane in a specific way (R_C = 224 μm), cells in the central region resulted to be polarized along the longitudinal direction (Section 3.3.2.3). The same result was not obtained in terms of FAs polarization, In fact, in both undeformed and deformed configurations (Figure 3.12A-B) a heterogeneous FAs orientation was observed. Analysing the images of ASCs (Figure 3.12C-D), FAs manifest no polarization into undeformed configuration. The same occurs for deformed one; in fact, even if the actin cytoskeleton stress fibers are polarized along the microchannel direction, some FAs were aligned with the actin filaments whereas others were oriented in other directions.

The FAs size distribution between undeformed and 24 h deformed configurations (Figure 3.12E) did not show statistically significant differences.

Focusing the attention on the FAs size distribution into undeformed configuration expressed in function of their polarization with respect to the longitudinal direction (Figure 3.12F), there were not relevant differences of values. Conversely, statistically significant results were observed in 24h deformed case (Figure 3.12G). Particularly, a difference in the percentage of FAs having an area ≤ 2.5 μm² was quantified for FAs aligned along the longitudinal and orthogonal axes. The same occurred for FAs having size ≥ 7.5 μm². The percentage of large FAs (≥ 7.5 μm²) aligned along the longitudinal axis were significantly higher than the orthogonal ones. An opposite result was observed for small FAs (≤ 2.5 μm²).

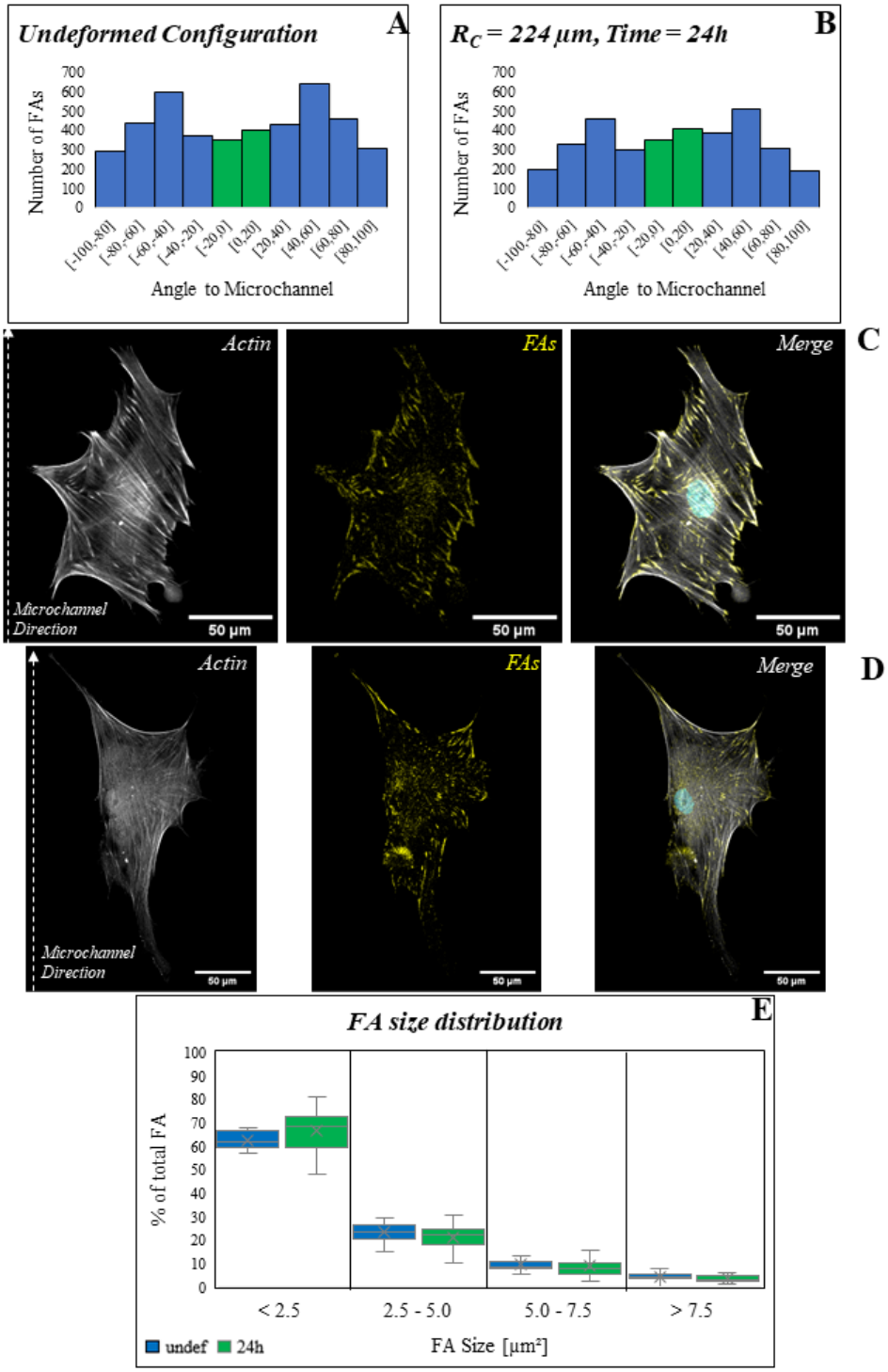
A
Undeformed Configuration
Number of FAs
700
600
500
400
300
200
100
0
[-100,-80]
[-80,-60]
[-60,-40]
[-40,-20]
[-20,0]
[0,20]
[20,40]
[40,60]
[60,80]
[80,100]
Angle to Microchannel
B
R_C = 224 µm, Time = 24h
Number of FAs
Angle to Microchannel
C
Actin
FAs
Merge
Microchannel Direction
50 µm
D
Actin
FAs
Merge
Microchannel Direction
50 µm
E
FA size distribution
% of total FA
100
90
80
70
60
50
40
30
20
10
0
< 2.5
2.5 - 5.0
5.0 - 7.5
> 7.5
undef
24h
FA Size [µm²]

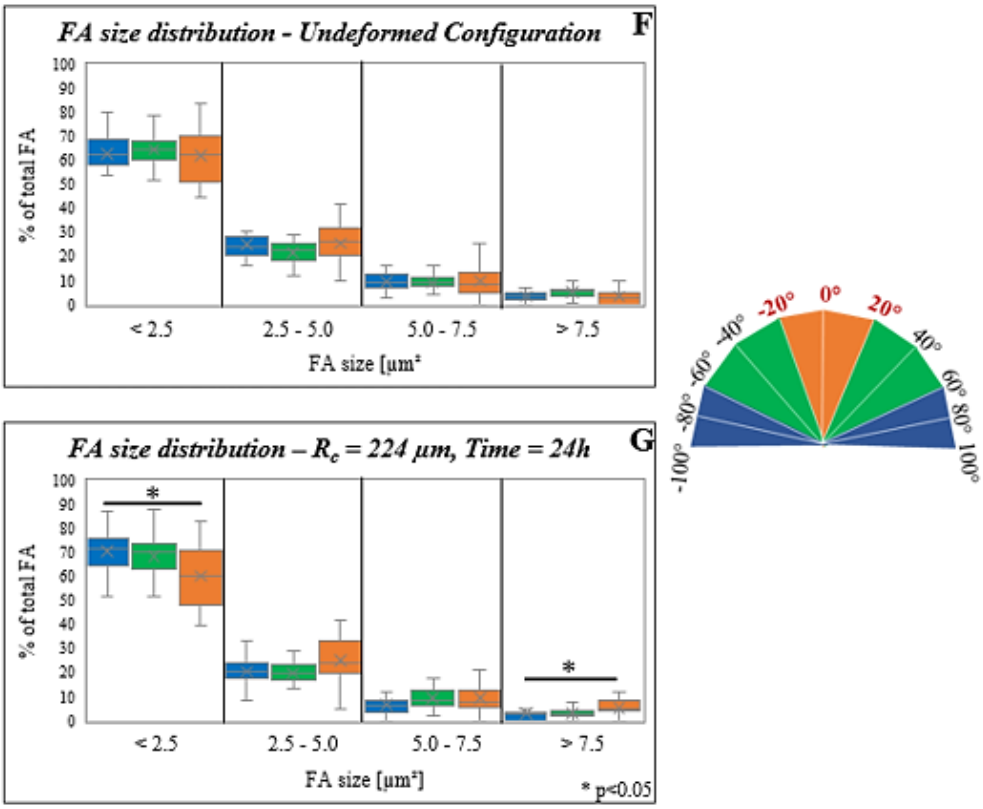

*Figure 3.12: Focal adhesions (FAs) behaviour induced by a curvature variation of 0.0045 μm^{-1} on the microfluidic platform. A-B: Histograms showing FAs polarization with respect to the microchannel direction (0°) into flat (A) and deformed (B) configurations. C: Confocal acquisition of a single adipose derived mesenchymal stem cell into undeformed configuration. Gray: Actin Cytoskeleton, Yellow: Focal Adhesions, Cyan: Nucleus. Scale bar: 50 µm. D: Confocal acquisition of a single adipose derived mesenchymal stem cell into deformed configuration. Gray: Actin Cytoskeleton, Yellow: Focal Adhesions, Cyan: Nucleus. Scale bar: 50 µm. E-G: Focal adhesions size distribution. E: Comparison of FA size distribution between deformed and deformed configuration. F: FA size distribution in function of polarization angle into undeformed configuration. G: FA size distribution in function of polarization angle into deformed configuration. Data are expressed as mean value ± standard deviation and each experiment was repeated three times on independent microfluidic platform. * $p<0.05$.*

3.3.4.4 Focal adhesions response to R_c = 191 µm

A curved membrane with a radius of curvature of 191 µm was able to induce a re-organization of the actin stress fibers along longitudinal axis of the microfluidic platform (Section 3.3.2.4). Interestingly, FAs did not manifest the same polarization (Figure 3.13A-B). Particularly, on the undeformed configuration, a random FAs polarization was observed; whereas on the deformed profile the number of FAs along the microchannel direction increases with respect to the undeformed one, but the histogram profile did not show a clear peak along the longitudinal line. The same was showed by z-projection confocal images of ASCs (Figure 3.13C-D) with an actin stress fibers polarization and only a fraction of FAs polarized along longitudinal axis.

Furthermore, no statistically significant differences were found in the FAs size before and 24 h after mechanical insult application (Figure 3.13F).

Finally, the FAs size distributions expressed in terms of the angle formed between FAs and microchannel showed that into undeformed case (Figure 3.13F) no statistically significant differences were observed; whereas on the deformed one (Figure 3.13G) a consistent reduction of the percentage was obtained for FAs aligned along the microchannel direction with respect to the orthogonal ones when the FAs size was lower than 2.5 µm².

For all the cases analysed so far, a polarization of FAs along the longitudinal direction was not relevant as observed for the actin stress fibers which re-organized along that direction. This finding indicates that amplitude of the curvature applied on low density ASCs controls in a different way cytoskeleton and focal adhesions behaviour.

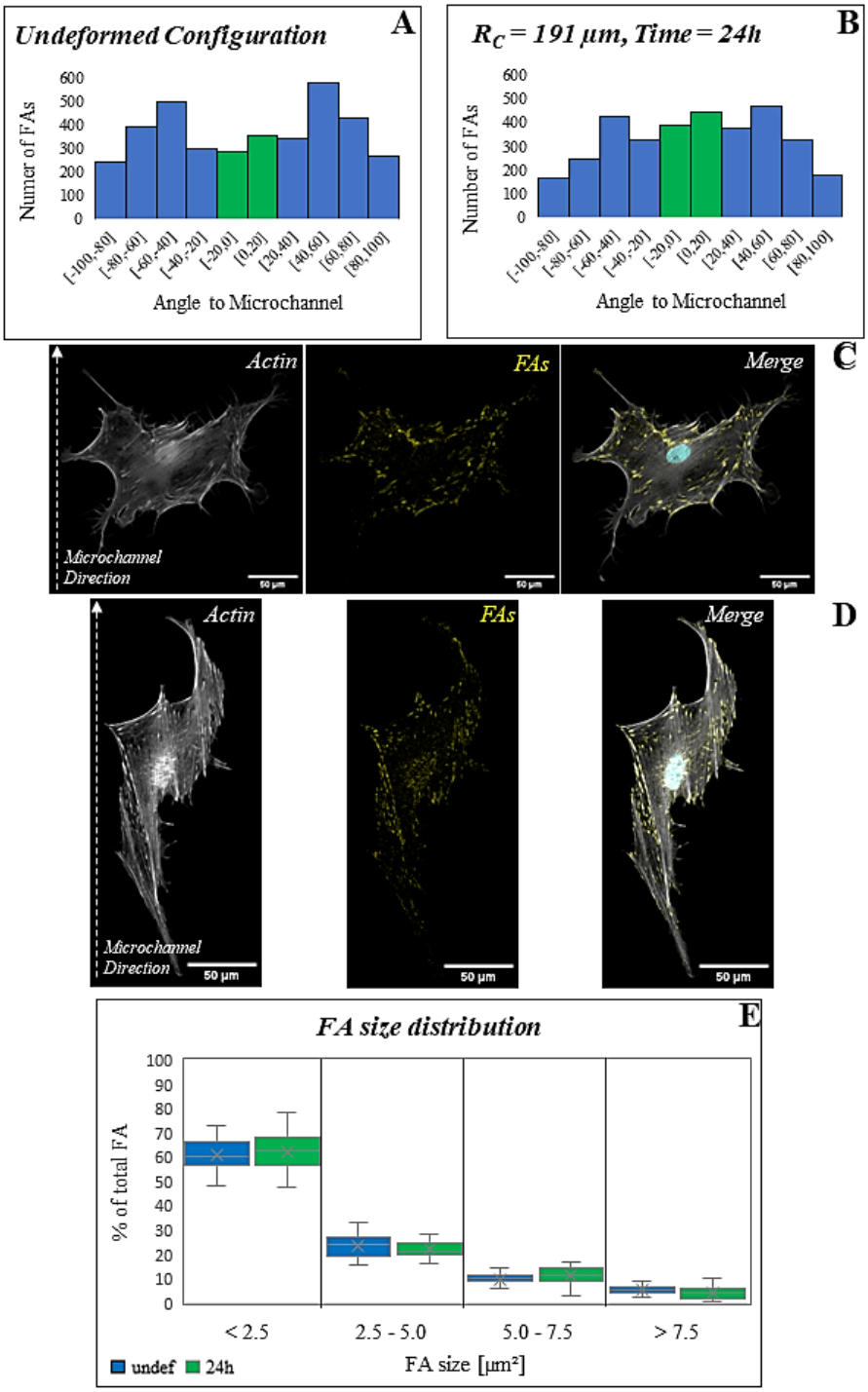
A
Undeformed Conftguration
Numer of FAs
600
500
400
300
200
100
0
[-100,-80]
[-80,-60]
[-60,-40]
[-40,-20]
[-20,0]
[0,20]
[20,40]
[40,60]
[60,80]
[80,100]
Angle to Microchannel
B
R_C = 191 µm, Time = 24h
Number of FAs
Angle to Microchannel
C
Actin
FAs
Merge
Microchannel Direction
50 µm
D
E
FA size distribution
% of total FA
100
90
80
70
60
50
40
30
20
10
0
< 2.5
2.5 - 5.0
5.0 - 7.5
> 7.5
undef
24h
FA size [µm²]

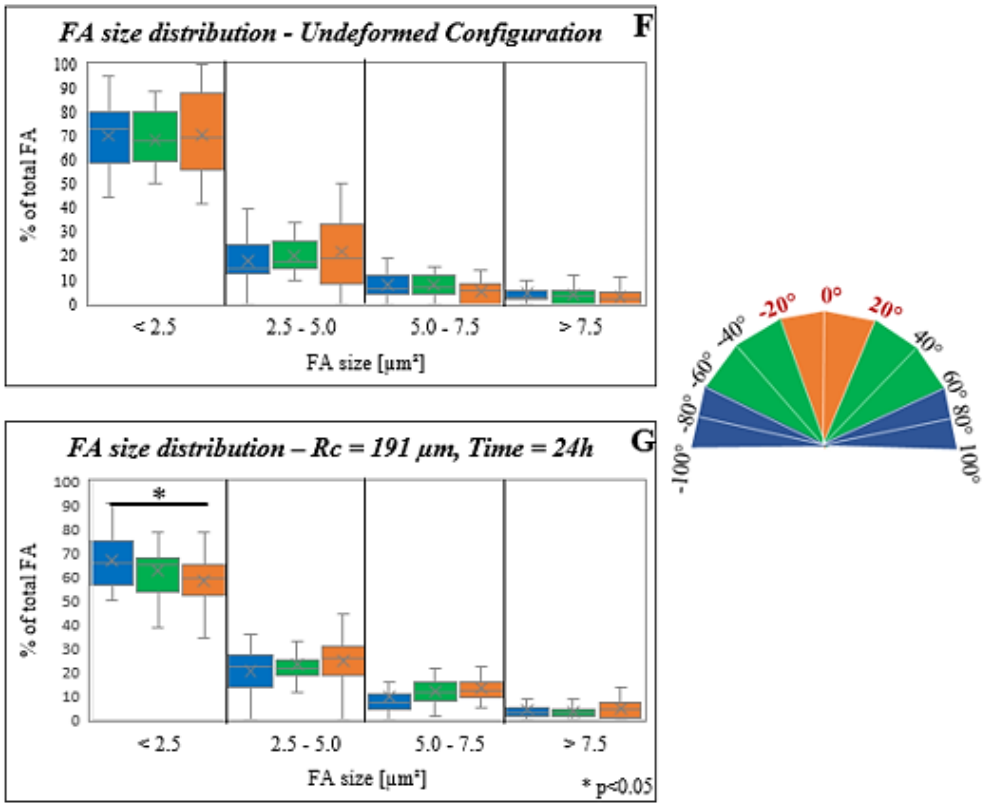

*Figure 3.13: Focal adhesions (FAs) behaviour induced by a curvature variation of 0.0052 μm^{-1} on the microfluidic platform. A-B: Histograms showing FAs polarization with respect to the microchannel direction (0°) into flat (A) and deformed (B) configurations. C: Confocal acquisition of a single adipose derived mesenchymal stem cell into undeformed configuration. Gray: Actin Cytoskeleton, Yellow: Focal Adhesions, Cyan: Nucleus. Scale bar: 50 µm. D: Confocal acquisition of a single adipose derived mesenchymal stem cell into deformed configuration. Gray: Actin Cytoskeleton, Yellow: Focal Adhesions, Cyan: Nucleus. Scale bar: 50 µm. E-G: Focal adhesions size distribution. E: Comparison of FA size distribution between deformed and deformed configuration. F: FA size distribution in function of polarization angle into undeformed configuration. G: FA size distribution in function of polarization angle into deformed configuration. Data are expressed as mean value ± standard deviation and each experiment was repeated three times on independent microfluidic platform. * $p<0.05$.*

3.3.4.5 Focal adhesions response to R_c = 175 µm

A polarization of FAs along the microchannel direction occurred applying a mechanical signal able to form a curved membrane having a R_C = 175 µm. In fact, starting from a random FAs organization (Figure 3.14A) for flat condition, a well-defined FAs re-alignment was observed 24 h after the mechanical load (Figure 3.14B). A higher number of FAs are aligned along the longitudinal axis into curved profile with respect to the un-curved one. Also the z-projection confocal images (Figure 3.14C-D) show this peculiar FAs behaviour specifically induced by the curvature.

Analysing the FA size distribution (Figure 3.14E), no relevant differences in terms of FA area was observed between undeformed and deformed configurations.

On the contrary, the FA size distribution expressed as function of FA angle to microchannel gives important information. Starting from undeformed configuration (Figure 3.14F), no relevant differences between the different ranges were quantified. A different outcome was observed at 24 h (Figure 3.14G); particularly, the percentage of small FAs (size $\leq$ 2.5 µm²) aligned along the longitudinal axis was statistically smaller with respect to the same FAs belonging to the other ranges. This means that the specific morphology of the cell-seeded membrane was able to control not only the polarization of these structures but also their size. Having smaller focal adhesions in the orthogonal direction to the microchannel than in the longitudinal one means having fewer stable structures in the first case than in the second case. That is, it would seem that starting from this curvature (0.0052 μm^{-1}) the maturation of focal adhesions is preferred along the longitudinal axis and disadvantaged in the orthogonal direction.

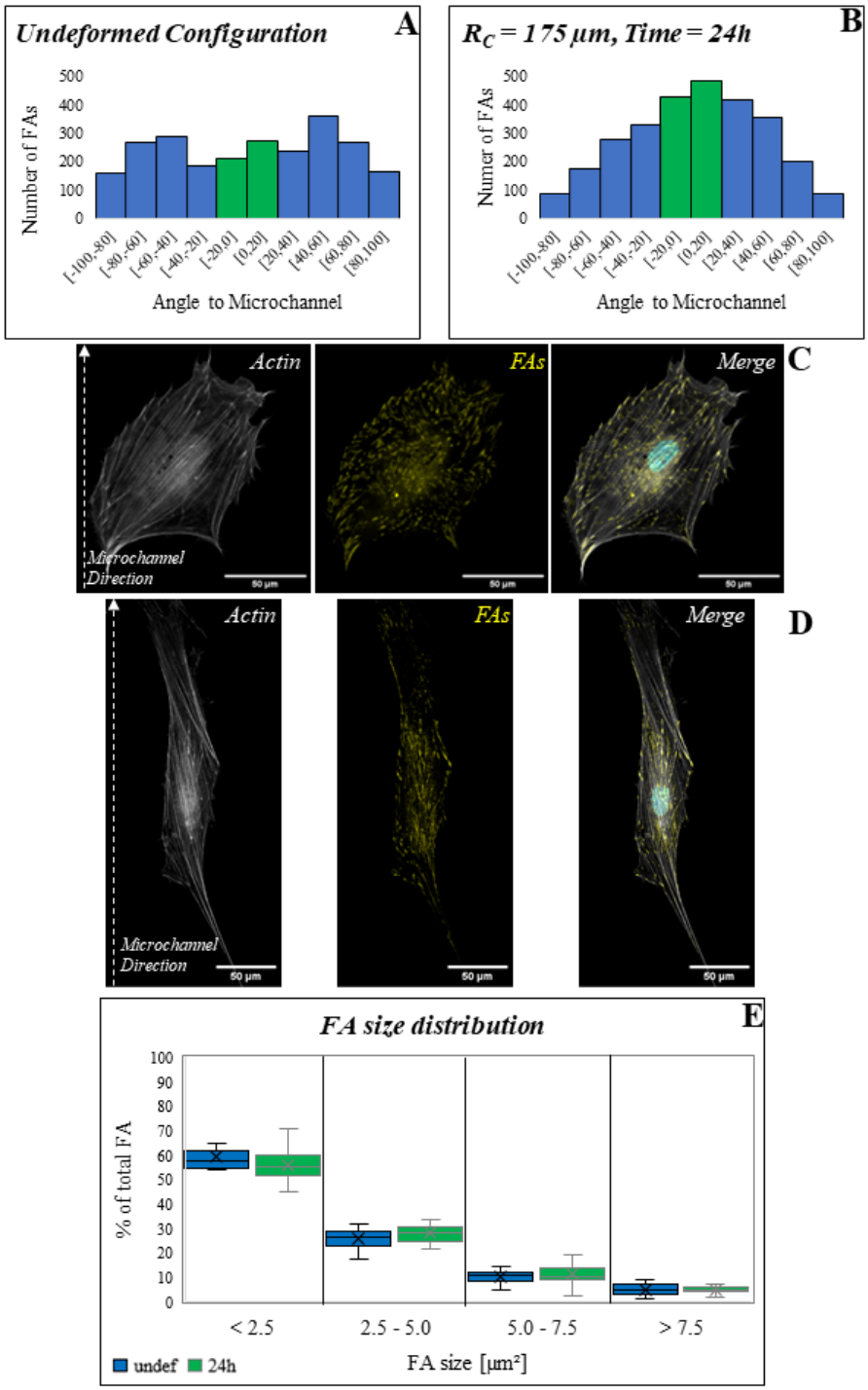
A
Undeformed Configuration
Number of FAs
500
400
300
200
100
0
[-100,-80]
[-80,-60]
[-60,-40]
[-40,-20]
[-20,0]
[0,20]
[20,40]
[40,60]
[60,80]
[80,100]
Angle to Microchannel
B
$R_C = 175\ \mu m$, Time = 24h
Numer of FAs
Angle to Microchannel
C
Actin
FAs
Merge
Microchannel Direction
50 µm
D
E
FA size distribution
% of total FA
100
90
80
70
60
50
40
30
20
10
0
< 2.5
2.5 - 5.0
5.0 - 7.5
> 7.5
undef
24h
FA size [µm²]

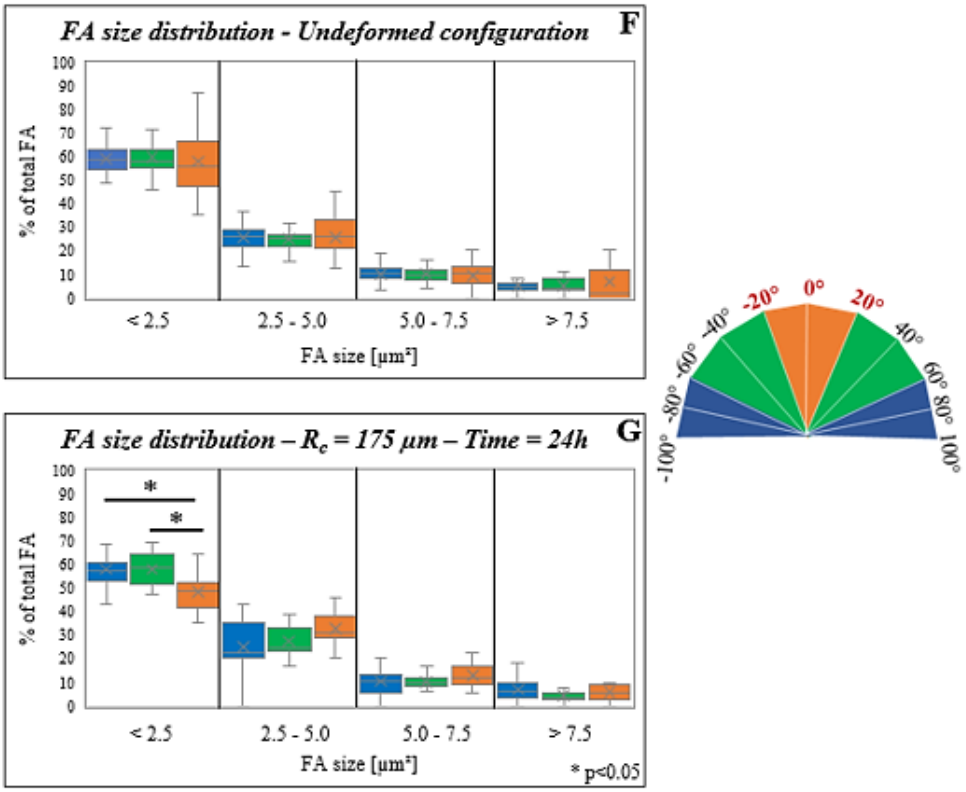

*Figure 3.14: Focal adhesions (FAs) behaviour induced by a curvature variation of 0.0057 μm^{-1} on the microfluidic platform. A-B: Histograms showing FAs polarization with respect to the microchannel direction (0°) into flat (A) and deformed (B) configurations. C: Confocal acquisition of a single adipose derived mesenchymal stem cell into undeformed configuration. Gray: Actin Cytoskeleton, Yellow: Focal Adhesions, Cyan: Nucleus. Scale bar: 50 µm. D: Confocal acquisition of a single adipose derived mesenchymal stem cell into deformed configuration. Gray: Actin Cytoskeleton, Yellow: Focal Adhesions, Cyan: Nucleus. Scale bar: 50 µm. E-G: Focal adhesions size distribution. E: Comparison of FA size distribution between deformed and deformed configuration. F: FA size distribution in function of polarization angle into undeformed configuration. G: FA size distribution in function of polarization angle into deformed configuration. Data are expressed as mean value ± standard deviation and each experiment was repeated three times on independent microfluidic platform. * $p<0.05$.*

3.3.4.6 Focal adhesions response to R_c = 151 µm

The last but not least case was that related to FAs response to a curvature radius of 151 µm. Also in this configuration the curved membrane was able to control the FAs polarization; that is, from a random orientation into undeformed configuration (Figure 3.15A) to a well-polarized FAs (Figure 3.15B) along the longitudinal axis after 24 h.

Observing the confocal images, both actin stress fibers and FAs are aligned with microchannel direction (Figure 3.15D) into deformed configuration with respect to undeformed one (Figure 3.15C).

In terms of size distribution (Figure 3.15E), statistically significant differences were occurred only for small FAs ($\leq$ 2.5 µm²) between flat and curved cases.

Furthermore, a detailed study of FA size distribution in function of their orientation was made for each configuration: undeformed and deformed. The former (Figure 3.15F) was characterized by non-statistical differences between the different ranges. Otherwise, the latter (Figure 3.15G) has relevant statistical differences. Starting from FAs size $\leq$ 2.5 µm², relevant statistical changes occurred between FAs polarized along the channel and other intervals. The percentage reduction of polarized small FAs was correlated with an increase of FAs size in other ranges. In fact, for [2.5 – 5] µm², [5 – 7.5] µm² and $\geq$ 7.5 µm² the percentage of polarized FAs was higher than the orthogonal ones.

So, in agreement with the results obtained for R_C = 175 µm, this specific mechanical insult was able to control the architecture of both actin stress fibers and FAs observing ASCs more stable when aligned along the microchannel direction generated by an anisotropic/uniaxial mechanical stretching.

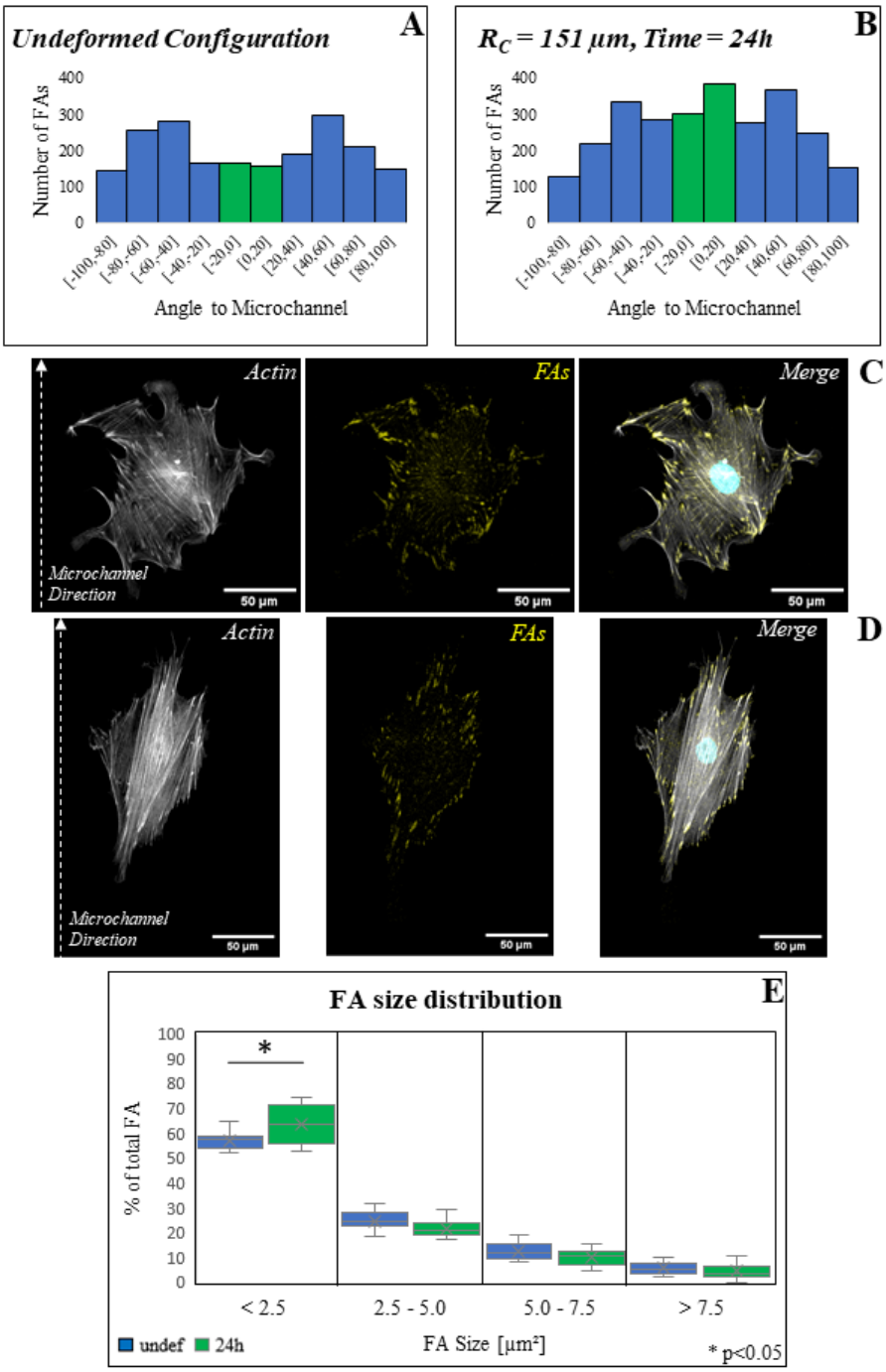
A
Undeformed Configuration
Number of FAs
400
300
200
100
0
[-100,-80]
[-80,-60]
[-60,-40]
[-40,-20]
[-20,0]
[0,20]
[20,40]
[40,60]
[60,80]
[80,100]
Angle to Microchannel
B
R_C = 151 μm, Time = 24h
Number of FAs
Angle to Microchannel
C
Actin
FAs
Merge
Microchannel Direction
50 μm
D
Actin
FAs
Merge
Microchannel Direction
50 μm
E
FA size distribution
% of total FA
100
90
80
70
60
50
40
30
20
10
0
*
< 2.5
2.5 - 5.0
5.0 - 7.5
> 7.5
undef
24h
FA Size [μm²]
* p<0.05

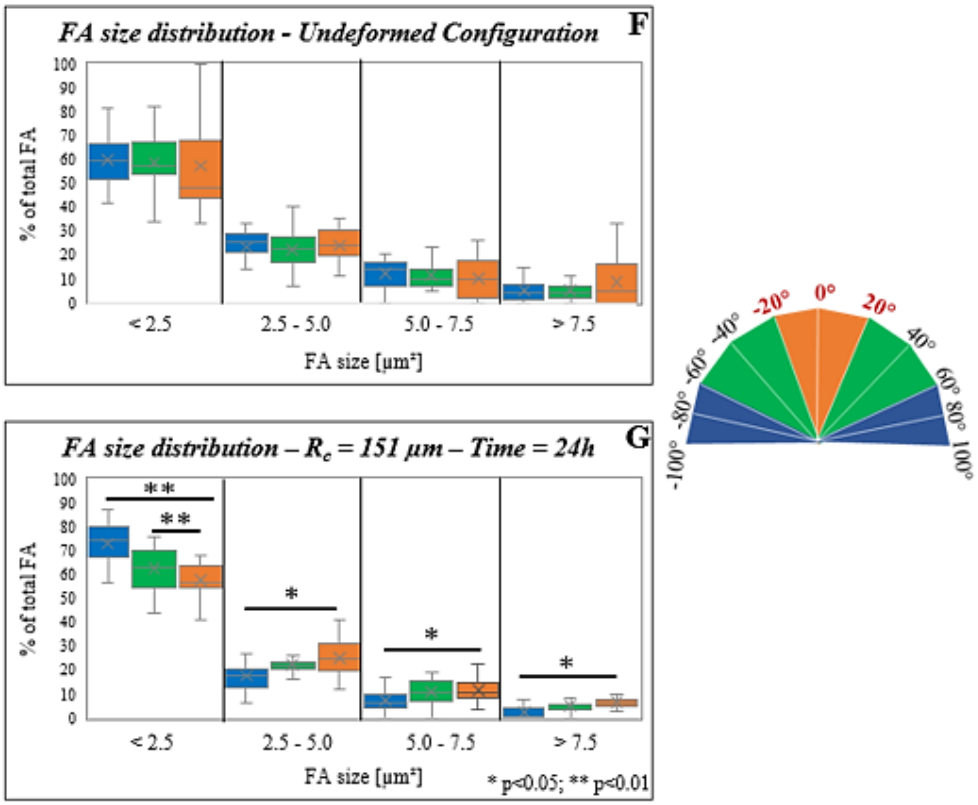

*Figure 3.15: Focal adhesions (FAs) behaviour induced by a curvature variation of 0.0066 µm^{-1} on the microfluidic platform. A-B: Histograms showing FAs polarization with respect to the microchannel direction (0°) into flat (A) and deformed (B) configurations. C: Confocal acquisition of a single adipose derived mesenchymal stem cell into undeformed configuration. Gray: Actin Cytoskeleton, Yellow: Focal Adhesions, Cyan: Nucleus. Scale bar: 50 µm. D: Confocal acquisition of a single adipose derived mesenchymal stem cell into deformed configuration. Gray: Actin Cytoskeleton, Yellow: Focal Adhesions, Cyan: Nucleus. Scale bar: 50 µm. E-G: Focal adhesions size distribution. E: Comparison of FA size distribution between deformed and deformed configuration. F: FA size distribution in function of polarization angle into undeformed configuration. G: FA size distribution in function of polarization angle into deformed configuration. Data are expressed as mean value ± standard deviation and each experiment was repeated three times on independent microfluidic platform. * p<0.05 ** p<0.01.*

3.4 Discussion and Conclusions

The microfluidic platform was designed to study the influence of curvature on low-density human adipose derived mesenchymal stem cells. Particularly, the role of curvature on actin stress fibers re-organization and focal adhesions response to different mechanical cues has been analysed.

Applying a static uniaxial mechanical signal along the longitudinal direction of the microfluidic channel, an actin stress fibers re-organization was observed when the membrane curvature results equal to 0.0045 μm^{-1}; on the contrary a polarization of FAs along the longitudinal axis was obtained with a greater curvature of 0.0057 μm^{-1}. These behaviours are localized only on the central part of the microfluidic channel, indicating that only the ASCs adhered in this region are able to respond to this mechanical stimulus. A heterogeneous response for all the different mechanical configurations in both cytoskeletal and FA rearrangements occurred on the lateral parts.

These results are supported by previous findings in which high-density cells tend to align along the direction of uniaxial stress when appropriately stimulated [14,15], which accords well to the common knowledge that cells elongate along given chemical or physical structural patterns [16-20]. The actin cytoskeleton filaments and FAs polarization along the longitudinal axis indicates the preferential organization of the cell along the minimum curvature surface. In fact, from a cellular point of view, in the central part of the curved PDMS membrane, the amplitude of curvature results smaller with respect to the side regions. Also the stresses and strains of the PDMS membrane in the curved profile result homogeneous in the middle part than in the lateral ones. In this regard, curvature-controlled cell orientation has been postulated to be a consequence of the energetic optimization of the actomyosin stress fibers aiming to minimize their deformation [21,22]. Stress fibers in a bent configuration require more energy to maintain a curved morphology and a functional cytoskeleton due to the fragmentation of the F-actin fibers [22-24], thus limiting the capacity of the cell to adopt unfavourable curvatures [25] and inducing a preferred migration towards longitudinal direction [9].

The FAs create an adhesive contact between the cell and the ECM in order to mediate the link between them and permit the propagation of mechanical signals [26]. The FA size distributions show statistically significant variations of FA dimension in function of

their orientation for high curvature profile. As well known, the dimension of FAs results a useful parameter to divide them into nascent and mature focal complexes [27,28]. The fact that, for high curvature configurations, the larger structures are aligned with the longitudinal direction with respect to the smaller ones directed in the orthogonal way means that these specific profiles are able to vehiculate the focal adhesions formation. That is, the curvature discourages the formation of mature focal adhesions in the direction of the radius of curvature and at the same time favours their formation in the longitudinal direction. Larger FAs allowed to exert significantly higher forces on the actin stress fibers with respect to the smaller ones [13,29,30].

So, the continuous interplay between ECM, FAs, and actin stress fibers, but more generally cytoskeleton filaments, permit to single ASCs to respond in a specific way to each mechanical insult applied.

Consequently, the novelties related to this project are: (i) the design of a microfluidic platform accessible in real time to the confocal microscopy in order to observe co-transfected live cells; (ii) the analysis of ASCs at low seeding densities useful for understanding in detail the role played by the mechanical stimuli on the response of the cytoskeleton and of FAs on single cells; (iii) the choice of the cell line (human mesenchymal stem cells extracted by patients' adipose tissue) and, as a consequence, the importance to understand its mechanosensing and mechanotransduction pathways, due to the enormous potential of stem cells in the field of mechanobiology, regenerative medicine, tissue engineering, and so on.

It is known from literature [14,15] that uniaxial stimuli on cells with high seeding densities induce an alignment in the longitudinal direction but a heterogeneous behaviour was observed at low seeding densities for the same mechanical cues [14]. Given the lack of such information on the response of single stem cells to such mechanical stimuli, this project aims at increasing knowledge on the mechanisms that control stem cell ability to perceive them and to mechano-adapt by controlling cytoskeleton and FA organization. Obviously, the cells in living systems are not subjected to a static mechanical stimulation, but, generally, they are involved in periodic dynamic one, so a study of cyclic dynamic mechanical stimulation on low-density ASCs was developed and explained in the next chapter.

References

[1] Li, Linqing, Jeroen Eyckmans, and Christopher S. Chen. "Designer biomaterials for mechanobiology." *Nature materials* 16.12 (2017): 1164-1168.

[2] Vining, Kyle H., and David J. Mooney. "Mechanical forces direct stem cell behaviour in development and regeneration." *Nature reviews Molecular cell biology* 18.12 (2017): 728-742.

[3] Meirelles, Lindolfo da Silva, Pedro Cesar Chagastelles, and Nance Beyer Nardi. "Mesenchymal stem cells reside in virtually all post-natal organs and tissues." *Journal of cell science* 119.11 (2006): 2204-2213.

[4] Lee, Ryang Hwa, et al. "Characterization and expression analysis of mesenchymal stem cells from human bone marrow and adipose tissue." *Cellular physiology and biochemistry* 14.4-6 (2004): 311-324.

[5] Mizuno, Hiroshi, Morikuni Tobita, and A. Cagri Uysal. "Concise review: adipose-derived stem cells as a novel tool for future regenerative medicine." *Stem cells* 30.5 (2012): 804-810.

[6] Markarian, Carolina Franke, et al. "Isolation of adipose-derived stem cells: a comparison among different methods." *Biotechnology letters* 36.4 (2014): 693-702.

[7] Geiger, Benjamin, Joachim P. Spatz, and Alexander D. Bershadsky. "Environmental sensing through focal adhesions." *Nature reviews Molecular cell biology* 10.1 (2009): 21-33.

[8] Shemesh, Tom, et al. "Focal adhesions as mechanosensors: a physical mechanism." *Proceedings of the National Academy of Sciences* 102.35 (2005): 12383-12388.

[9] Pieuchot, Laurent, et al. "Curvotaxis directs cell migration through cell-scale curvature landscapes." *Nature communications* 9.1 (2018): 1-13.

[10] Kim, Dong-Hwee, and Denis Wirtz. "Predicting how cells spread and migrate: focal adhesion size does matter." *Cell adhesion & migration* 7.3 (2013): 293-296.

[11] Mitra, Satyajit K., Daniel A. Hanson, and David D. Schlaepfer. "Focal adhesion kinase: in command and control of cell motility." *Nature reviews Molecular cell biology* 6.1 (2005): 56-68.

[12] Kadrmas, Julie L., and Mary C. Beckerle. "The LIM domain: from the cytoskeleton to the nucleus." *Nature reviews Molecular cell biology* 5.11 (2004): 920-931.

[13] Martino, Fabiana, et al. "Cellular mechanotransduction: from tension to function." *Frontiers in physiology* 9 (2018): 824.

[14] Yamashita, Tadahiro, et al. "Air-pressure-driven separable microdevice to control anisotropic curvature of cell culture surface." *Analytical Sciences* (2020): 20A001.

[15] Zhou, Jing, and Laura E. Niklason. "Microfluidic artificial "vessels" for dynamic mechanical stimulation of mesenchymal stem cells." *Integrative Biology* 4.12 (2012): 1487-1497.

[16] Jeon, H., C. G. Simon Jr, and G. J. Kim. "Biomed Mater Res." *Part B* 102 (2014): 1580-1594.

[17] Iannone, Maria, et al. "Nanoengineered surfaces for focal adhesion guidance trigger mesenchymal stem cell self-organization and tenogenesis." *Nano letters* 15.3 (2015): 1517-1525.

[18] Ventre, Maurizio, and Paolo A. Netti. "Engineering cell instructive materials to control cell fate and functions through material cues and surface patterning." *ACS applied materials & interfaces* 8.24 (2016): 14896-14908.

[19] Ventre, Maurizio, et al. "Topographic cell instructive patterns to control cell adhesion, polarization and migration." *Journal of the royal society Interface* 11.100 (2014): 20140687.

[20] Saporito, Stefania, et al. "A role for nuclear stretching and NPCs changes in the cytoplasmic-nuclear trafficking of YAP: An experimental and numerical modelling approach." *Materials Today Bio* 15 (2022): 100335.

[21] Vicente-Manzanares, Miguel, et al. "Non-muscle myosin II takes centre stage in cell adhesion and migration." *Nature reviews Molecular cell biology* 10.11 (2009): 778-790.

[22] Dunn, G. A., and JP182511 Heath. "A new hypothesis of contact guidance in tissue cells." *Experimental cell research* 101.1 (1976): 1-14.

[23] Bade, Nathan D., et al. "Gaussian curvature directs stress fiber orientation and cell migration." *Biophysical journal* 114.6 (2018): 1467-1476.

[24] Biton, Y. Y., and S. A. Safran. "The cellular response to curvature-induced stress." *Physical biology* 6.4 (2009): 046010.

[25] Bade, Nathan D., et al. "Curvature and Rho activation differentially control the alignment of cells and stress fibers." *Science advances* 3.9 (2017): e1700150.

[26] Stutchbury, Ben, et al. "Distinct focal adhesion protein modules control different aspects of mechanotransduction." *Journal of cell science* 130.9 (2017): 1612-1624.

[27] Kim, Dong-Hwee, and Denis Wirtz. "Focal adhesion size uniquely predicts cell migration." *Biophysical Journal* 104.2 (2013): 319a.

[28] Wehrle-Haller, Bernhard. "Structure and function of focal adhesions." *Current opinion in cell biology* 24.1 (2012): 116-124.

[29] Sigaut, Lorena, et al. "Correlation of cellular traction forces and dissociation kinetics of adhesive protein zyxin revealed by multi-parametric live cell microscopy." *Plos one* 16.5 (2021): e0251411.

[30] Burridge, Keith, and Christophe Guilluy. "Focal adhesions, stress fibers and mechanical tension." *Experimental cell research* 343.1 (2016): 14-20.

Chapter 4

Adipose stem cell behaviour to cyclic mechanical cues: cytoskeleton and focal adhesions response

4.1 Introduction

At the cellular level, the mechanical stimuli can act as a key driver in the regulation of cellular functions such as cellular differentiation, polarization, migration, and proliferation [1-3]. This occurs thank to two specific cells abilities known as mechanosensing and mechanotransduction, that are defined as the capacity of a cell to sense and to transduce a mechanical cue into a biochemical response, respectively [4-6]. These mechanical signals can be either intracellular or extracellular forces generated by the continuous interaction between cells and extracellular matrix. The physical pathway between ECM-cytoskeleton-nucleus responsible of mechanical stimuli propagation is well known; conversely, how the mechanical cues are transduced into biochemical ones remains an open challenge [7,8].

As previously introduced, the cells are able to discriminate between planar, convex, and concave surfaces. Moreover, there is a spatio-temporal dependence in the influence of cell response from its surrounding environment which has to be considered [9,10]. In fact, in the body, cells especially those from blood, bone marrow, lungs, heart, and musculoskeletal tissues, are subjected to cyclic mechanical loading.

Generally, to mimic such mechanical microenvironment, the controlled stress/strain is applied to cell-seeded biomaterials designing specific microfluidic devices. Different microfluidic platforms have been designed in order to apply uniaxial [11,12] or biaxial [13-18] cyclic mechanical cues on high density cell-seeded membranes at specific frequencies. One of the most studied frequencies of cyclic mechanical loading is 1Hz, which corresponds to the frequency to which cells and tissues of the vascular and musculoskeletal systems are subjected. Seeding the cells in high-density conditions, a

polarization along the longitudinal direction was induced by uniaxial cyclic mechanical stimulation [11,12] but the same result was not observed on low cell seeding cases [12]. Moreover, to evaluate the cellular polarization in confluent conditions, the nuclear orientation with respect to the stimulation direction has been quantified [11,12]

Since it is not clear the role played by cyclic curvature variations on low-density cells, particularly the response of actin cytoskeleton and FAs to these specific signals, the microfluidic platform, previously introduced, has been used to dynamically stimulate these cells. Particularly, the response of ASCs was studied in flat conditions and 24 h after the application of the dynamic mechanical cues. As detailed explained in the chapter 3, a polarization of both actin stress fibers and FAs along the longitudinal axis occurred with a curvature of 0.0057 μm^{-1}. So, applying this specific curvature variation in a dynamic manner, the actin stress fibers and FAs response was acquired after 24 h.

In detail, three different stimulation periods (T) have been studied: (i) T = 1s (duty cycle 50%), (ii) T = 1 min (duty cycle 50%), (iii) T = 10 min (duty cycle 50%) applying a curvature variation of 0.0057 μm^{-1}. In this way we tried to understand how the periodicity could influence the cellular response to a specific mechanical signal which is known to be able to manipulate cellular and focal adhesions polarization in stationary conditions.

4.2 Materials and Methods

As previously introduced in the materials and methods sections of the chapter 3, the ASCs have been extracted from human adipose tissue (section 3.2.1), electroporated (section 3.2.3) and seeded (5000 cells/cm^2 – low cell density) (section 3.2.5) on fibronectin-functionalized microfluidic platforms.

The only difference for these experiments with respect to the previous ones resides in the mechanical stimulation applied. In fact, in the previous chapter, the role of curvature variation on actin stress fibers and focal adhesions responses was analyzed in static mechanical configuration for different curvatures. Conversely, here the response of these structures in cyclic mechanical conditions has been considered. Three different stimulation periods were tested: T = 1 s, T = 1 min and T = 10 min applying for the all T(s) the same curvature variation. Starting from T = 1 s, the cell-seeded microfluidic platform was linked to the pressure controller OB1 in order to apply a curvature variation

of 0.0057 μm^{-1} (R_C = 175 μm) each second with a duty cycle of 50% for 24 h. At the end of cyclic mechanical stimulation, the actin stress fibers and FAs responses have been opportunely acquired with a confocal microscope using the strategy explained in section 3.2.7. The same approach was used for T = 1 min and T = 10 min where the only difference was the stimulation period. In fact, the single ASCs were periodically stimulated each minute or each 10 minutes with a duty cycle of 50% modifying the curvature of 0.0057 μm^{-1}. Every experiment was repeated three different times on independent microfluidic platforms; particularly, at least, 70 cells/device were acquired to study the response of actin cytoskeleton filaments and at least 7 cells/device to study the FAs behaviour. Using histograms and box and whisker plots, a detailed analysis of size and polarization on actin fibers and FAs was performed. All data are reported as mean ± standard deviation and a statistical comparison was made with ANOVA followed by Tukey's test for multiple comparisons. P values of < 0.01 (**) or < 0.05 (*) denote statistically significant differences.

4.3 Results

4.3.1 Actin cytoskeleton reorganization induced by cyclic dynamic changes of cell-seeded membrane curvature

Cellular cytoskeleton is highly involved in the mechanosensing and mechanotransduction mechanisms due to its linkage with focal adhesions and nuclear membrane.

In fact, the mechanical signals propagate from the extracellular matrix to the nucleus through the actin stress fibers, microtubules, and intermediate filaments. Particularly, the actin stress fibers are able to re-organize their orientation and structure as a response to a specific mechanical cue. Moreover, cells in living systems are continuously subjected to cyclic mechanical signals and the understanding of actin cytoskeleton re-organization induced by a specific cyclic mechanical insult could be very useful. Indeed, it is clear the physical pathways through mechanical signals are able to propagate from the ECM to the nucleus and *viceversa*, but how these are transduced in biochemical ones remains unknown.

So, to study the actin stress fibers response to a specific cyclic mechanical stimulation, a curvature variation of 0.0057 μm^{-1} was applied in different periodicities. This curvature

has been chosen because, as previously explained in the Chapter 3, it is able to induce an actin filaments re-polarization along the longitudinal direction of the microchannel into a static mechanical configuration.
In order to analyse in detail the actin stress fibers response to each tested periodicity, every case will be detailed studied in the next paragraphs.

4.3.1.1 Actin stress fibers response to R_C = 175 µm – T = 1 s

On three different independent microfluidic platforms, the response of actin stress fibers to a cyclic mechanical curvature variation of 0.0057 μm^{-1} (R_C = 175 µm) was studied. Particularly, this stimulus was applied with a periodicity of 1 s and a duty cycle of 50% for 24 h on low-density adipose derived mesenchymal stem cells. In this way, the cellular and cytoskeletal responses are not influenced by cell-cell interaction.
In undeformed configuration, the actin stress fibers and, as a consequence ASCs cells, have a random polarization with respect to the microfluidic channel (0°) direction (Figure 4.1A). Then, 24h after the application of this specific cyclic mechanical insult, all cells are polarized along the longitudinal direction (Figure 4.1B). From the 3D FEM model the von Mises stress and strain distributions along the radius of curvature direction have been calculated. The former is constant in the central part ≈ 86 kPa and heterogeneous in the side parts [109-415] kPa (Figure 4.1C, S2I-L); and the latter has the same colour map with approximatively 14.4% strain in the central part and [14.4 – 60.1] % on the lateral ones (Figure 4.1D, S3I-L).
Since the stress and strain fields are generated not only by the pressure applied on the microfluidic platform, but also by the side effects created by the irreversible bonding between PMMA and PDMS layers, the actin stress fibers response was studied in specific microchannel regions in both undeformed and deformed cases in order to take or not into account all these effects.
On the lateral parts, the actin cytoskeleton randomly organized in the undeformed configuration (Figure 4.1E) became highly polarized along the longitudinal axis at the end of mechanical stimulation (Figure 4.1F). An analogous result was observed in the central part. From a heterogeneous organization of cells in flat cases (Figure 4.1G) up to a well-oriented actin cytoskeleton along the microfluidic direction after 24 h of

stimulation (Figure 4.1H). These results show that, independently from the microchannel regions analyzed, the cyclic curvature variation was able to induce an actin cytoskeleton re-organization in the direction of uniaxial stretching. This means that the amplitude and, particularly, the periodicity of the stimulation applied control the ASCs polarization. Unlike the previously analyzed static case (3.3.2.5 Section) in which edge effects had a key role on the cytoskeleton un-polarization on lateral regions, in this case they can be neglected and there are not differences on the cellular and actin stress fibers response between central and side sectors of the microchannel.

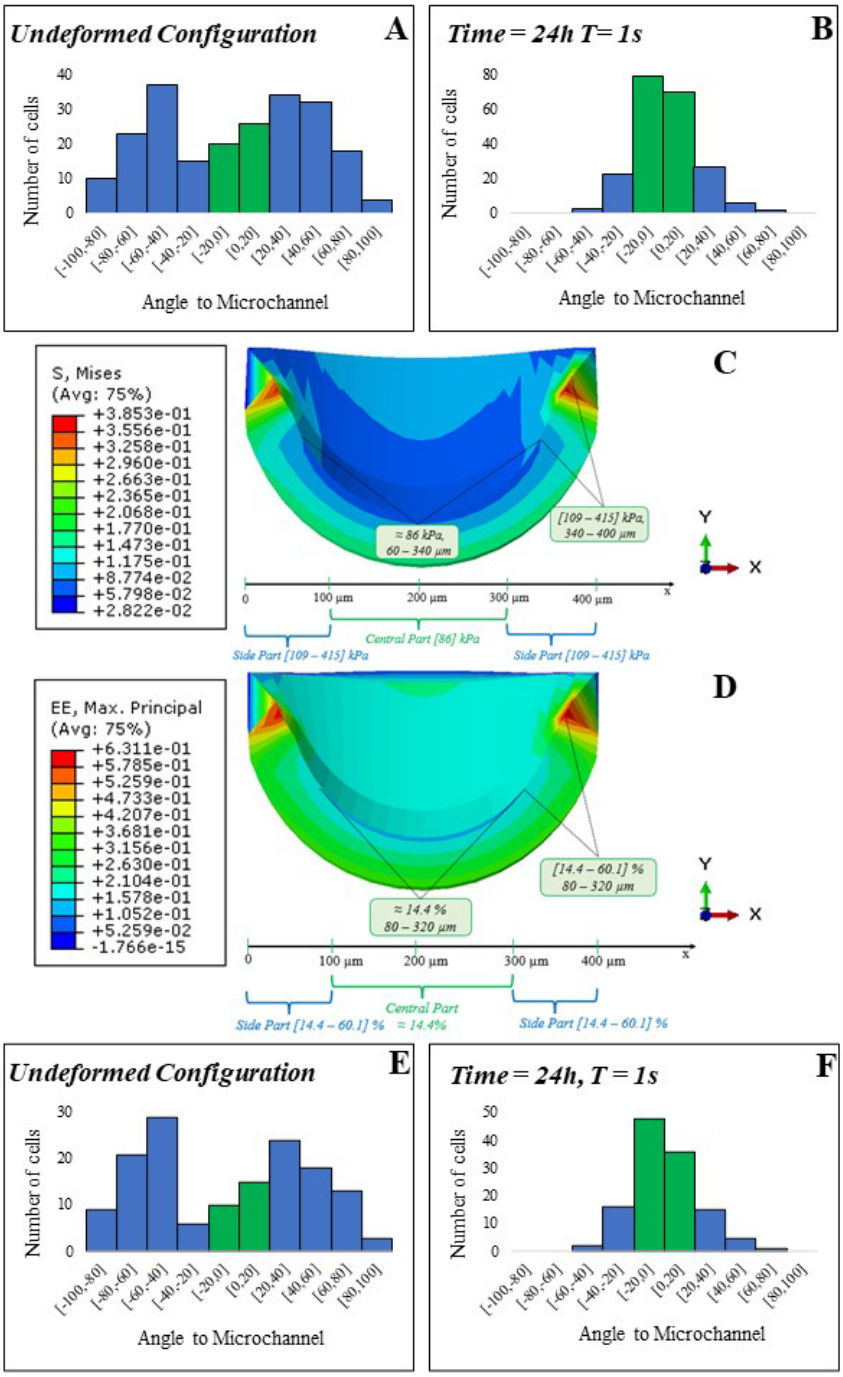
Undeformed Configuration
A
Number of cells
Angle to Microchannel
Time = 24h T= 1s
B
Number of cells
Angle to Microchannel
S, Mises
(Avg: 75%)
+3.853e-01
+3.556e-01
+3.258e-01
+2.960e-01
+2.663e-01
+2.365e-01
+2.068e-01
+1.770e-01
+1.473e-01
+1.175e-01
+8.774e-02
+5.798e-02
+2.822e-02
C
≈ 86 kPa,
60 – 340 µm
[109 – 415] kPa,
340 – 400 µm
Y
X
0
100 µm
200 µm
300 µm
400 µm
x
Central Part [86] kPa
Side Part [109 – 415] kPa
Side Part [109 – 415] kPa
EE, Max. Principal
(Avg: 75%)
+6.311e-01
+5.785e-01
+5.259e-01
+4.733e-01
+4.207e-01
+3.681e-01
+3.156e-01
+2.630e-01
+2.104e-01
+1.578e-01
+1.052e-01
+5.259e-02
-1.766e-15
D
[14.4 – 60.1] %
80 – 320 µm
≈ 14.4 %
80 – 320 µm
Y
X
0
100 µm
200 µm
300 µm
400 µm
x
Central Part
Side Part [14.4 – 60.1] %
≈ 14.4%
Side Part [14.4 – 60.1] %
Undeformed Configuration
E
Number of cells
Angle to Microchannel
Time = 24h, T = 1s
F
Number of cells
Angle to Microchannel

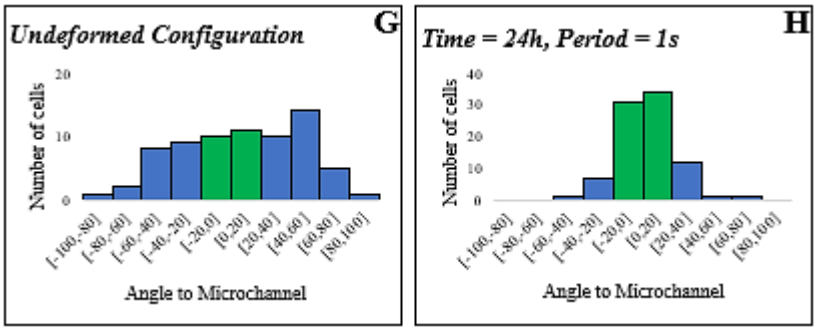

Figure 4.1: Adipose stem cells behaviour induced by a curvature variation of 0.0057 μm^{-1} with a period T of 1s on the microfluidic platform. A-B: Histograms showing ASCs polarization with respect to the microchannel direction (0°) into flat (A) and deformed (B) configurations. C: von Mises stress distribution on the curved cell-seeded PDMS membrane (colour map express the von Mises stress in MPa) D: maximum elastic strain distribution on the curved cell-seeded PDMS membrane (colour map express the strain in a-dimensional way. E-F: Histograms showing ASCs polarization with respect to the microchannel direction (0°) into flat (E) and deformed (F) configurations on the lateral regions. G-H: Histograms showing ASCs polarization with respect to the microchannel direction (0°) into flat (G) and deformed (H) configurations on the central region.

4.3.1.2 Actin stress fibers response to R_C = 175 µm – T = 1min

A cyclic dynamic mechanical curvature variation of 0.0057 μm^{-1} (R_C = 175 µm) was applied on low-density ASCs with a periodicity of 1 min and a duty cycle of 50%.

As a result, starting from a random actin cytoskeleton polarization in flat condition (Figure 4.2A), a well polarized cytoskeleton along the uniaxial stretching direction was observed at the end of 24 h stimulation (Figure 4.2B). In terms of von Mises stress and strain distribution, there are the same ranges, previously introduced (Figure 4.2C-D, S2I-L, S3I-L).

In fact, compared to the above case, there are no differences in terms of the amplitude of the applied curvature, but rather in terms of stimulation periodicity.

Due to the side effects, the ASCs polarization was detailed studied in the different regions of the microfluidic platform: side parts and central one.

In the former, a heterogeneous polarization of actin stress fibers has occurred in both undeformed and 24 h deformed configurations (Figure 4.2E-F). Conversely, in the latter, starting from a heterogeneous cell orientation (Figure 4.2G), well-polarized stem cells were observed after 24 h of cyclic mechanical stimulation (Figure 4.2H).

The results obtained with a periodicity of 1 min are similar to that described in 3.3.2.5 section, where the same curvature variation was applied in static conditions. Using this

periodicity (1 min), the side effects on the lateral parts cannot be neglected observing a different response between the different microchannel regions.

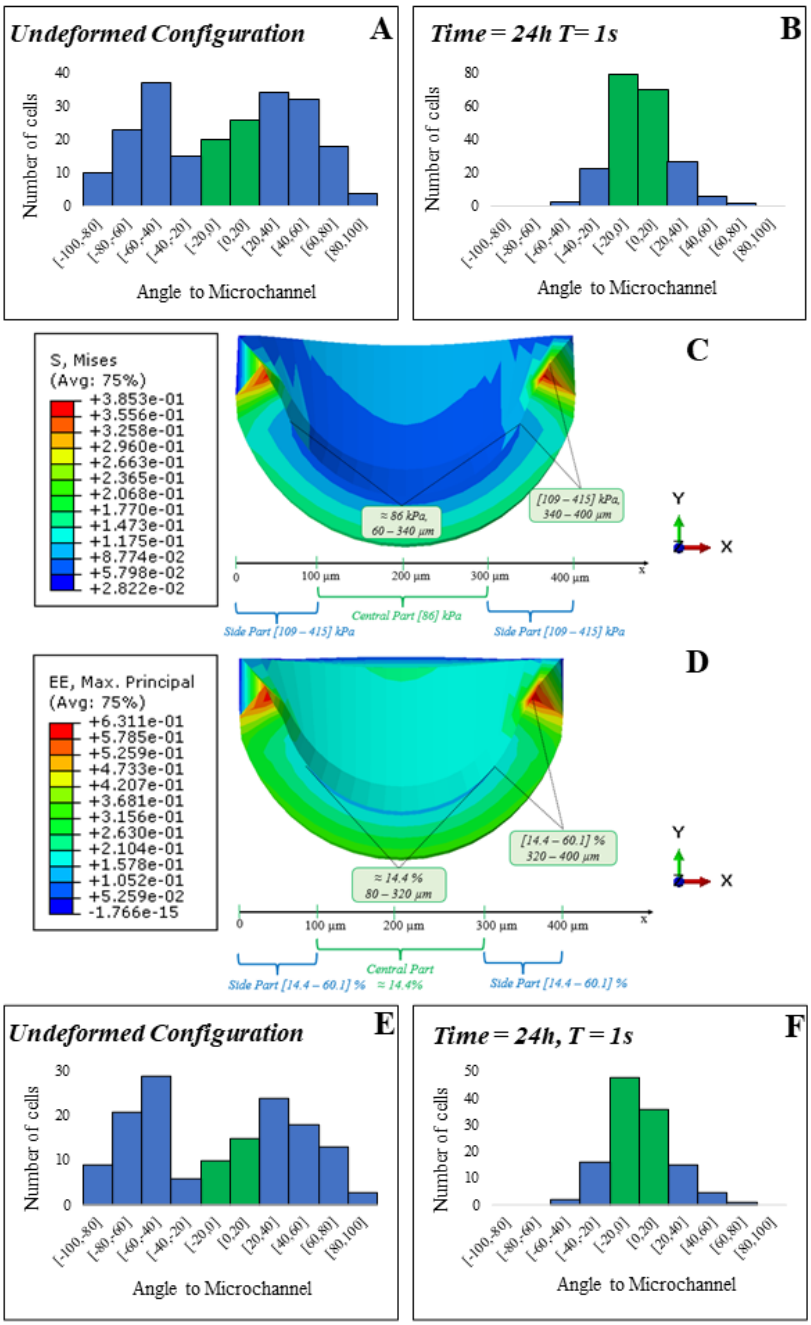

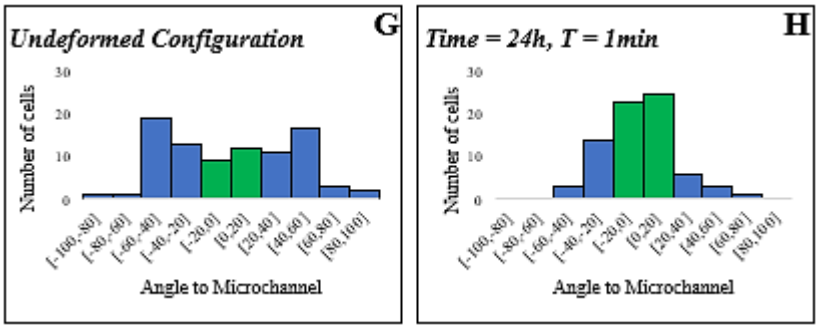

Figure 4.2: Adipose stem cells behaviour induced by a curvature variation of 0.0057 μm^{-1} with a period T of 1min on the microfluidic platform. A-B: Histograms showing ASCs polarization with respect to the microchannel direction (0°) into flat (A) and deformed (B) configurations. C: von Mises stress distribution on the curved cell-seeded PDMS membrane (colour map express the von Mises stress in MPa) D: maximum elastic strain distribution on the curved cell-seeded PDMS membrane (colour map express the strain in a-dimensional way. E-F: Histograms showing ASCs polarization with respect to the microchannel direction (0°) into flat (E) and deformed (F) configurations on the lateral regions. G-H: Histograms showing ASCs polarization with respect to the microchannel direction (0°) into flat (G) and deformed (H) configurations on the central region.

4.3.1.3 Actin stress fibers response to R_C = 175 µm – T = 10 min

To test the role of cyclic mechanical insults on single ASCs cytoskeleton response, specific signals with a periodicity of 10 min and a curvature variation of 0.0057 μm^{-1} were studied. Starting from a random cytoskeleton organization in flat condition (Figure 4.3A), a response of cells was observed after 24 h of stimulation (Figure 4.3B). Particularly, there is an increase in the number of cells aligned along the longitudinal direction with respect to the undeformed configuration, but the differences are not that significant. That is, the cyclic mechanical insults are able to induce a re-organization of actin stress fibers, but the cells are not consistently aligned along the direction of uniaxial stretching. The von Mises stress and strain distributions (Figure 4.3C-D, S2I-L, S3I-L) are always the same but developed on PDMS membrane with a periodicity different with respect to the previous cases.

To analyse in detail the ASCs response, their behaviour was studied on the central and lateral parts of the microfluidic channel. Starting from side parts, a random actin stress fiber polarization has occurred in both undeformed (Figure 4.3E) and 24 h deformed (Figure 4.3F) configurations. A similar result was obtained on the central region of the channel between the two cases (Figure 4.3G-H), even if into stimulated configuration a slight polarization along the uniaxial stretching direction was observed.

So, the periodicity of mechanical stimulation plays a vital role on the adipose stem cell response. In fact, even if the curvature variation applied was able to control the actin cytoskeleton organization in static conditions, in dynamic ones the response depends on the period with which curvature variation occurred. In conclusion, not only the mechanical stimulus in terms of amplitude but also the way in which it is applied are responsible for cellular behaviour.

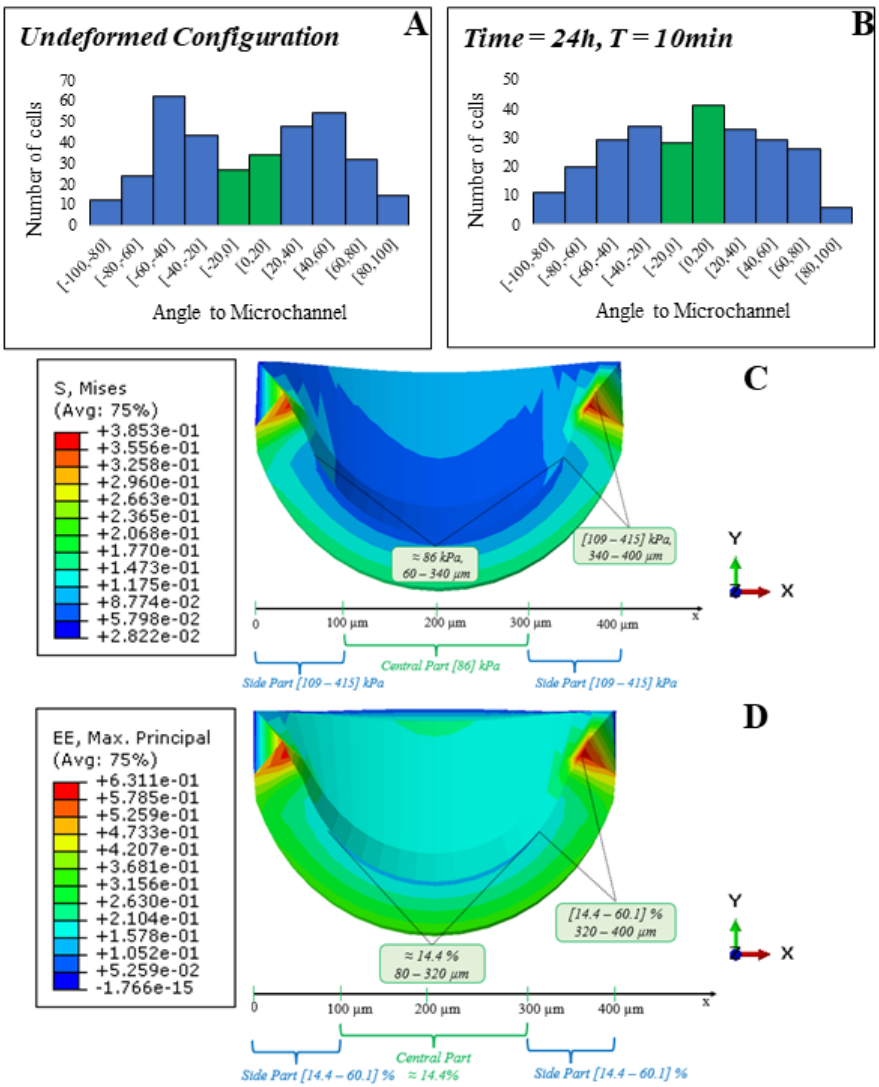

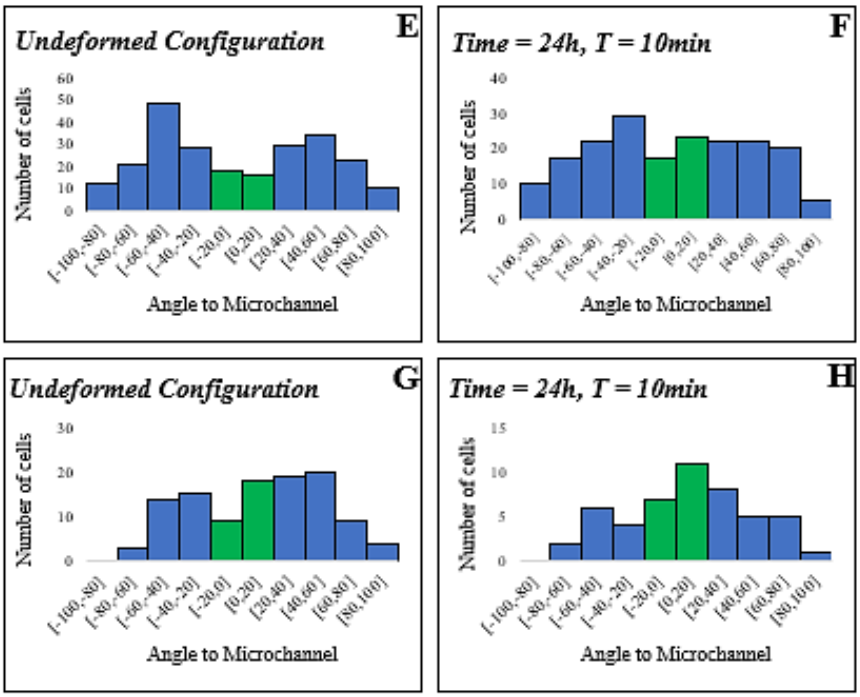

Figure 4.3: Adipose stem cells behaviour induced by a curvature variation of 0.0057 μm^{-1} with a period T of 10min on the microfluidic platform. A-B: Histograms showing ASCs polarization with respect to the microchannel direction (0°) into flat (A) and deformed (B) configurations. C: von Mises stress distribution on the curved cell-seeded PDMS membrane (colour map express the von Mises stress in MPa) D: maximum elastic strain distribution on the curved cell-seeded PDMS membrane (colour map express the strain in a-dimensional way. E-F: Histograms showing ASCs polarization with respect to the microchannel direction (0°) into flat (E) and deformed (F) configurations on the lateral regions. G-H: Histograms showing ASCs polarization with respect to the microchannel direction (0°) into flat (G) and deformed (H) configurations on the central region.

4.3.2 Cell morphology induced by cyclic dynamic changes of cell-seeded membrane curvature

To understand the response of single adipose derived mesenchymal stem cells to cyclic dynamic mechanical cues applied as curvature variation, the cellular morphology has been studied. Particularly, the occupied cell area on PDMS membrane could be modified as a consequence of dynamic curvature change. Knowing the von Mises stress and strain fields generated by the curvature modification, the microchannel was divided into three different regions: two lateral parts and a single central one. On these sections, the cell area distribution between the undeformed and deformed configurations was analyzed.

Starting from the cell area observed with a curvature variation of 0.0057 μm^{-1} and a period of stimulation of 1 s (Figure 4.4A), a statistically significant difference was

observed on the side parts between flat and mechanically stimulated cases. Conversely, non-statistically significant evidence occurred in the central part. As previously explained in the section 4.3.1.1, the actin stress fibers of ASCs adhered on the side parts at the end of mechanical stimulation were polarized along the longitudinal direction regardless of side effects. This cytoskeleton re-organization could be responsible of cell area reduction with respect to the undeformed case.

Non-statistically significant differences were obtained stimulating the ASCs with a periodicity of 1 min for 24 h (Figure 3.4B) in both regions.

Finally, the stimulation period of 10 min generates a specific cell area distribution characterized by a non-statistical variation between undeformed and deformed configurations on lateral parts and a statistical one on the central region (Figure 4.4C). Particularly, it has been showed in the section 4.3.1.3 that this stimulation period was not able to induce a consistent cytoskeleton re-organization along the longitudinal axis even if a response in terms of cell morphology change has occurred.

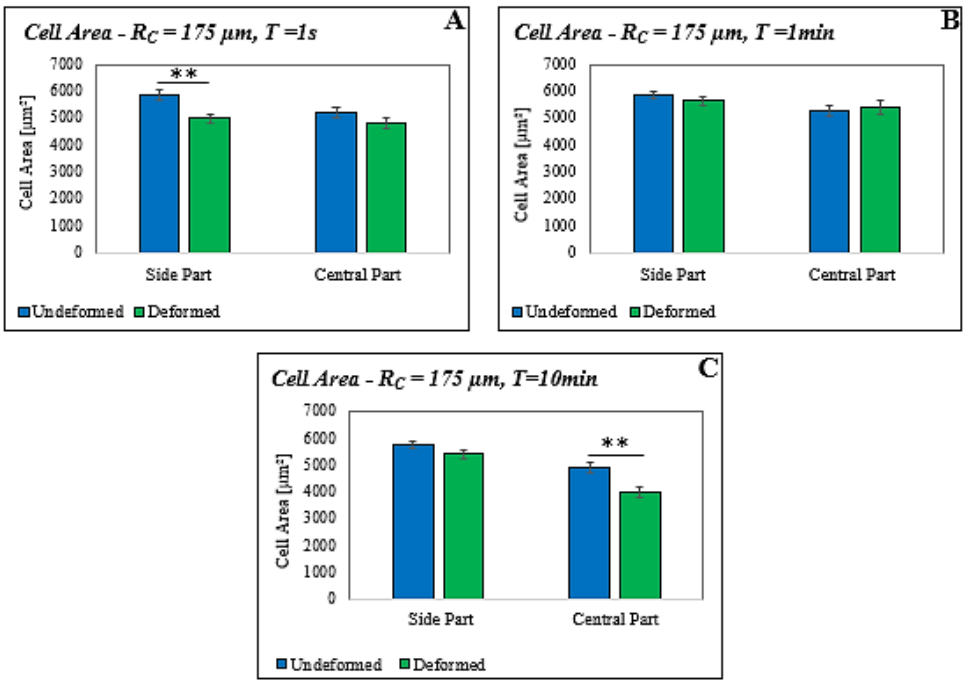

*Figure 4.4: Cell area distribution for undeformed and deformed configurations on both side and central regions of the microfluidic channel. A: Cell area distribution for R_C = 175 µm and T = 1s. B: Cell area distribution for R_C = 175 µm and T = 1min. C: Cell area distribution for R_C = 175 µm and T = 10 min. Each experiment was repeated three times on three different microfluidic platform and the histograms show the mean cell area ± s.e.m. ** p<0.01*

4.3.3 Focal Adhesions assembly induced by cyclic dynamic changes of cell-seeded membrane curvature

The FAs are involved in the mechanosensing and mechanotransduction pathways since one of their essential roles consist of sensing mechanical microenvironment changes and propagate them inside the cells. In fact, they are able to create a direct communication between extracellular matrix and cell cytoskeleton.

The cyclic mechanical curvature variation can be classified as a microenvironmental change that could generate a response of FAs. This response could be highlighted considering the FA size and polarization at the end of mechanical stimulation compared to unstimulated case. In order to analyse the FA behaviour to each cyclic mechanical stimulation, that is every period, a specific analysis was made in the next paragraphs.

4.3.1.1 Focal Adhesion response to R_C = 175 µm – T = 1 s

The focal adhesions behaviour was relevantly influenced by the cyclic mechanical stimulation of R_C = 175 µm and T = 1 s. Starting from Figure 4.5A, the FAs are randomly organized on the microfluidic platform; conversely, they result well polarized along the longitudinal direction at the end of stimulation (Figure 4.5B). The same can be observed with representative confocal images (Figure 4.5C-D) highlighting how the dynamic stimulation is responsible for this result.

FAs polarization agrees with the actin stress fibers response underlining the continuous interaction between cell and extracellular matrix.

Not only an orientation analysis, but also a FA size distribution was performed. Comparing the percentage of FAs having a specific dimension between the undeformed and deformed configurations (Figure 4.5E), no statistically significant differences were observed. Moreover, for each specific case, the number of FAs in a defined size range was organized with respect to their orientation on the microfluidic platform. In flat case (Figure 4.5F), there are no relevant differences; conversely, a lot of variations has occurred in the deformed one (Figure 4.5G). Starting from FAs with an area smaller than 2.5 µm², the percentage of FAs aligned along the longitudinal axis was relevantly smaller with respect to those oriented in other directions. Then, for other ranges, the difference was observed only between those aligned along the microfluidic channel and those

orthogonally to the same direction, where the percentage of the former was higher than the percentage of the latter. Larger focal adhesions mean more mature and stable structures than the smaller ones. That is, the uniaxial cyclic mechanical stimulation was able to induce the formation of FAs along a specific direction controlling not only their orientation but also their size and, as a consequence, their stability.

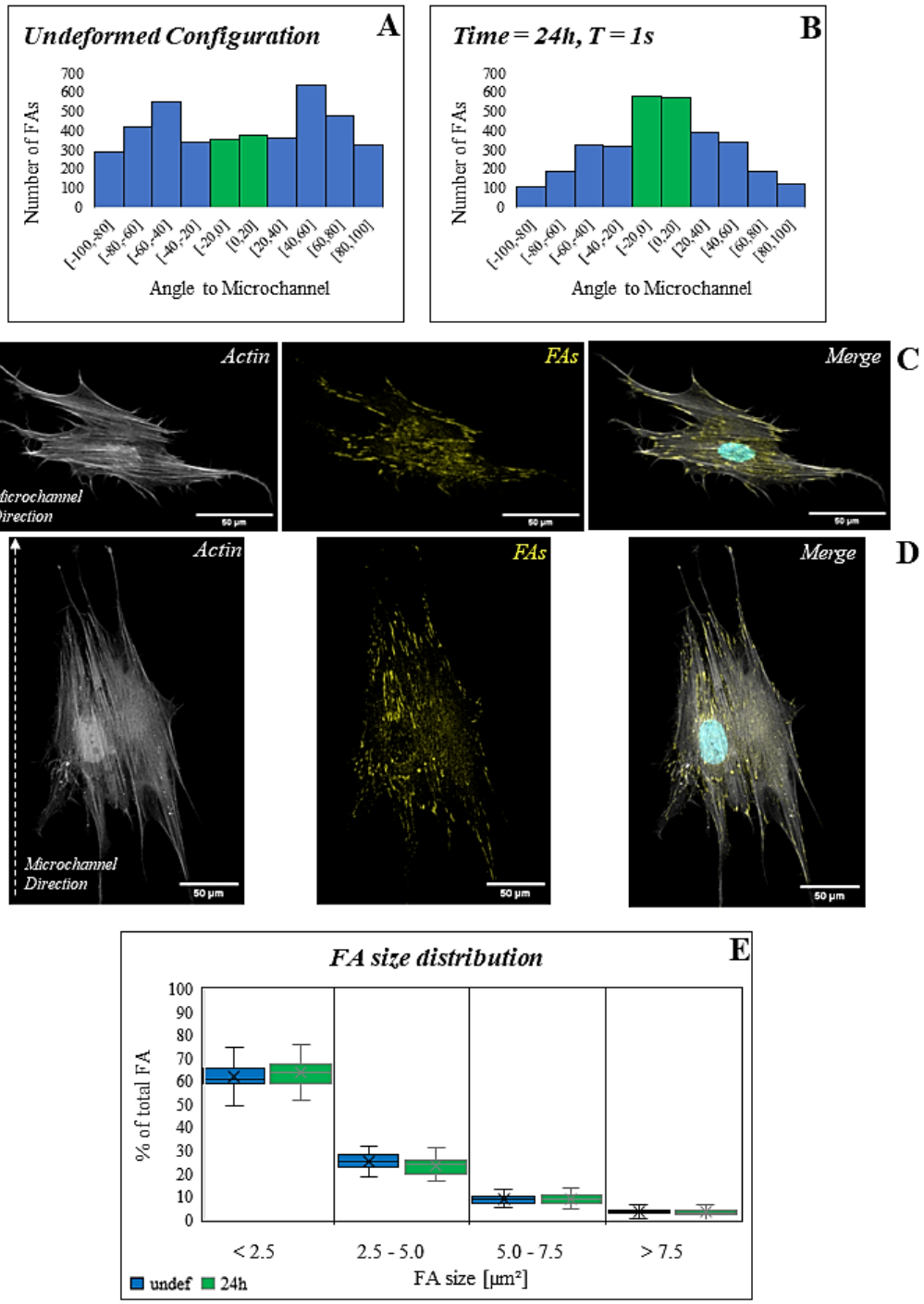
Undeformed Configuration
A
Number of FAs
Angle to Microchannel
Time = 24h, T = 1s
B
Number of FAs
Angle to Microchannel
[-100,-80]
[-80,-60]
[-60,-40]
[-40,-20]
[-20,0]
[0,20]
[20,40]
[40,60]
[60,80]
[80,100]
Actin
FAs
Merge
C
Microchannel Direction
50 µm
D
E
FA size distribution
% of total FA
< 2.5
2.5 - 5.0
5.0 - 7.5
> 7.5
FA size [µm²]
undef
24h

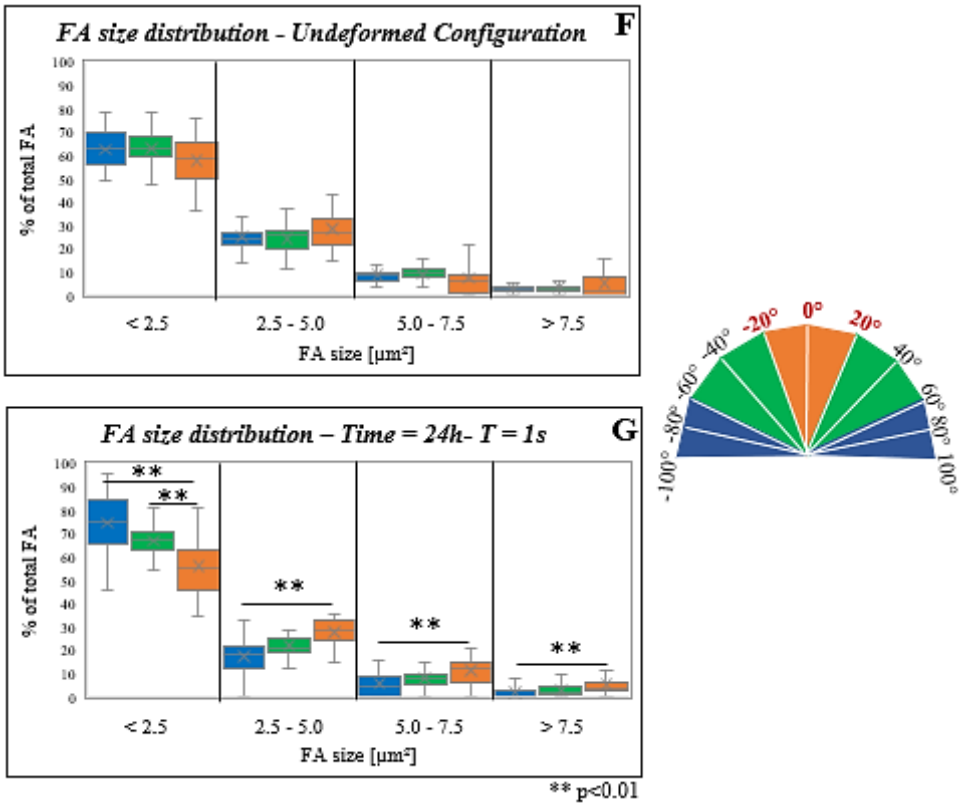

*Figure 4.5: Focal adhesions (FAs) behaviour induced by a curvature variation of 0.0056 µm^{-1} with a T = 1s on the microfluidic platform. A-B: Histograms showing FAs polarization with respect to the microchannel direction (0°) into flat (A) and deformed (B) configurations. C: Confocal acquisition of a single adipose derived mesenchymal stem cell into undeformed configuration. Gray: Actin Cytoskeleton, Yellow: Focal Adhesions, Cyan: Nucleus. Scale bar: 50 µm. D: Confocal acquisition of a single adipose derived mesenchymal stem cell into deformed configuration. Gray: Actin Cytoskeleton, Yellow: Focal Adhesions, Cyan: Nucleus. Scale bar: 50 µm. E-G: Focal adhesions size distribution. E: Comparison of FA size distribution between deformed and deformed configuration. F: FA size distribution in function of polarization angle into undeformed configuration. G: FA size distribution in function of polarization angle into deformed configuration. Data are expressed as mean value ± standard deviation and each experiment was repeated three times on independent microfluidic platform. ** p<0.01.*

4.3.1.2 Focal Adhesion response to R_C = 175 µm – T = 1 min

A periodicity of 1 min with a radius of curvature variation of 175 µm was able to control the FAs response. In fact, starting from ASCs with a random FA organization (Figure 4.6A), a polarization of these ones along the longitudinal axis occurred. The same was highlighted by confocal representative z-projections (Figure 4.6C-D).

Comparing the undeformed and deformed FA size distribution (Figure 4.6E), statistically differences were observed for FA size lower than 2.5 µm² and in the interval [5 – 7.5] µm² with an increment of smaller FA with respect to the larger ones (Figure 4.6E) for deformed configuration.

Analysing the FA size distribution taking into account their orientation, different results can be outlined. Obviously, the FA size distribution of undeformed configuration did not show relevant variations (Figure 4.6F). Conversely, a consistent percentage reduction of smaller FAs polarized along the longitudinal axis occurred comparing with other directions (Figure 4.6G) which was opportunely balanced by relevant differences in the range [2.5 – 5] µm². Also in this case, as in the previous one, the cyclic mechanical insults were able to control the structure and direction of focal adhesions in a specific way.

Finally, the mechanical cues create periodic curvature variations that are sensed by cells through focal adhesions and transduced into cytoskeleton re-organization and variations of FAs themselves.

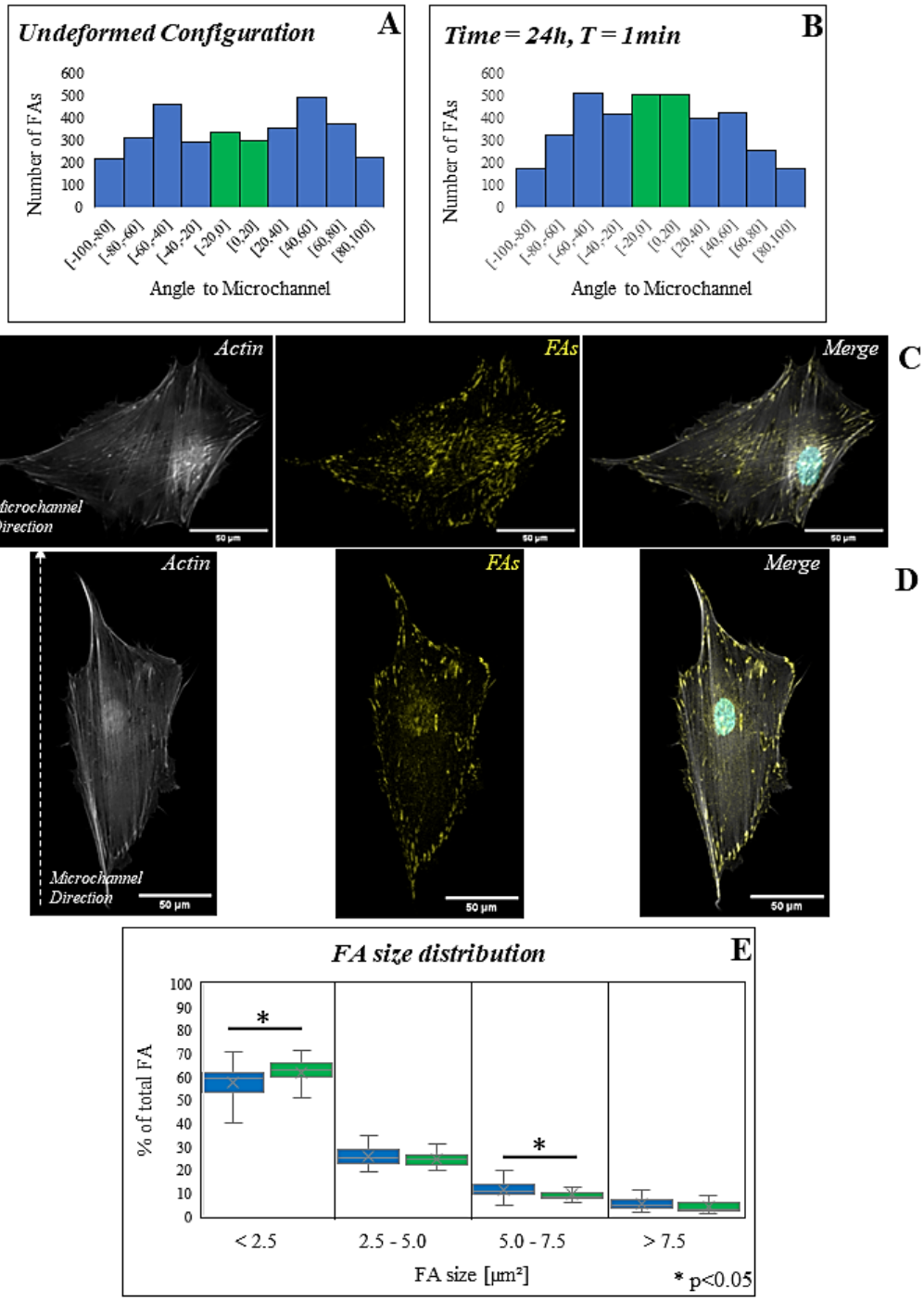
Undeformed Configuration
A
Number of FAs
600
500
400
300
200
100
0
[-100,-80]
[-80,-60]
[-60,-40]
[-40,-20]
[-20,0]
[0,20]
[20,40]
[40,60]
[60,80]
[80,100]
Angle to Microchannel
Time = 24h, T = 1min
B
Number of FAs
Angle to Microchannel
Actin
FAs
Merge
C
Microchannel Direction
50 µm
D
FA size distribution
E
% of total FA
100
90
80
70
60
50
40
30
20
10
0
*
*
< 2.5
2.5 - 5.0
5.0 - 7.5
> 7.5
FA size [µm²]
* p<0.05

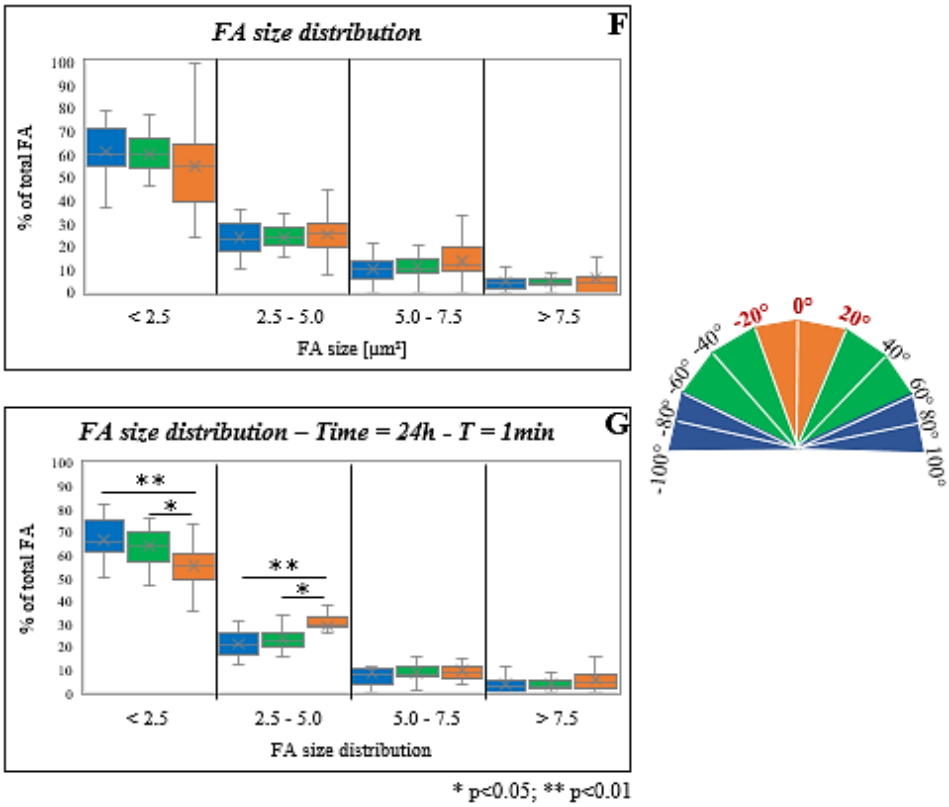

*Figure 4.6: Focal adhesions (FAs) behaviour induced by a curvature variation of 0.0056 µm^{-1} with a T = 1min on the microfluidic platform. A-B: Histograms showing FAs polarization with respect to the microchannel direction (0°) into flat (A) and deformed (B) configurations. C: Confocal acquisition of a single adipose derived mesenchymal stem cell into undeformed configuration. Gray: Actin Cytoskeleton, Yellow: Focal Adhesions, Cyan: Nucleus. Scale bar: 50 µm. D: Confocal acquisition of a single adipose derived mesenchymal stem cell into deformed configuration. Gray: Actin Cytoskeleton, Yellow: Focal Adhesions, Cyan: Nucleus. Scale bar: 50 µm. E-G: Focal adhesions size distribution. E: Comparison of FA size distribution between deformed and deformed configuration. F: FA size distribution in function of polarization angle into undeformed configuration. G: FA size distribution in function of polarization angle into deformed configuration. Data are expressed as mean value ± standard deviation and each experiment was repeated three times on independent microfluidic platform. * p<0.05; ** p<0.01.*

4.3.1.3 Focal Adhesion response to R_C = 175 μm – T = 10 min

The last periodicity studied was 10 minutes with a radius of curvature change of 175 μm. Starting from the FA polarization, in both undeformed and deformed configurations (Figure 4.7A-B), a random organization was observed. This means that the specific cyclic mechanical insults are not able to vehiculate the orientation of adhesion complexes. In fact, observing the representative images (Figure 4.7C-D), particularly into deformed configuration, all FAs are not well polarized along a specific direction.

Then, a FA size distribution was analyzed comparing flat and curved cases in function of specific FA size range (Figure 4.7E). Box and whisker plots show statistically significant differences between undeformed and deformed profiles, particularly an increase of smaller FAs in stimulated configuration with respect to unstimulated one. This increase of small FAs corresponds to a decrease of larger ones at 24 h. Studying the FA size distribution as function of their polarization (Figure 4.7F-G), no relevant changes were obtained in the different conditions.

So, these results show that the cyclic mechanical stimulation with a periodicity of 10 min was not able to control and vehiculate the re-organization of actin stress fibers and FAs in a consistent way. That is, even if the amplitude of the curvature applied was enough to influence the cellular behaviour in static conditions, considering another variable (periodicity), the ASCs response is completely different. Consequently, the way in which a mechanical signal was applied may be more important than the signal itself.

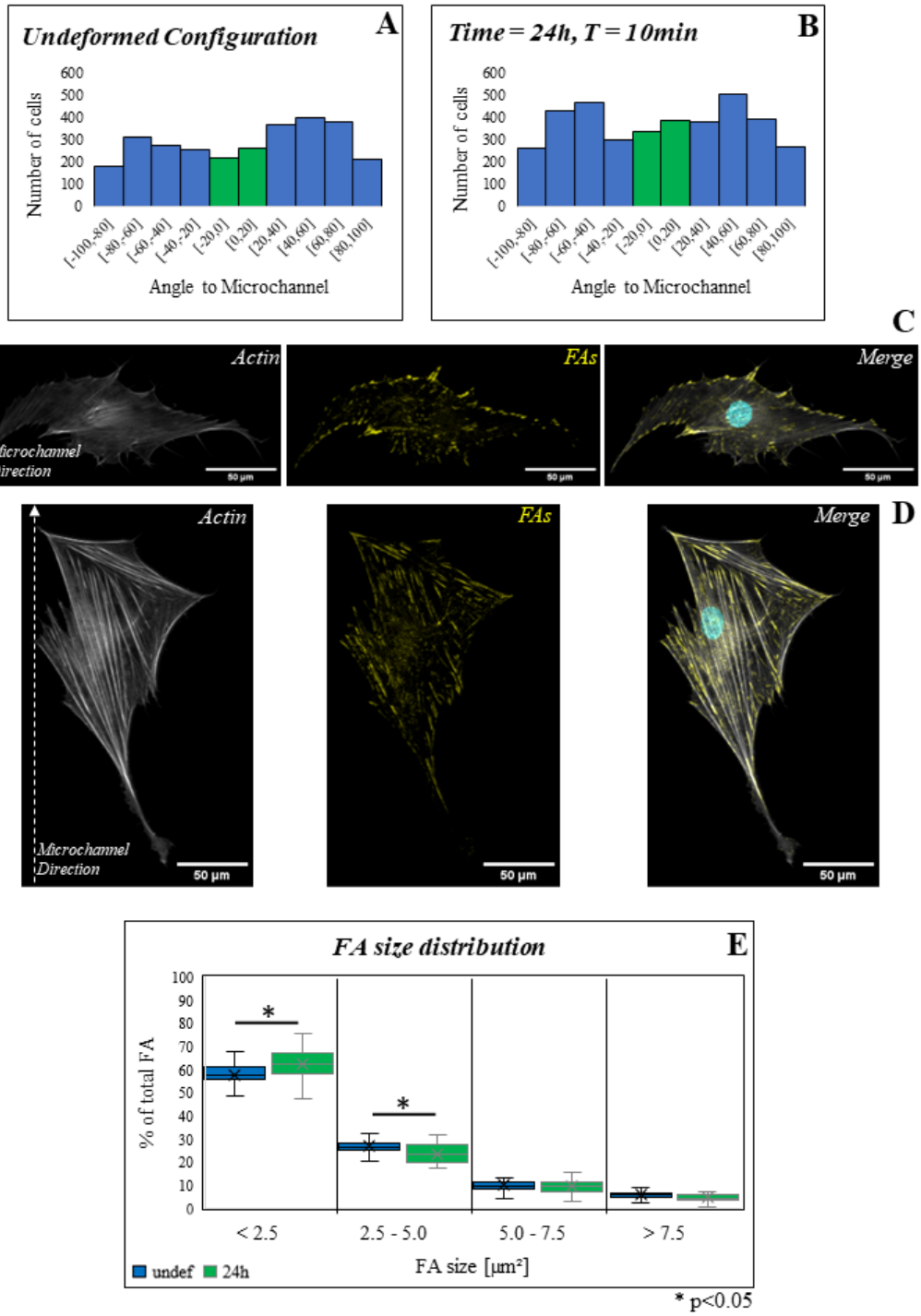
Undeformed Configuration
A
Number of cells
600
500
400
300
200
100
0
[-100,-80]
[-80,-60]
[-60,-40]
[-40,-20]
[-20,0]
[0,20]
[20,40]
[40,60]
[60,80]
[80,100]
Angle to Microchannel
Time = 24h, T = 10min
B
Number of cells
Angle to Microchannel
C
Actin
FAs
Merge
Microchannel Direction
50 µm
D
Actin
FAs
Merge
Microchannel Direction
50 µm
FA size distribution
E
% of total FA
100
90
80
70
60
50
40
30
20
10
0
*
*
< 2.5
2.5 - 5.0
5.0 - 7.5
> 7.5
FA size [µm²]
undef
24h
* p<0.05

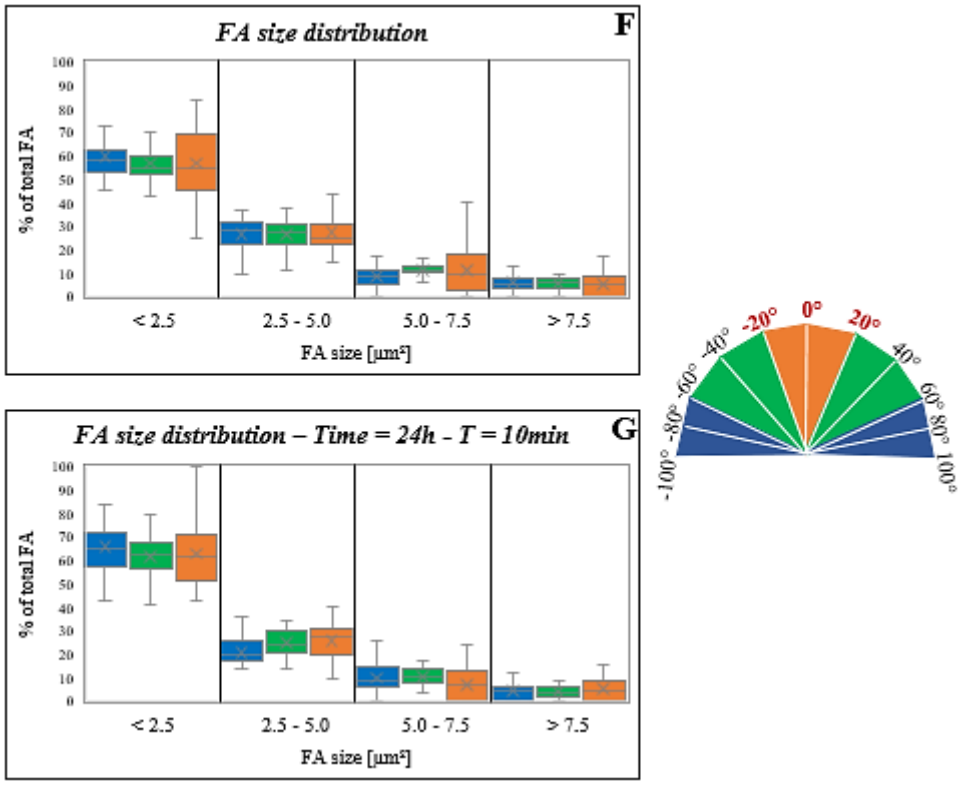

*Figure 4.7: Focal adhesions (FAs) behaviour induced by a curvature variation of 0.0056 µm^{-1} with a T = 10min on the microfluidic platform. A-B: Histograms showing FAs polarization with respect to the microchannel direction (0°) into flat (A) and deformed (B) configurations. C: Confocal acquisition of a single adipose derived mesenchymal stem cell into undeformed configuration. Gray: Actin Cytoskeleton, Yellow: Focal Adhesions, Cyan: Nucleus. Scale bar: 50 µm. D: Confocal acquisition of a single adipose derived mesenchymal stem cell into deformed configuration. Gray: Actin Cytoskeleton, Yellow: Focal Adhesions, Cyan: Nucleus. Scale bar: 50 µm. E-G: Focal adhesions size distribution. E: Comparison of FA size distribution between deformed and deformed configuration. F: FA size distribution in function of polarization angle into undeformed configuration. G: FA size distribution in function of polarization angle into deformed configuration. Data are expressed as mean value ± standard deviation and each experiment was repeated three times on independent microfluidic platform. * p<0.05; ** p<0.01.*

4.4 Discussion and Conclusions

Mechanical cues have broad effects on cell behaviour and play an essential role in guiding developmental, regenerative, and pathological processes [19,20]. For instance, the mechanical signals of the cellular microenvironment are able to direct the stem cells into a specific differentiation pathway [21,22]. Moreover, the mechanical microenvironments have significant impacts on disease progression, such as the development of cardiac fibrosis [23]. Since, in the body, cells, especially those from blood, bone marrow, lungs, heart, or musculoskeletal tissue, are subjected to cyclically mechanical loading, an in-depth investigation into the low-density adipose derived mesenchymal stem cells response could provide interesting insights.

Stress fibers and FAs are complex protein structures able to produce, transmit and sense mechanical cues [24-28]. Evidence accumulated over many years led to the conclusion that mechanical tensions generated within stress fibers contributes to the assembly of both stress fibers themselves and their associated focal adhesions [24,29,30]. However, a more complex situation has been highlighted by recent studies in which a continuous interaction between stress fibers, focal adhesions and extracellular or intracellular forces occurred. For example, *Geiger's et al.* [31,32] observed a close correlation between the size of FAs and the force that is transmitted across them using traction force microscopy technique, supporting the idea that growth of FAs requires both tension and actin polymerization. Since the FAs are defined as integrin-containing multiprotein complexes, the recruitment of these components can be controlled by both tension applied and actin polymerization level obtaining nascent or mature focal complexes [33,34].

Our results move in the same direction in agreement with different studies [35-40]. In fact, the curvature modification of cell-seeded membrane consists of a variation of extracellular stresses and strains on the substrate itself which is sensed by low-density ASCs. As a consequence, a modification of actin cytoskeleton polarization and FAs size and orientation was observed in function of stimulation type. Not only the amplitude of tension, but also the periodicity with which it was applied plays a fundamental role in the ASCs behaviour. In fact, increasing the stimulation period, which means a frequency reduction, the ASCs are not able to consistently change their configuration with respect to undeformed case. This means that, changing the membrane curvature in a static way

(as shown in Chapter 3), a specific curvature amplitude (0.0045 μm^{-1}) is necessary to obtain the actin polarization along the uniaxial loading axis; whereas a greater value of curvature (0.0057 μm^{-1}) occurred to observe the same polarization made at FAs level. Differently, applying the curvature variation in a dynamic manner, even if it has been studied a curvature variation case able to generate in a static way both actin and FA polarization along the stimulation direction, the periodicity controls their response.

Applying a uniaxial mechanical insult means impose forces along a specific direction that thank to the mechanosensing and mechanotransduction, ASCs respond by modulating the actin cytoskeleton polymerization and as a consequence the FAs assembly in a specific way. For high static curvature variations or high periodicity in a dynamic situation, the FAs are stimulated to form and assemble along the longitudinal direction and discouraged to form into the orthogonal one. In fact, the FAs along the microchannel are larger in size than the FAs orthogonally formed.

So, in conclusion, the designed microfluidic platform proved to be a good tool to study in real-time the ASCs behaviour in terms of actin cytoskeleton polarization and FAs response in both static and dynamic mechanical configurations. The attention has been focused on the study of low-density ASCs in order to deeply understand the role of uniaxial stretching on their behaviour without cell-cell interaction, but, in future, longer experiments could be developed in order to study how these specific mechanical signals could control stem cell differentiation. In fact, the combination of microfluidic technique, with confocal microscopy and transfection approach on human extracted stem cells has different potentialities that could be exploited, for example, the use of small amount of cells and reagents, the visualization in real-time and the possibility to apply different mechanical insults through the pressure controller for as long as you want.

References

[1] Zaidi, Mone, ed. *Skeletal Biology and Medicine: Bone and Cartilage Homeostasis and Bone Disease. I*. Blackwell Pub., 2011.

[2] Harshad, Kamble, et al. "An electromagnetic cell-stretching device for mechanotransduction studies of olfactory ensheathing cells." *Biomedical microdevices* 18.3 (2016): 1-10.

[3] Hoffman, Brenton D., Carsten Grashoff, and Martin A. Schwartz. "Dynamic molecular processes mediate cellular mechanotransduction." *Nature* 475.7356 (2011): 316-323.

[4] Silver, Frederick H., and Lorraine M. Siperko. "Mechanosensing and mechanochemical transduction: how is mechanical energy sensed and converted into chemical energy in an extracellular matrix?." *Critical Reviews™ in Biomedical Engineering* 31.4 (2003).

[5] Orr, A. Wayne, et al. "Mechanisms of mechanotransduction." *Developmental cell* 10.1 (2006): 11-20.

[6] Chen, Christopher S. "Mechanotransduction–a field pulling together?." *Journal of cell science* 121.20 (2008): 3285-3292.

[7] Wang, Ning, Jessica D. Tytell, and Donald E. Ingber. "Mechanotransduction at a distance: mechanically coupling the extracellular matrix with the nucleus." *Nature reviews Molecular cell biology* 10.1 (2009): 75-82.

[8] Nava, Michele M., Manuela T. Raimondi, and Riccardo Pietrabissa. "Bio-chemo-mechanical models for nuclear deformation in adherent eukaryotic cells." *Biomechanics and modeling in mechanobiology* 13.5 (2014): 929-943.

[9] Park, Joong Yull, et al. "Study of cellular behaviors on concave and convex microstructures fabricated from elastic PDMS membranes." *Lab on a Chip* 9.14 (2009): 2043-2049.

[10] Frost, Adam, Vinzenz M. Unger, and Pietro De Camilli. "The BAR domain superfamily: membrane-molding macromolecules." *Cell* 137.2 (2009): 191-196.

[11] Yamashita, Tadahiro, et al. "Air-pressure-driven separable microdevice to control anisotropic curvature of cell culture surface." *Analytical Sciences* (2020): 20A001.

[12] Zhou, Jing, and Laura E. Niklason. "Microfluidic artificial “vessels” for dynamic mechanical stimulation of mesenchymal stem cells." *Integrative Biology* 4.12 (2012): 1487-1497.

[13] Kamble, Harshad, et al. "Pneumatically actuated cell-stretching array platform for engineering cell patterns in vitro." *Lab on a Chip* 18.5 (2018): 765-774.

[14] Moraes, Christopher, et al. "Microfabricated arrays for high-throughput screening of cellular response to cyclic substrate deformation." *Lab on a Chip* 10.2 (2010): 227-234.

[15] Moraes, Christopher, et al. "Microdevice array-based identification of distinct mechanobiological response profiles in layer-specific valve interstitial cells." *Integrative Biology* 5.4 (2013): 673-680.

[16] Michielin, F., et al. "Microfluidic-assisted cyclic mechanical stimulation affects cellular membrane integrity in a human muscular dystrophy in vitro model." *RSC advances* 5.119 (2015): 98429-98439.

[17] Chiu, Chih-Hao, et al. "Self-renewal and differentiation of adipose-derived stem cells (ADSCs) stimulated by multi-axial tensile strain in a pneumatic microdevice." *Micromachines* 9.11 (2018): 607.

[18] Campillo, Noelia, et al. "A novel chip for cyclic stretch and intermittent hypoxia cell exposures mimicking obstructive sleep apnea." *Frontiers in physiology* 7 (2016): 319.

[19] Vining, Kyle H., and David J. Mooney. "Mechanical forces direct stem cell behaviour in development and regeneration." *Nature reviews Molecular cell biology* 18.12 (2017): 728-742.

[20] Doyle, Andrew D., et al. "Local 3D matrix microenvironment regulates cell migration through spatiotemporal dynamics of contractility-dependent adhesions." *Nature communications* 6.1 (2015): 1-15.

[21] Das, Rajat K., et al. "Stress-stiffening-mediated stem-cell commitment switch in soft responsive hydrogels." *Nature materials* 15.3 (2016): 318-325.

[22] Chaudhuri, Ovijit, et al. "Hydrogels with tunable stress relaxation regulate stem cell fate and activity." *Nature materials* 15.3 (2016): 326-334.

[23] Bonnans, Caroline, Jonathan Chou, and Zena Werb. "Remodelling the extracellular matrix in development and disease." *Nature reviews Molecular cell biology* 15.12 (2014): 786-801.

[24] Burridge, Keith. "Are stress fibres contractile?." *Nature* 294.5843 (1981): 691-692.

[25] Geiger, Benjamin, and Alexander Bershadsky. "Exploring the neighborhood: adhesion-coupled cell mechanosensors." *Cell* 110.2 (2002): 139-142.

[26] Hoffman, Brenton D., Carsten Grashoff, and Martin A. Schwartz. "Dynamic molecular processes mediate cellular mechanotransduction." *Nature* 475.7356 (2011): 316-323.

[27] Case, Lindsay B., and Clare M. Waterman. "Integration of actin dynamics and cell adhesion by a three-dimensional, mechanosensitive molecular clutch." *Nature cell biology* 17.8 (2015): 955-963.

[28] Burridge, Keith, and Erika S. Wittchen. "The tension mounts: stress fibers as force-generating mechanotransducers." *Journal of Cell Biology* 200.1 (2013): 9-19.

[29] D. Riveline, E. Zamir, N.Q. Balaban, U.S. Schwarz, T. Ishizaki, S. Narumiya, Z. Kam, B. Geiger, A.D. Bershadsky, Focal contacts as mechanosensors: externally applied local mechanical force induces growth of focal contacts by an mDia1-dependent and ROCK-independent mechanism, J. Cell. Biol. 153 (2001) 1175–1186.

[30] Chrzanowska-Wodnicka, Magdalena, and Keith Burridge. "Rho-stimulated contractility drives the formation of stress fibers and focal adhesions." *The Journal of cell biology* 133.6 (1996): 1403-1415.

[31] Balaban, Nathalie Q., et al. "Force and focal adhesion assembly: a close relationship studied using elastic micropatterned substrates." *Nature cell biology* 3.5 (2001): 466-472.

[32] Schwarz, Ulrich S., et al. "Calculation of forces at focal adhesions from elastic substrate data: the effect of localized force and the need for regularization." *Biophysical journal* 83.3 (2002): 1380-1394.

[33] Kuo, Jean-Cheng, et al. "Analysis of the myosin-II-responsive focal adhesion proteome reveals a role for β-Pix in negative regulation of focal adhesion maturation." *Nature cell biology* 13.4 (2011): 383-393.

[34] Schiller, Herbert B., et al. "Quantitative proteomics of the integrin adhesome show a myosin II-dependent recruitment of LIM domain proteins." *EMBO reports* 12.3 (2011): 259-266.

[35] Galbraith, Catherine G., Kenneth M. Yamada, and Michael P. Sheetz. "The relationship between force and focal complex development." *The Journal of cell biology* 159.4 (2002): 695-705.

[36] Choquet, Daniel, Dan P. Felsenfeld, and Michael P. Sheetz. "Extracellular matrix rigidity causes strengthening of integrin–cytoskeleton linkages." *Cell* 88.1 (1997): 39-48.

[37] Wang, Ning, James P. Butler, and Donald E. Ingber. "Mechanotransduction across the cell surface and through the cytoskeleton." *Science* 260.5111 (1993): 1124-1127.

[38] Matthews, Benjamin D., et al. "Cellular adaptation to mechanical stress: role of integrins, Rho, cytoskeletal tension and mechanosensitive ion channels." *Journal of cell science* 119.3 (2006): 508-518.

[39] Guilluy, Christophe, et al. "The Rho GEFs LARG and GEF-H1 regulate the mechanical response to force on integrins." *Nature cell biology* 13.6 (2011): 722-727.

[40] Burridge, Keith, and Christophe Guilluy. "Focal adhesions, stress fibers and mechanical tension." *Experimental cell research* 343.1 (2016): 14-20.

Chapter 5

Role of curvature on Yes-associated protein trafficking

5.1 Introduction

Yes-associated proteins, commonly known as YAP, are transcriptional regulators involved into cell proliferation, cell survival, stem cell self-renewal and cell differentiation [1]. This transcription factor can shuttle between the cytoplasm and the nucleus and, from recent evidence [2-6], it results inactive into the cytoplasm and active and able to interact with DNA-binding transcription factors in the nucleus. In this way, it contributes to gene expression regulation. The shuttling of YAP from the cytoplasm to the nucleus and *vice versa* is regulated by mechanical cues between ECM, cytoskeleton, and nucleus. Particularly, experimental evidence has demonstrated that in function of adhesive area available and substrate rigidity, the YAP can be localized in the cytoplasmic or nuclear regions [1]. As shown in Figure 5.1, for large adhesive area or stiff extracellular matrix, a YAP accumulation inside the nucleus has occurred; conversely, for small cell-spreading regions or soft ECM, a cytoplasmic YAP localization was performed.

As a consequence, YAPs can be classified as mechanotransducers because their nucleo/cytoplasmic shuttling can be not only a faithful read-out of ECM mechanical cues, but, also, a fundamental mechanism for cells, which can translate this information into coherent gene expression programs and cell behaviours.

For example, there is a link between mechanical cues and YAP activity for the differentiation of mesenchymal stem cells (MSCs). In particular, during osteogenic differentiation, developed in conditions of high cell spreading and rigid substrates, the YAP proteins were active and able to contribute to the differentiation mechanism; on the contrary, during neurogenic differentiation occurred on soft substrates, YAP was inactive [7]. Furthermore, they play an important role in breast cancer, as the stiffness of tumour

tissue is higher than healthy one, this allow the activation of YAP proteins that are able to control cell proliferation [1].

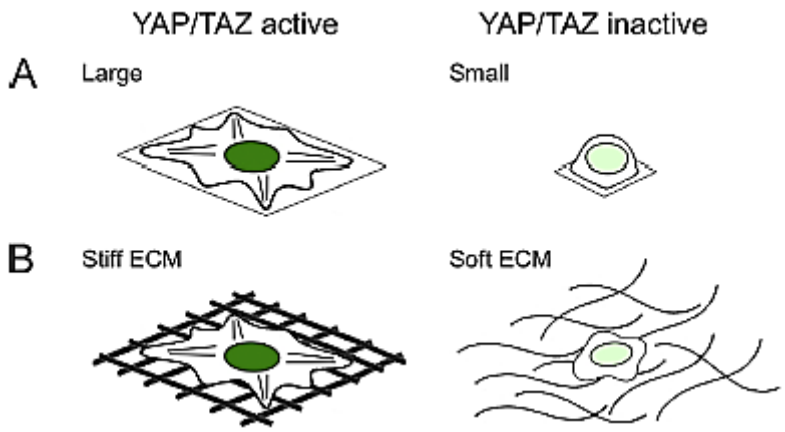

Figure 5.1 YAP' position in different conditions. A: large spreading area, YAP inside the nucleus (left-dark green) and soft spreading area, YAP outside the nucleus (right-light green); B Stiff ECM, YAP inside the nucleus (left-dark green) and soft ECM, YAP outside the nucleus (right-light green) [43].

Another important function of the transcription factor YAP consists in own ability to control both cell stiffness and focal adhesions formation. *Nardone et al.* [2] have reported that the translocation of YAP from the cytoplasm to the nucleus activates a specific mechanism able to form focal adhesions and increase cell stiffness. Conversely, if the translocation does not occur, the focal adhesions are less developed, and the cells have a smaller stiffness with respect to the previous case.

Finally, a correlation between YAP regulator and substrate curvature has been recently observed. As introduced before, on convex structure, the mechanotransduction is mediated by BAR domain proteins which release small GTPases such as Rac, Rho, and CDC42. Particularly, Rho molecules are able to play a fundamental role in YAP regulation that acting in conjunction with actomyosin cytoskeleton are able to transcriptionally activate the transcription factor shuttling from the cytoplasm to the nucleus inducing proliferation of epithelial and endothelial cells [5,8].

Conversely, the relationship between concave morphologies and YAP regulation is not well understood. It is known that concave substrates stimulate tight junction formation on confluent cells [9] and a protein into these junctions (zona occludens 2 – ZO-2) interacts with YAP factor [10,11]. Generally, tight junctions are able to trap YAP

molecules to prevent them from inducing transcription pathways and this would lead to proteasomal degradation which, in turn, would favour apoptosis and growth arrest [1]. So, due to the tight junction formation stimulated by concave morphologies and the role of these structures on YAP trafficking, a possible relation between cellular concave sensing and YAP activity could be possible. To study this possible correlation, the designed microfluidic platform, detailed described in the chapter 2, has been used to analyse the behaviour of high-density adipose derived mesenchymal stem cells to a specific curvature variation in terms of YAP shuttling between cytoplasm and nucleus.
That is, in undeformed and deformed configuration the nuclear/cytoplasmic YAP concentration has been evaluated and compared in order to understand if a possible relationship exists. Particularly, these experiments have been made using YAP electroporated ASCs in order to acquire on the same cells a real-time response.

5.2 Materials and Methods

5.2.1 Design and testing of the microfluidic platform

The microfluidic platform design was detailed explained in the section 2.2.1 of the chapter 2, but to study the role of curvature on YAP behaviour, it was necessary to change the fluorescent nanoparticles embedded in the PDMS membrane. This change was due to the fluorescent molecule associated with the YAP plasmid which was identical to that associated with the polystyrene nanoparticles and, therefore, both excited by the same wavelength. In order to avoid this overlapping, the PDMS membrane was embedded with red fluorescent polystyrene nanoparticles which are identical to the green ones except for the associated fluorophore molecule (Fluoresbrite Carboxy NYO 0.50 Micron Microspheres – Polysciences). The “new” microfluidic platforms have opportunely tested to the different pressures in order to verify their correct functionality and compared with the “old” one. All the tests have been made on three different microfluidic platforms.

5.2.2 Electroporation of ASCs

The electroporation of human adipose derived mesenchymal stem cells was performed with Neon Transfection system (Catalog Number: MPK1096 – ThermoFisher Scientific); in particular the Yes-associated protein was transfected using the plasmid pEGFP-C3-hYAP1 (cat. 17843 – addgene). One-week cultured ASCs (passages 1-2) were trypsinized for 5 minutes and centrifuged at 1100 rpm for 5 minutes. Then, after removal of supernatant, PBS was added to ASCs for a second centrifuge (300 x g for 5 min) to remove all culture medium residues from cells.

The electroporation mechanism can be done using two different buffers: buffer E into electroporator tube and buffer R to the pellet of ASCs. In addition to the buffer R, the YAP plasmid in concentration of 0.6 μg was added in order to have a final volume of cells, buffer, and plasmid of 10 μL equal to the electroporator tip volume. Particularly, 300000 cells for each electroporation have been used. The instrument was set with specific parameters: pulse voltage = 1200V, pulse width = 20ms and pulse number = 2.

At the end of electroporation, the total volume contained in electroporator tip was put into a 6-well with 2mL of ASCs culture medium without Pen-Strep.

5.2.3 Cell culture and cell seeding on microfluidic platform

After the electroporation step, a time equal to 48 h is necessary for ASCs to adhere and recover their morphology. So, after 48 h, the transfected ASCs were detached with trypsin (Catalog. N° 25200056 Gibco, Thermo Fisher Scientific) and seeded at passages 3-4 on the fibronectin functionalized microfluidic platform at a density of 10000 cells/cm^2 (see 3.2.4 section). The ASCs mechanical load was induced 24 h after seeding to be sure that all cells were correctly adhered to the PDMS membrane.

To visualize not only YAP transcription factor but also cell nuclei and actin stress fibers in real-time, specific ASCs staining have been carried out. The former was made 24 h after the cell seeding on the microfluidic platform using Hoechst dye (1:10000 for 15 min at 37 °C; Hoechst 33342, Catalog. N° H3570, Invitrogen). The latter was performed after the nuclear staining using a live cell fluorogenic F-actin labelling probe (1:100 Spy650-FastAct SC505 – Spirochrome). Due to its non-toxic feature, the probe can be added to the ASCs culture medium and kept inside it for the whole time of experiment. So, after

1-2 h the actin stress fibers of ASCs can be perfectly visualized with the confocal microscope and the experiments can start.

5.2.4 Static mechanical stimulation of ASCs

To change the curvature of the cell-adhered PDMS membrane, the pressure inside the underneath microfluidic channel was modified using the OB1 pressure controller. Particularly, a pressure reduction of -400 mbar was applied as linear ramp (-100mbar/min) on high-density ASCs in order to study the YAP shuttling between cytoplasm and nucleus. Due to the microfluidic platform accessibility using the confocal microscopy, the cellular behaviour was acquired before and 24 h after the application of the mechanical insult; particularly, 24 h is a sufficient time for cells to sense and respond to the curvature variation reaching their homeostatic configuration.

5.2.5 Confocal z-stacks acquisitions

As for the study of single ASCs behaviour induced by static and dynamic mechanical configurations, also here the confocal microscope (Confocal Zeiss Axio Observer.Z1) has been opportunely equipped with a stage incubator (Okolab S.r.l) in order to reproduce the same temperature, humidity, and CO_2 conditions of a cell culture incubator.

Due to the transparency and thickness of the microfluidic platform, low and high magnification objectives can be used. Particularly, to study the role of curvature on YAP trafficking, the high-density ASCs have been acquired using water immersed 40x long distance objective. For each z-stacks YAPs, actin stress fibers and nuclei have been captured in both undeformed and 24h deformed configuration. Particularly, samples were excited at 380 nm (Nuclei), 488 nm (Yes-associated proteins) and 639 nm (Actin stress fibers); whereas the emissions were collected in the 400-420 nm, 500-530 nm, and 660-690 nm ranges, respectively.

5.2.6 Confocal image analysis

To study the trafficking of YAP between cytoplasm and nucleus, the concentration of this transcription factor was determined in both regions by z-stacks analysis. Particularly, it can be made using an image analysis software called FiJi and the strategy to quantify the nuclear/cytoplasmic YAP ratio has been developed by *Nardone and colleagues* [2]. Briefly, the quantification of nuc/cyt YAP ratio was made using the equation below (1):

$$\frac{\sum_{nuc}^{I} pixels/A_{nuc}}{\sum_{cyto}^{I} pixels/A_{cyto}} \quad (1)$$

where $\sum_{nuc}^{I} pixels$ and $\sum_{cyto}^{I} pixels$ represent the sum of the intensity values for the pixels of YAP proteins in the nuclear and cytoplasmic region, respectively; whereas A_{nuc} and A_{cyto} are the areas of the corresponding regions. All these parameters can be calculated using a specific plug-in of the FiJi software called "Measure".

5.2.7 Statistical analysis

Each experiment has been performed on two independent microfluidic platforms acquiring for the study of nuclear-cytoplasmic YAP ratio at least 10 cells/device. All data are reported as mean ± standard error of the mean. Statistical comparisons were performed with ANOVA and P values of < 0.01 (**) or < 0.05 (*) denote statistically significant differences.

5.3 Results

5.3.1 Operating tests of the microfluidic platform

As previously introduced, the nanoparticles (NPs) embedded in the PDMS membrane have been changed to avoid an overlapping between NPs and YAP signals at the same wavelength. So, red fluorescent polystyrene nanoparticles have been entrapped in the cell-seeded membrane. Since the characteristics and dimensions of these NPs are equal to the green ones used for other experiments, the microfluidic platform should response in the same way to a specific pressure. To be sure about that, different tests on independent microfluidic platforms with red NPs have been made and compared with

green NPs chips. Even if those experiments have been performed for each pressure in the range [-100; -600] mbar, here it has been reported only the comparison at -400mbar, that is the pressure applied to study YAP response to curvature variation. As shown in Figure 5.2A, a perfect match was observed between devices having PDMS membrane with red NPs and those with green ones (R^2 = 0.998). Obviously, each experiment has been repeated three times on three different microfluidic platforms in order to be sure of their reproducibility. Then, a 3D view of the PDMS membrane with red polystyrene nanoparticles embedded is shown in Figure 5.2B.

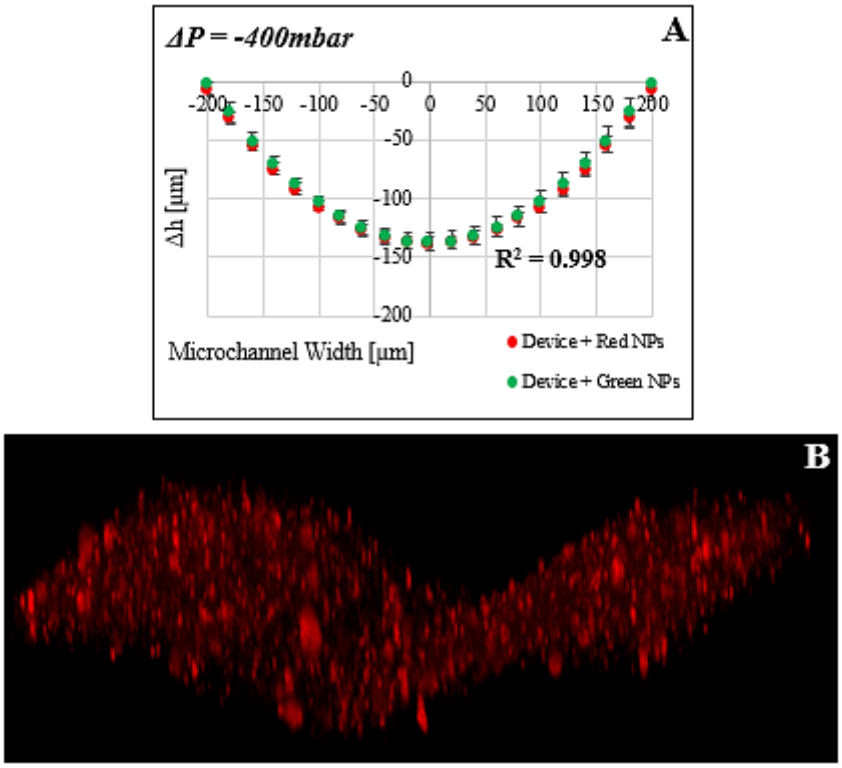

Figure 5.2 Microfluidic platform with red polystyrene nanoparticles embedded in the PDMS membrane. A: Comparison of operating tests between a microfluidic platform with red polystyrene nanoparticle PDMS membrane and that with green polystyrene nanoparticles. B: 3D images of red PDMS membrane behaviour at -400 mbar. Each experiment has been repeated three different times on three independent microfluidic platforms.

5.3.2 Nuclear-cytoplasmic YAP trafficking influenced by curvature

The relationship between Yes-associated protein trafficking and curvature of the cell-seeded substrate is not very clear, as a consequence, a specific curvature variation has been applied on YAP-electroporated high-density ASCs to study their response to this specific mechanical insult. The pressure applied was equal to -400mbar, which means a curvature of 0.0052 μm^{-1} and a R_C = 191 μm. It has been applied to ASCs this specific curvature variation since, from chapter 3, it results able to induce the alignment of actin stress fibers of low-density ASCs along the uniaxial stretching direction. With respect to the previous experiments where the influence of static or dynamic curvature variations were studied on low-density cells, now, high-density ASCs have been considered. In fact, as shown in Figure 5.3A, the communication between cells cannot be neglected but it is possible to recognize the different cells and quantify for each one the nuclear-cytoplasmic YAP trafficking. Using *Nardone et al.* approach [2], the nuclear and cytoplasmic concentration have been quantified before and 24h after the mechanical stimulation. Into undeformed configuration, the nuc/cyt YAP ratio results equal to ≈ 1.80 whereas into deformed one approx. 1.55 (Figure 5.3B). *Nardone et al.* establish a uniform distribution of YAP between cytoplasm and nucleus when this parameter is close to 2; whereas smaller or larger than 2 means cytoplasmic or nuclear accumulation, respectively. In this case, into undeformed configuration, the YAP is approximatively uniformly distributed inside ASCs, whereas after 24 h from the application of curvature change, a statistically significant reduction of ≈ 15% of nuc/cyt YAP ratio has occurred. This should mean that the curvature variation induces a translocation of YAP from the nucleus to the cytoplasm able to reduce this parameter. As representative ASCs, Figures 5.3C-D show cells into undeformed (uniform nuc/cyt YAP ratio) and deformed (cytoplasmic accumulation of YAP) configuration, respectively.

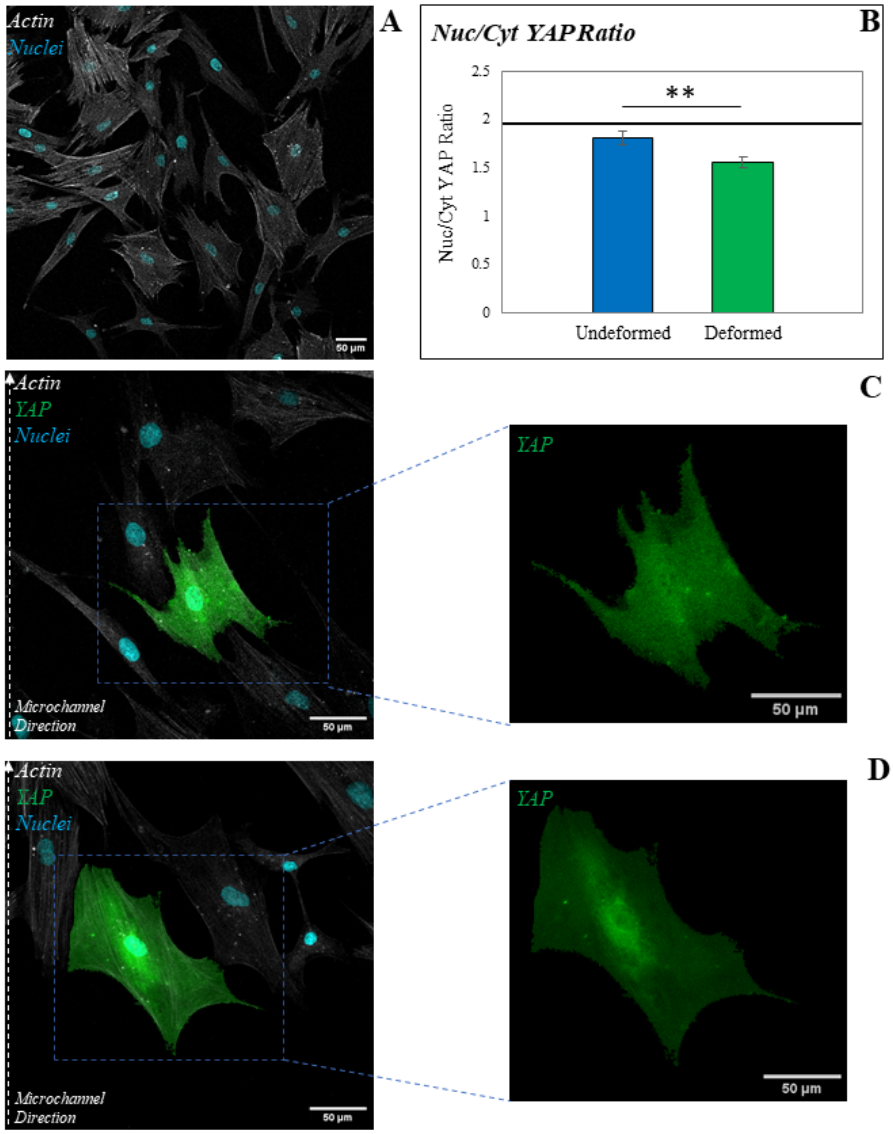

*Figure 5.3 Role of curvature on YAP trafficking. A: Confocal image acquired with 10X objective showing ASCs on high density condition; Gray: Actin, Cyan: Nuclei, scale bar 50 µm. B: Nuclear/cytoplasmic YAP ratio in undeformed and 24h deformed configurations, black straight line represents uniform concentration of YAP between cytoplasm and nucleus. C-D: Representative images of ASCs in undeformed (C) and deformed (D) cases with a zoom on YAP localization acquire with 40X. Gray: Actin, Green: YAP, Cyan: Nuclei, scale bar 50 µm. Each experiment was repeated two times on independent microfluidic devices. Data expressed as mean ± s.e.m. **p<0.001*

5.4 Discussion and conclusions

The cytoplasmic/nuclear shuttling of transcription factors is an important process that regulates different cellular behaviour with high efficiency, such as cell proliferation, differentiation, migration and so on [2-4,12]. Several models have been proposed to describe the dynamics of TFs translocation. For instance, the binding of Myocardin-related transcription factor A with monomeric G-actin prevents the translocation of TFs into the nucleus. Sequestration of G-actin caused by actin polymerization and cytoskeleton assembling frees the TFs making it available for nuclear transport [13]. YAP belongs to those TFs whose shuttling dynamics is sensitive to the cell's cytoskeleton structure [14,15]. It is a transcriptional coactivator downstream of the Hippo pathway that regulates many cellular functions, such as proliferation, migration, differentiation, and apoptosis [2-4,12]. Many findings have demonstrated that YAP is also a protein that respond to: extracellular environment signals as its rigidity and geometry, cell density and polarity and the intracellular status of the actin cytoskeleton, altogether determining a peculiar nuclear/cytoplasmic localization [16,17].

Moreover, the curvature should have a role on the nuclear-cytoplasmic trafficking of YAP which, as a consequence, could control cellular pathways. Since the cells are able to discriminate between planar, concave, and convex substrates, a specific YAP translocation could occur for each configuration. On convex substrates, a YAP shuttling from the cytoplasm to the nucleus is activated by the interaction between Rho molecules and actomyosin cytoskeleton controlling cell proliferation [5,8]. Conversely, on concave surfaces a translocation of YAP from the nucleus to the cytoplasm could occur [18] but the phenomenon is not well understood. For this reason, the designed microfluidic platform has been used to test the response of ASCs to curvature variations. Particularly, the curvature applied was able to control the cytoskeleton architecture through the actin stress fibers re-alignment along the uniaxial stretching direction. As a result, from a uniform concentration of YAP between cytoplasm and nucleus into undeformed configuration, an increase of cytoplasmic YAP was observed 24 h after the application and maintenance of curvature variation. This translocation should be controlled by the combination of curvature and cell-cell interaction [18]. In fact, as known [9-11], the concave substrates stimulate the formation of tight junctions, whereas one of their

constituent proteins (zona occludens 2 – ZO-2) is able to interact with YAP molecules avoiding the activation of transcription pathways. Since the YAP factors are inactive inside the cytoplasm and active into the nucleus, to prevent the activation of these mechanisms, the YAP sequestration has to occur in the cytoplasm.

With respect to low-density cells where YAP localization is only controlled by the actin cytoskeleton and well-structured filaments means YAP nuclear localization [14,15], on confluent ones the interaction between them plays a fundamental role.

So, the stimulation applied in these experiments is only one of the possible curvature variations that can be tested using the designed microfluidic platform. In fact, the versatility of the device permit to test different mechanical insults controlling not only the amplitude but also the time with which they can be applied. Furthermore, a study of YAP translocation on low-density ASCs could be of interest to neglect the cell-to-cell interaction and only study in depth the influence of curvature on YAP translocation.

Finally, as future perspectives, the application of this approach to the study of other transcription factors involved in mechanosensing and mechanotransduction pathways could also be very interesting.

References

[1] Aragona, Mariaceleste, et al. "A mechanical checkpoint controls multicellular growth through YAP/TAZ regulation by actin-processing factors." *Cell* 154.5 (2013): 1047-1059.

[2] G. Nardone, J. Oliver-De La Cruz, J. Vrbsky, J. et al. 2017. YAP regulates cell mechanics by controlling focal adhesion assembly. Nat Commun 8, 15321. https://doi.org/10.1038/ncomms15321.

[3] Elosegui-Artola, Alberto, et al. "Force triggers YAP nuclear entry by regulating transport across nuclear pores." *Cell* 171.6 (2017): 1397-1410.

[4] Bruyère, Céline, et al. "Actomyosin contractility scales with myoblast elongation and enhances differentiation through YAP nuclear export." *Scientific reports* 9.1 (2019): 1-14.

[5] Dupont, Sirio, et al. "Role of YAP/TAZ in mechanotransduction." *Nature* 474.7350 (2011): 179-183.

[6] García-González, Alberto, et al. "The effect of cell morphology on the permeability of the nuclear envelope to diffusive factors." *Frontiers in physiology* 9 (2018): 925.

[7] Lv, Hongwei, et al. "Mechanism of regulation of stem cell differentiation by matrix stiffness." *Stem cell research & therapy* 6.1 (2015): 1-11.

[8] Low, Boon Chuan, et al. "YAP/TAZ as mechanosensors and mechanotransducers in regulating organ size and tumor growth." *FEBS letters* 588.16 (2014): 2663-2670.

[9] Soscia, David A., et al. "Salivary gland cell differentiation and organization on micropatterned PLGA nanofiber craters." *Biomaterials* 34.28 (2013): 6773-6784.

[10] Oka, T., A. P. Schmitt, and M. Sudol. "Opposing roles of angiomotin-like-1 and zona occludens-2 on pro-apoptotic function of YAP." *Oncogene* 31.1 (2012): 128-134.

[11] Oka, Tsutomu, et al. "Functional complexes between YAP2 and ZO-2 are PDZ domain-dependent, and regulate YAP2 nuclear localization and signalling." *Biochemical Journal* 432.3 (2010): 461-478.

[12] S. Dupont. 2016. Role of YAP/TAZ in cell-matrix adhesion-mediated signalling and mechanotransduction. . Exp Cell Res. 343(1):42-53. doi: 10.1016/j.yexcr.2015.10.034.

[13] E. Sidorenko, M.K. 2019. Vartiainen. Nucleoskeletal regulation of transcription: Actin on MRTF.. Exp Biol Med (Maywood). 244(15):1372-1381. doi:10.1177/1535370219854669

[14] Das, A., Fischer, R.S., Pan, D., Waterman, C. M. 2016. YAP nuclear localization in the absence of cell-cell contact is mediated by a filamentous actin-dependent, myosin II- and phospho-YAP-independent pathway during extracellular matrix mechanosensing. J Biol Chem. 291(12):6096-110. doi: 10.1074/jbc.M115.708313.

[15] M. Kofler et al. 2018. Mediated nuclear import and export of TAZ and underlying molecular requirements. Nat Commun 9, 4966. https://doi.org/10.1038/s41467-018-07450-0.

[16] Wolf et al. 2009. Mechanotransduction: Role of nuclear pore mechanics and nucleocytoplasmic transport, in Cellular Mechanotransduction: Diverse Perspectives from Molecules to Tissues, edited by M. Mofrad and R. Kamm (Cambridge University Press, New York, 2009), pp. 415-435.

[17] Saporito, Stefania, et al. "A role for nuclear stretching and NPCs changes in the cytoplasmic-nuclear trafficking of YAP: An experimental and numerical modelling approach." *Materials Today Bio* 15 (2022): 100335.

[18] Baptista, Danielle, et al. "Overlooked? Underestimated? Effects of substrate curvature on cell behavior." *Trends in biotechnology* 37.8 (2019): 838-854.

Chapter 6

Design of micropatterned substrates to control adipose stem cell organization

6.1 Introduction

Biochemical and biophysical cues are able to control different aspects of cellular behaviour such as cell proliferation, migration, and differentiation [1-5]. Generally, these signals born inside the extracellular microenvironment (ECM) that, through the focal adhesions, can be propagated inside the cells. Particularly, integrins are able to transduce extracellular physical information into intracellular signalling pathways.

To finely control and guide the cell behaviour, it is possible to manipulate specific properties of the extracellular microenvironment such as chemistry [2,6], stiffness [7,8], and topography [9,10]. Particularly, the attention has been focused on topographic changes of the ECM due to their high potentialities in controlling cell differentiation, proliferation, and motility. Particularly, in function of topographic scales, specific cellular responses can be observed. Starting from the macroscale (>100 μm), the cell arrangement can be controlled at level of cell colonies [11]; conversely, at the microscale (0.1-100 μm) the topographies are of the same order of magnitude of single cells. As a consequence, a guidance of single cells can be performed. For example, parallel microstructures that have diameter from 10 μm to 30 μm can manipulate fibroblasts alignment along the longitudinal direction [12-14].

The last but not least are the nano-topographies designed at nanoscopic scale (1-100nm) which are of the same order of magnitude of cell receptors such as integrins. As previously introduced, integrins are specific proteins which work from a mechanical point of view ensuring a cell cytoskeleton attachment to the ECM and biochemically by sensing whether adhesion has occurred [15,16]. These cell receptors are able to propagate extracellular cues inside the cells, controlling the formation of both focal adhesions and cytoskeleton filaments. As a consequence, nano and micro-patterns are able to finely

manipulate cellular behaviour and, particularly, cell differentiation. Tissue culture micro-grooves of polystyrene or polydimethylsiloxane developed by *Yim et al.* [17] having 350 nm linewidth and 700 nm pitch or 500 nm linewidth and 1 μm pitch, respectively, are able to induce a specific arrangement of FAs and cytoskeleton on human mesenchymal stem cells. Also, poly(lactic-co-glycolic acid) micro-patches that have ridges and grooves of 800 nm and a height of 600 nm can induce osteogenic differentiation on primary osteoblasts [18]. Furthermore, micro and nano-topographies can significantly influence YAP mechanotransduction which regulates gene expression and, as a consequence, cellular pathways [19].

The designed microfluidic platform can induce on high- or low-density ASCs macroscopic mechanical extracellular signals inasmuch both microchannel width and radii of curvature have a dimension larger than 100 μm. Nevertheless, a control of both cytoskeleton and focal adhesions by applying uniaxial stretching along microchannel direction has occurred. In order to transform this microfluidic platform in a tool with which apply different mechanical insults on adipose stem cells, a specific micro-topography can be designed on the cell-seeded PDMS membrane. Having the ability to induce different mechanical signals means mimicking as much as possible the condition to which cells are subjected in vivo. To fabricate PDMS substrate with a specific feature needs to create a specific micropatterned master on which the membrane can be replicated.

Detailly, micropatterned masters having ridges and grooves features have been designed and fabricated using the two-photon polymerization technique, then their characterization and also that of the PDMS replica was made using atomic force microscopy (AFM) and scanning electron microscopy (SEM). These features also induce a preferential direction on the ASCs, and, within the microfluidic platform, they can be aligned along the microfluidic channel or directed orthogonally to it, so as to obtain coupled or de-coupled mechanical signals.

6.2 Materials and Methods

6.2.1 Micropattern fabrication process

Micropatterned substrates were fabricated by means of two-photon polymerization (2PP) technique using the 3D printing Nanoscribe Photonic Professional GT System (Nanoscribe GmbH). This instrument uses a 780 nm Ti-sapphire laser emitting ≈ 100 fs pulsed at 80 MHz with a maximum power of 150 mW and is equipped with a 63x oil immersion objective (1.4 N.A.). A specific photoresist called Ip-Dip (Nanoscribe GmbH) was used to accurately fabricate structures with submicrometric resolutions. Particularly, the topography was characterized by ridges and grooves of 700nm, with a pitch of 1.4 µm and a thickness of 450 nm, which corresponds to the voxel dimension, that is minimum resolution. These structures were fabricated on 25x25 mm² fused silica substrates (3D SF DiLL - Nanoscribe GmbH). Using the 63x objective, the maximum scan field is equal to 150 µm x 150 µm, this means that to create a micropatterned surface of 15x15 mm² a single structure of 100 µm x 100 µm has to be repeated a number of times ensuring the continuity of the features on x-y plane. Thus, fabrication parameters were iteratively determined to ensure correct topography and continuity over the whole surface. Particularly, the laser power was set to 35% and the scan speed to 15mm/s.

Briefly, the first step of fabrication procedure consists of place and fix the substrates in a holder and then pouring in the center the Ip-Dip avoiding the bubble formation. After, the holder is placed into a piezoelectric x/y/z stage using an invert z-axis configuration where a galvo scanner determines the laser trajectories. At the end of process, a photoresist development needs to fix the fabricated topographies. So, 10 min into Mr-Dev developed liquid, 10 min into IPA and 5 minutes at 50 °C are sufficient to remove photoresist in excess and solidify micropatterns.

Starting from the fabricated micropatterns in Ip-Dip, using the replica molding technique, specific PDMS patterned substrates (19:1 pre-polymer/cross-linker ratio) can be obtained. In order to finely replicate the nanometric features, the PDMS was poured on the master, degassed to remove air bubbles, and cured at 130 °C for 20min. After cooling, a peeling off of the PDMS membrane from the Ip-Dip master was done and then, the same masters can be used a lot of times to reproduce other replicas.

6.2.2 AFM and SEM characterization techniques

The morphological investigation of Ip-Dip patterned substrates was performed using Atomic Force Microscopy (AFM), whereas Scanning Electron Microscopy (SEM) approach was used to PDMS replicas characterization.

AFM is a type of scanning probe microscopy with resolution of few nanometres characterized by three different major abilities: force measurement, topographic imaging, and manipulation. To study the morphological features of fabricated micropatterns, the topographic imaging approach has been applied. The reaction of the probe to the force that the sample imposes on it, can be used to form an image of the three-dimensional shape (topography) of the sample surface at high resolution. Using the Dimension Icon AFM (Bruker) in contact mode with a specific probe (ScanAsyst-Fluid – Bruker), in air, and at room temperature, a detailed topography of the Ip-Dip substrate was performed. Finally, the scale indicating the sample height was adjusted to limit the gap between high (ridges) and low (grooves) regions.

SEM is an electron microscopy technique able to produce images of samples by scanning the surface with a focused beam of electrons. Briefly, electrons interact with atoms in the sample and various signals that contain information about the surface topography and composition were produced. The electron beam is scanned, and the position of the beam is combined with the intensity of the detected signal to produce an image. Generally, secondary electrons emitted by atoms after electron beam excitation are detected using a secondary electron detector.

The PDMS replicas were cut in the middle of the pattern and small samples were 90° rotated and deposited onto carbon tape attached to the surface of aluminium stub in order to visualize the ridges and grooves profiles. After a gold sputter-coated of 15nm in a Cressington sputter coated HR208, the image acquisitions were made with Focused Ion Beam Scanning Electron Microscope (FIBSEM) Helios CX5 (ThermoFisher Scientific). Particularly, a voltage of 2-3 kV, a current of 0.34 nA, a magnification from 10 kX to 70 kX and a tilting angle of 0° or 52° were used as acquisition parameters.

6.2.3 Micropattern sterilization, functionalization and cell seeding

PDMS micropatterned replicas are opportunely sterilized and functionalized before adipose stem cell seeding. The sterilization approach consists of 15 minutes in ethanol and 1 h under UV. Then, the functionalization was made through oxygen plasma treatment (1 min – Plasma Surface Technology – Diener Electronic) and 50 µg/ml fibronectin (F0895-2MG – Sigma-Aldrich) in PBS (D8537 – Merck) for 1 h at 37 °C.

At the end of micropatterned substrates functionalization, 1-week cultured adipose derived mesenchymal stem cells were seeded at a low-density of 5000 cells/micropattern. The ASCs were cultured into a specific cell culture medium composed by: Minimum Essential Medium Eagle (Alpha modification) (AL081 – Microtech S.R.L.), 10% of fetal bovine serum (F7524 - Merck), 1% of L-Glutamine (G7513 - Merck) and 1% of Pen-Strep (P4333 - Merck). After 24 h from the cell seeding, the ASCs response to the micropatterned features has been analysed.

6.2.4 Cell fixation and immunofluorescence

ASCs cultured on all micropatterned substrates were fixed 24 h after cell seeding with 4% paraformaldehyde (Alfa Aesar-Thermo Fisher, Karlsruhe, Germany) in PBS for 15 min. The cells were then permeabilized with 0.1% Triton X-100 (Sigma Aldrich-Merck KGaA, Darmstadt, Germany) in 1x PBS (TPBS) for 10 min and blocked in 3% bovine serum albumin in PBS (Sigma-Aldrich) for 1 h to avoid non-specific binding.

Actin stress fibers were labelled using 1:500 Alexa Fluor 488 Phalloidin (Alexa Fluor ™ Thermo Fisher Scientific) for 1 h and nuclei were stained incubating samples with DAPI (4',6-Diamidino-2-Phenylindole, Dihydrochloride, Thermo Fisher Scientific) solution (dilution 1:10000) for 15 minutes. Fluorescent images of nuclei and actin stress fibers were collected with Confocal Zeiss Axio Observer.Z1 using a 40x objective. Samples were excited at 380 nm (Nuclei), and 488 nm (actin filaments), and the emissions were collected in the 400-420 nm, and 500-530nm, respectively. Moreover, Z-stacks have been acquired with the optimal interval suggested by the software, followed by the application of a maximum intensity algorithm.

6.2.5 Image analysis

The images were analyzed using an image processing package of ImageJ, called FiJi, with which a quantification of cellular/nuclear major and minor axes and aspect ratio (AR) was performed. Each image acquired is composed of different z-stacks where both actin stress fibers and nuclei can be recognized. To quantify their AR, major and minor axes a specific plug-in of the software called “Measure” has been used. Briefly, starting from the z-stacks, a z-projection was made, and, after an improvement of contrast, the cellular and nuclear parameters have been determined by the plug-in.

6.2.6 Statistical analysis

Each experiment was performed on three independent PDMS micropatterned substrates acquiring for the study of cellular and nuclear morphology at least 10 cells/substrate. All data are reported as mean ± standard error of the mean.

6.3 Results

6.3.1 Micropatterned substrates morphology

The micropatterned Ip-Dip masters were fabricated with the two-photon polymerization technique using specific parameters which are detailly explained in the materials and methods section. Their analysis from a qualitative and quantitative point of view was made using optical microscopy and atomic force microscopy, respectively. As shown in Figure 6.1A, the fabricated parameters have been optimized to occur a large micropatterned substrate composed of continuous smaller squared structures. Furthermore, from the AFM images (Figure 6.1B) a quantification of micropatterned substrate thickness and distance between ridges and grooves was performed. The thickness of the fabricated structures results equal to 460 ± 14 nm, whereas the ridges and grooves are equally spaced with a pitch of 1377 ± 77 nm ≈ 1400 nm.

Knowing the topographic characteristics of the fabricated masters, specific PDMS replicas were obtained using the replica molding approach. A quantification of morphological parameters was made using the SEM images (Figure 6.1C) obtaining a micropattern pitch of 1410 ± 0.01 nm and a thickness of 354 ± 9 nm. The depth reduction of PDMS replicas should be due to the difficulties of material to enter inside the

nanoscopic ridges and grooves or should be due to the shrinkage effects of PDMS during the curing process. Nevertheless, as previously explained in the introduction section, the order of magnitude of these specific topographic parameters is able to control cellular response at level of integrins and this thickness reduction can be neglected.

Finally, the Ip-Dip masters can be used to fabricate a lot of PDMS replicas. In fact, after 50 replications, the topographic characteristics of PDMS substrates are comparable to those of the first ones.

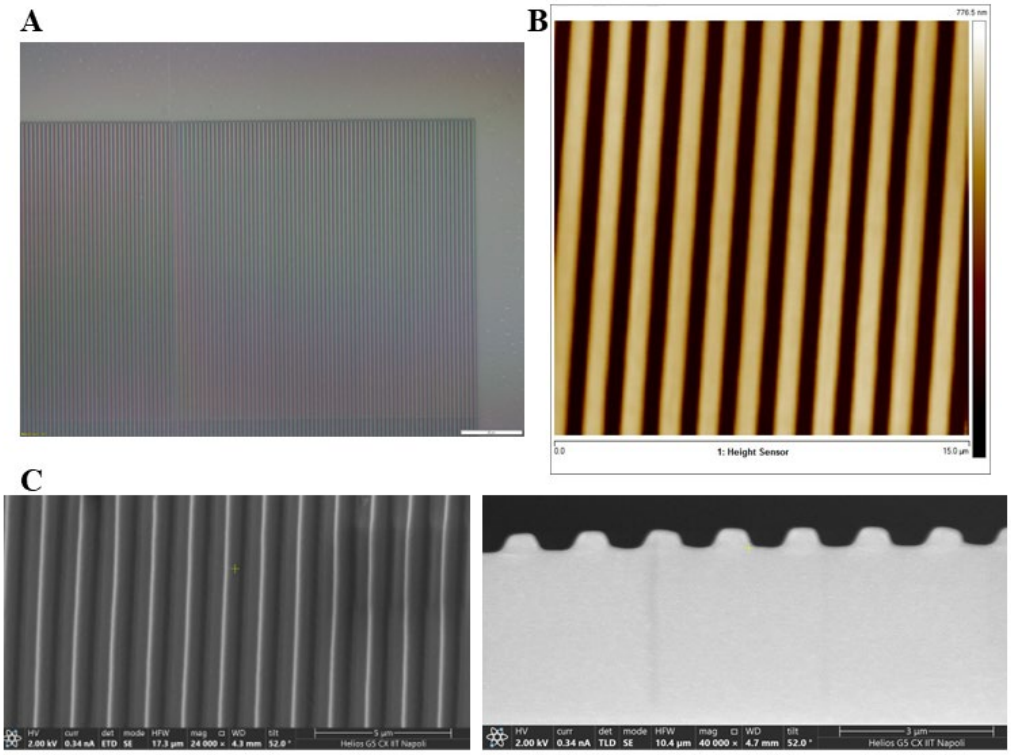

Figure 6.1: Micropatterned Ip-Dip substrate morphology. A: Image acquired using an optical microscope showing the Ip-Dip master topography from a qualitative point of view (scale bar: 20 µm). B: AFM scan useful to quantify pitch and depth values of master. C: SEM acquisitions showing in the x-y plane (left image) and y-z plane (right image) the PDMS replicas topographies (scale bar 5 µm - 3 µm)

6.3.2 ASCs response on micropatterned substrates

On three different micropatterned PDMS substrates (19:1 pre-polymer/cross-linker ratio), low-density ASCs were seeded in order to study their response to these specific features after 24 h. Particularly, cellular, and nuclear morphology in terms of major-minor axes and AR were evaluated. As shown in Figure 6.2A-C, the actin stress fibers and nucleus are perfectly aligned along the micropatterned direction. Particularly, cells are characterized by a major axis = 102.77 ± 4.69 µm, a minor axis = 15.71 ± 0.94 µm and an aspect ratio = 7.21 ± 0.61 µm; conversely, the nuclei have a major axis = 15.42 ± 0.25 µm, a minor axis = 8.33 ± 0.19 µm and an AR = 1.88 ± 0.06 µm. Analysing these outcomes, a preferential polarization of ASCs on ridges and groove direction was observed. In fact, for example, the AR of ASCs equal to 7.21 represents a length of cells along micropatterned direction 7 times larger than the width along the orthogonal one.

So, knowing the response of ASCs to time and space curvature variations and, also, to specific micropatterned substrates, as future perspective these features could be introduced in the microfluidic platform in order to couple or de-couple these different biophysical signals.

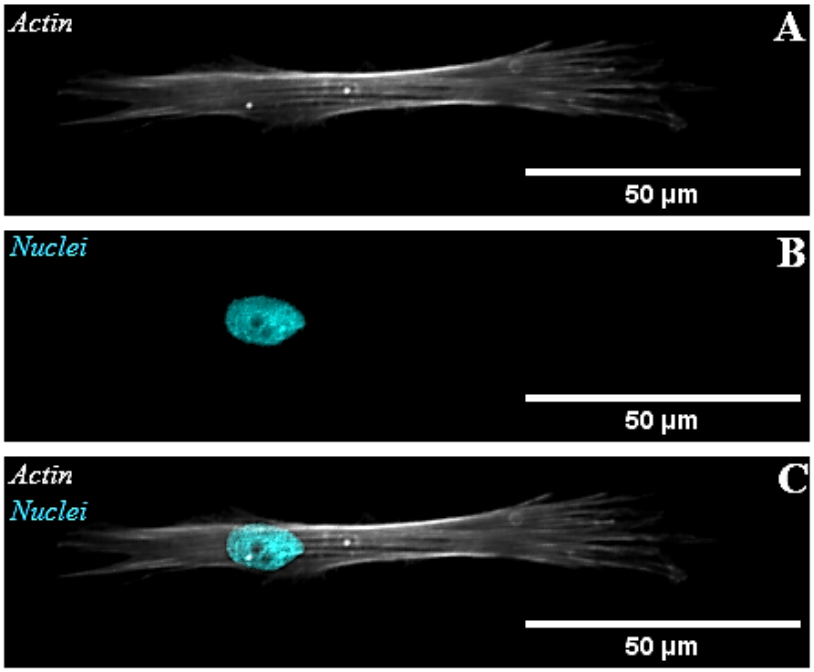

Figure 6.2: ASC response to micropatterned topographies. A-B: Actin stress fibers (A) and nucleus (B) polarization along the ridges and grooves direction; C: Merge of actin stress fibers and nucleus. (Gray; actin stress fibers, Cyan; Nucleus. Scale bar: 50 µm.

6.4 Discussion and Conclusions

Biomaterials are able to actively regulate cellular functions such as cell proliferation, differentiation, and motility; particularly, these materials induce on cells chemical or physical signals. The former includes material modifications integrating growth factors [20], peptides [21] or extracellular matrices [22,23], whereas the latter employs mainly topographical structures to play instructive roles [24]. Particularly, the topographical cues are able to induce osteogenic, neurogenic, and cardiovascular differentiation [25-29].

For example, round mesenchymal stem cells are able to differentiate toward chondrogenic lineages with respect to the rectangular one that tend to osteogenic pathways [30]. The relationship between stem cells shape and their differentiation should be related to the different cytoskeletal tensions induced by specific topographical cues [30]. Particularly, circular shape induces stresses/strains smaller with respect to the rectangular one which, as a consequence, generate different cellular behaviours.

Knowing the potentialities of topographical cues, specific micropatterned substrates have been designed to finely control cellular and nuclear shape using the two-photon polymerization technique. The ridges and grooves dimensions of hundreds of nanometres (700 nm) classifies these materials as microscopic patterns, this means that they are able to act at level of focal adhesions. Due to the physical pathway between extracellular matrix, focal adhesions, cytoskeleton and nucleus, an ECM modification could generate the activation or not of specific mechanisms inside the nucleus. In these experiments, 24 h after cell seeding, a complete alignment of actin stress fibers and nuclei was observed on low-density ASCs.

A polarization of actin stress fibers and focal adhesions has occurred on the microfluidic platform previously described where curvature changes were applied in time and space. Moreover, the nuclear-cytoplasmic trafficking was influenced by curvature changes. Due to the dimension of microfluidic channel (400 μm width), the topographical signals applied could be considered macroscopic with respect to the microscopic ones applied through the patterns. Since both signals are able to control the adipose derived mesenchymal stem cells response in a specific way, a combination of these different biophysical cues should be very interested. Particularly, these signals can be coupled

aligning the ridges and grooves orientation with the microchannel direction or they may compete by aligning the micropatterns orthogonally to the device.

So, as future perspective the patterned cell seeded membrane will be integrated into the microfluidic platform in order to study the effects of these signals on cellular behaviour. Moreover, longer experiments will be performed to analyse how the combination of these signals could control the cell differentiation.

References

[1] Dalby, Matthew J., Andrés J. García, and Manuel Salmeron-Sanchez. "Receptor control in mesenchymal stem cell engineering." *Nature Reviews Materials* 3.3 (2018): 1-14.

[2] Benoit, Danielle SW, et al. "Small functional groups for controlled differentiation of hydrogel-encapsulated human mesenchymal stem cells." *Nature materials* 7.10 (2008): 816-823.

[3] Engler, Adam J., et al. "Matrix elasticity directs stem cell lineage specification." *Cell* 126.4 (2006): 677-689.

[4] McBeath, Rowena, et al. "Cell shape, cytoskeletal tension, and RhoA regulate stem cell lineage commitment." *Developmental cell* 6.4 (2004): 483-495.

[5] McMurray, Rebecca J., et al. "Nanoscale surfaces for the long-term maintenance of mesenchymal stem cell phenotype and multipotency." *Nature materials* 10.8 (2011): 637-644.

[6] Curran, Judith M., Rui Chen, and John A. Hunt. "The guidance of human mesenchymal stem cell differentiation in vitro by controlled modifications to the cell substrate." *Biomaterials* 27.27 (2006): 4783-4793.

[7] Wen, Jessica H., et al. "Interplay of matrix stiffness and protein tethering in stem cell differentiation." *Nature materials* 13.10 (2014): 979-987.

[8] Trappmann, Britta, et al. "Extracellular-matrix tethering regulates stem-cell fate." *Nature materials* 11.7 (2012): 642-649.

[9] Dalby, Matthew J., et al. "The control of human mesenchymal cell differentiation using nanoscale symmetry and disorder." *Nature materials* 6.12 (2007): 997-1003.

[10] Dalby, Matthew J., Nikolaj Gadegaard, and Richard OC Oreffo. "Harnessing nanotopography and integrin–matrix interactions to influence stem cell fate." *Nature materials* 13.6 (2014): 558-569.

[11] Desai, Tejal A. "Micro-and nanoscale structures for tissue engineering constructs." *Medical engineering & physics* 22.9 (2000): 595-606.

[12] Curtis, A. S. G., and Malini Varde. "Control of cell behavior: topological factors." *Journal of the National Cancer Institute* 33.1 (1964): 15-26.

[13] Clark, Petal, et al. "Cell guidance by ultrafine topography in vitro." *Journal of cell science* 99.1 (1991): 73-77.

[14] Curtis, A. S. G. "The mechanism of adhesion of cells to glass: a study by interference reflection microscopy." *The Journal of cell biology* 20.2 (1964): 199-215.

[15] Hynes, Richard O. "Integrins: bidirectional, allosteric signaling machines." *cell* 110.6 (2002): 673-687.

[16] Harburger, David S., and David A. Calderwood. "Integrin signalling at a glance." *Journal of cell science* 122.2 (2009): 159-163.

[17] Heng, Boon C., et al. "Role of YAP/TAZ in cell lineage fate determination and related signaling pathways." *Frontiers in cell and developmental biology* 8 (2020): 735.

[18] Saporito, Stefania, et al. "A role for nuclear stretching and NPCs changes in the cytoplasmic-nuclear trafficking of YAP: An experimental and numerical modelling approach." *Materials Today Bio* 15 (2022): 100335.

[19] Piccolo, Stefano, Sirio Dupont, and Michelangelo Cordenonsi. "The biology of YAP/TAZ: hippo signaling and beyond." *Physiological reviews* (2014).

[20] Bruggeman, Kiara F., Richard J. Williams, and David R. Nisbet. "Dynamic and responsive growth factor delivery from electrospun and hydrogel tissue engineering materials." *Advanced healthcare materials* 7.1 (2018): 1700836.

[21] Tsuchiya, Kousuke, and Keiji Numata. "Chemoenzymatic synthesis of polypeptides for use as functional and structural materials." *Macromolecular Bioscience* 17.11 (2017): 1700177.

[22] Freytes, Donald O., et al. "Preparation and rheological characterization of a gel form of the porcine urinary bladder matrix." *Biomaterials* 29.11 (2008): 1630-1637.

[23] Wolf, Matthew T., et al. "A hydrogel derived from decellularized dermal extracellular matrix." *Biomaterials* 33.29 (2012): 7028-7038.

[24] Jun, Indong, et al. "Ultrathin metal films with defined topographical structures as in vitro cell culture platforms for unveiling vascular cell behaviors." *Advanced Healthcare Materials* 5.18 (2016): 2396-2405.

[25] Arjmand, Monireh, et al. "Osteogenic differentiation potential of mesenchymal stem cells cultured on nanofibrous scaffold improved in the presence of pulsed electromagnetic field." *Journal of Cellular Physiology* 233.2 (2018): 1061-1070.

[26] Chen, Honglin, et al. "Tailoring surface nanoroughness of electrospun scaffolds for skeletal tissue engineering." *Acta biomaterialia* 59 (2017): 82-93.
[27] Jung, Ae Ryang, et al. "Nanoengineered polystyrene surfaces with nanopore array pattern alters cytoskeleton organization and enhances induction of neural differentiation of human adipose-derived stem cells." *Tissue Engineering Part A* 21.13-14 (2015): 2115-2124.
[28] Tan, Kenneth KB, et al. "Enhanced differentiation of neural progenitor cells into neurons of the mesencephalic dopaminergic subtype on topographical patterns." *Biomaterials* 43 (2015): 32-43.
[29] Tallawi, M., et al. "Novel PGS/PCL electrospun fiber mats with patterned topographical features for cardiac patch applications." *Materials Science and Engineering: C* 69 (2016): 569-576.
[30] Kilian, Kristopher A., et al. "Geometric cues for directing the differentiation of mesenchymal stem cells." *Proceedings of the National Academy of Sciences* 107.11 (2010): 4872-4877.

Conclusion and future perspectives

This thesis reports the design of a microfluidic platform useful to apply specific curvature variations in time and space on adipose derived mesenchymal stem cells. Particularly, this platform has been designed in order to visualize in real time the response of ASCs due to the combination of confocal microscopy technique with the transfection strategy. As detailed explained in the different chapters, a correlation between geometric form and biological functions exists on cellular level. In fact, the ASCs response is related to the amplitude of curvature and the periodicity with which it has been applied. This correlation was analysed considering the actin stress fibers and focal adhesions behaviour in different configurations. Particularly, on static curvature variations specific curvature thresholds have been quantified for the re-organization of actin stress fibers and FAs, respectively. Furthermore, on dynamic cases, the periodicity becomes the relevant parameter in controlling cellular response.

Generally, topographical cues are not only able to manipulate cellular response in terms of cytoskeleton and FAs re-organization, but also the translocation of specific transcription factors between cytoplasm and nucleus can be regulated. In fact, the curvature is able to influence the trafficking of Yes-associated proteins into ASCs observing an accumulation of YAPs inside the cytoplasm.

So, the curvature variation is only one of the different biophysical signals able to finely control in time and space adipose stem cells behaviour. Since in human body, cells are continuously subjected to different types of cues, the design of a microfluidic multi-signal platform could be very useful. For this reason, specific micropatterned substrates have been designed and fabricated in order to produce patterned cell-seeded membranes that will be integrated into the microfluidic devices. Moreover, long experiments will be developed in order to verify the role of these different signals on the ASCs differentiation. In conclusion, the combination of these different strategies could be a useful tool to finely manipulate cellular responses in vitro in order to try to approach to the in-vivo conditions.

Supplementary Material

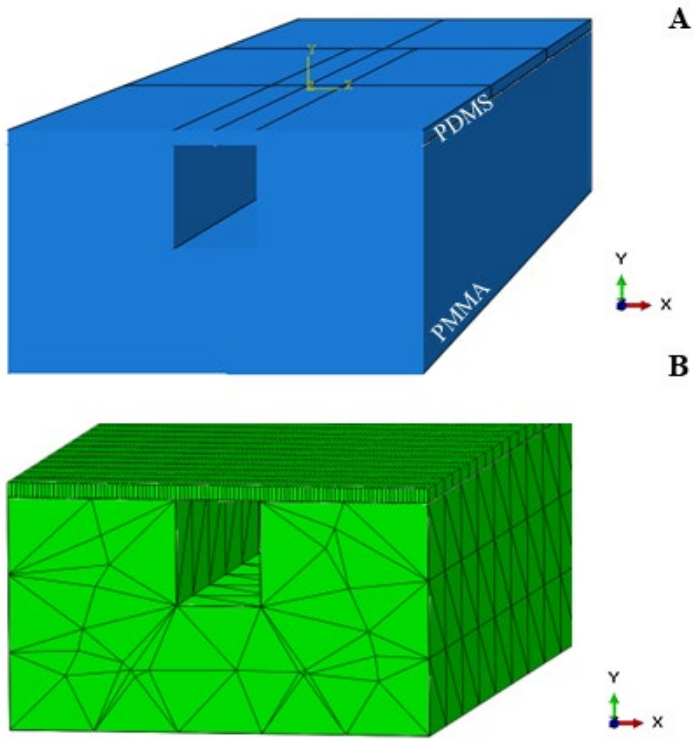

Figure S1:3D finite element method (FEM) model of the microfluidic platform. A: The full 3D model of the microfluidic device is composed by the PDMS membrane and the PMMA channel layer. B: The PMMA 3D mesh is formed by tetrahedron elements whereas the PDMS membrane 3D meshing needs solid continuum elements, in particular they are coarse and fine, respectively.

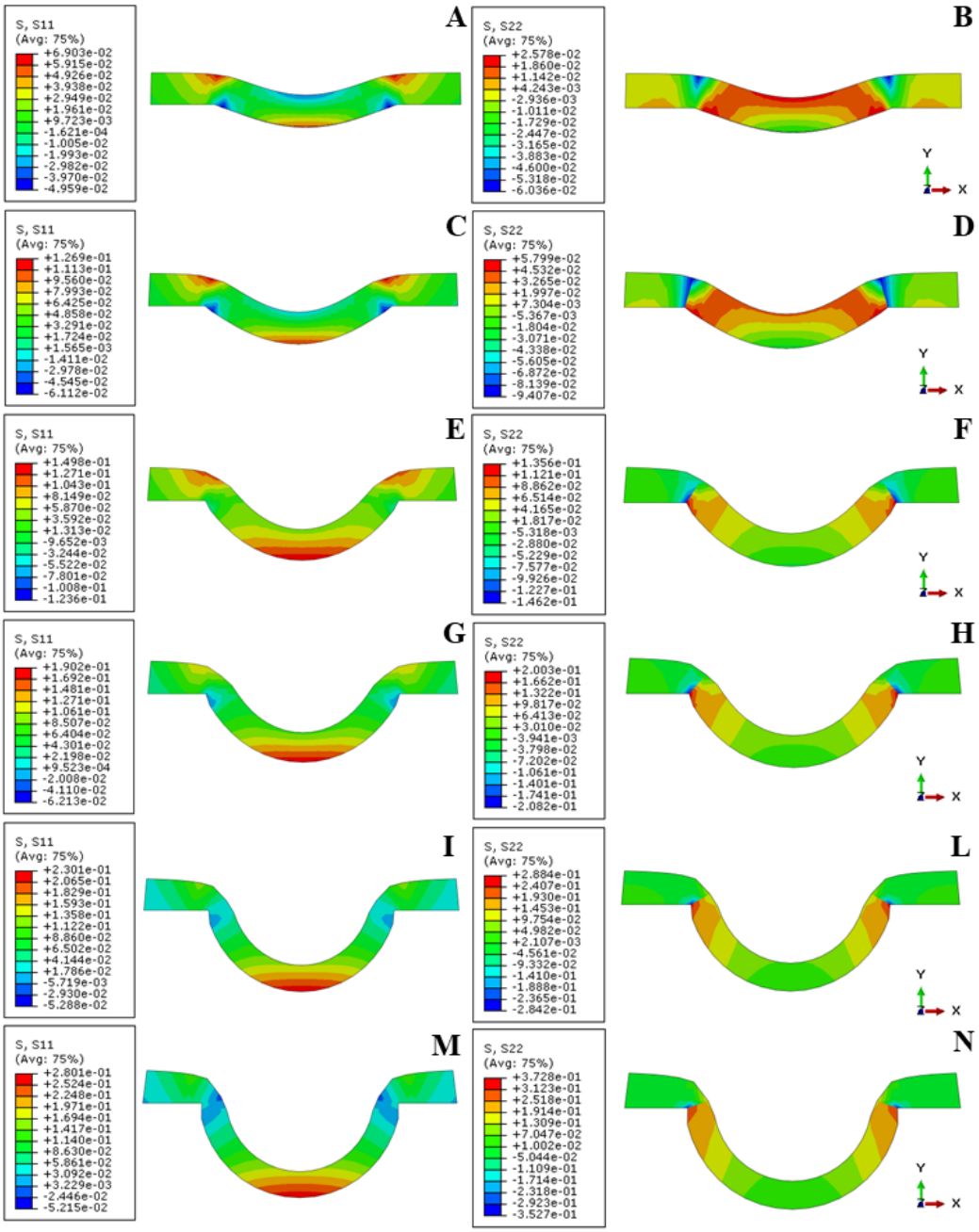

Figure S2:Maps of stress components in directions transverse to the channel axis (z-axis). 1,2 and 3 axes correspond to x, y and z, respectively. A-B: S11 and S22 stress components for pressure of -100mbar; C-D: S11 and S22 stress components for pressure of -200mbar; E-F: S11 and S22 stress components for pressure of -300mbar; G-H: S11 and S22 stress components for pressure of -400mbar; I-L: S11 and S22 stress components for pressure of -500mbar; M-N: S11 and S22 stress components for pressure of -600mbar (stress expressed in MPa on the color maps). The components considered are the most relevant on the von Mises stress field.

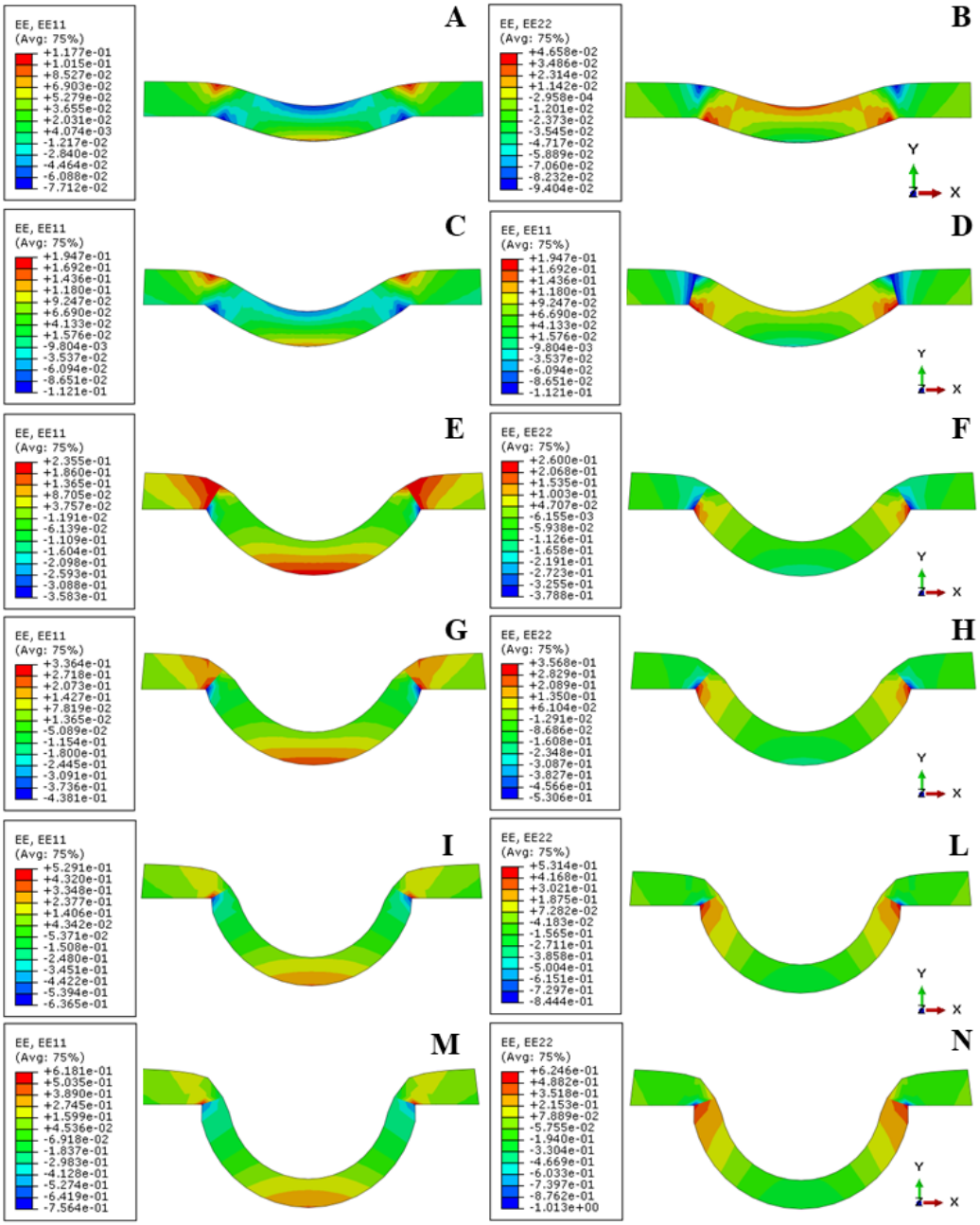

Figure S3:Maps of strain components in directions transverse to the channel axis. 1,2 and 3 axis correspond to x, y and z, respectively. A-B: E11 and E22 strain components for pressure of -100mbar; C-D: E11 and E22 strain components for pressure of -200mbar; E-F: E11 and E22 strain components for pressure of -300mbar; G-H: E11 and E22 strain components for pressure of -400mbar; I-L: E11 and E22 strain components for pressure of -500mbar; M-N: E11 and E22 strain components for pressure of -600mbar). The component considered are the most relevant on the total strain.